(12) INTERNATIONAL APPLICATION PUBLISHED UNDER THE PATENT COOPERATION TREATY (PCT)

(19) World Intellectual Property Organization
International Bureau

(43) International Publication Date
19 January 2012 (19.01.2012)

PCT

(10) International Publication Number
WO 2012/007931 A2

(51) International Patent Classification:
H01M 4/92 (2006.01)

(21) International Application Number:
PCT/IE20 11/000038

(22) International Filing Date:
15 July 201 1 (15.07.201 1)

(25) Filing Language: English

(26) Publication Language: English

(30) Priority Data:
2010/0445 16 July 2010 (16.07.2010) IE

(71) Applicant *(for all designated States except US):* **DUBLIN CITY UNIVERSITY** [IE/IE]; Glasnevin, Dublin 9 (IE).

(72) Inventors; and

(75) Inventors/Applicants *(for US only):* **KILLARD, Anthony, Joseph** [IE/GB]; 6 Elmer Close, Malmesbury, Wiltshire SN16 9UE (GB). **MORRIN, Aoife** [IE/IE]; 77 Parkmore Drive, Terenure, Dublin 6W (IE). **GONZALES-MACIA, Laura** [ES/ES]; Gonzalo Bilbao #29, BL2 4C, E-41003 Seville (ES). **CARTON, James, G.** [IE/IE]; Clonmore, Bree, Enniscorthy, County Wexford (IE).

(74) Agents: **O'BRIEN, John, A.** et al; c/o John A. O'Brien & Associates, Third Floor, Duncairn House, 14 Carysfort Avenue, Blackrock, County Dublin (IE).

(81) Designated States *(unless otherwise indicated, for every kind of national protection available):* AE, AG, AL, AM, AO, AT, AU, AZ, BA, BB, BG, BH, BR, BW, BY, BZ, CA, CH, CL, CN, CO, CR, CU, CZ, DE, DK, DM, DO, DZ, EC, EE, EG, ES, FI, GB, GD, GE, GH, GM, GT, HN, HR, HU, ID, IL, IN, IS, JP, KE, KG, KM, KN, KP, KR, KZ, LA, LC, LK, LR, LS, LT, LU, LY, MA, MD, ME, MG, MK, MN, MW, MX, MY, MZ, NA, NG, NI, NO, NZ, OM, PE, PG, PH, PL, PT, RO, RS, RU, SC, SD, SE, SG, SK, SL, SM, ST, SV, SY, TH, TJ, TM, TN, TR, TT, TZ, UA, UG, US, UZ, VC, VN, ZA, ZM, ZW.

(84) Designated States *(unless otherwise indicated, for every kind of regional protection available):* ARIPO (BW, GH, GM, KE, LR, LS, MW, MZ, NA, SD, SL, SZ, TZ, UG, ZM, ZW), Eurasian (AM, AZ, BY, KG, KZ, MD, RU, TJ, TM), European (AL, AT, BE, BG, CH, CY, CZ, DE, DK, EE, ES, FI, FR, GB, GR, HR, HU, IE, IS, IT, LT, LU, LV, MC, MK, MT, NL, NO, PL, PT, RO, RS, SE, SI, SK, SM, TR), OAPI (BF, BJ, CF, CG, CI, CM, GA, GN, GQ, GW, ML, MR, NE, SN, TD, TG).

Published:

— *without international search report and to be republished upon receipt of that report (Rule 48.2(g))*

WO 2012/007931 A2

(54) Title: SILVER ELECTRODE CATALYST

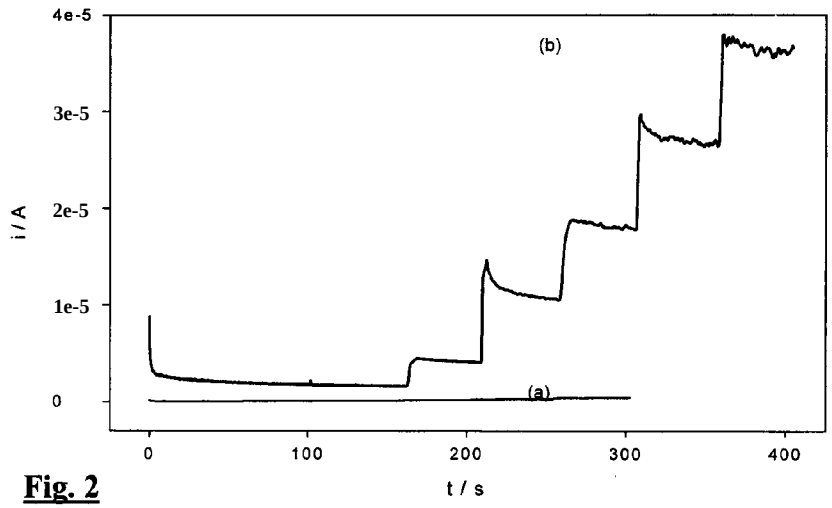

Fig. 2

(57) Abstract: A catalyst comprises a silver electrode wherein the electrode has been modified with a surfactant - salt solution. The electrode may comprise silver colloids, silver particles, or silver nanoparticles, especially a silver paste electrode. The electrode may be a screen printed electrode. The catalyst may be a non-enzymatic hydrogen peroxide catalyst. It may be used in a sensor system such as a glucose or a cholesterol sensor.

"SILVER ELECTRODE CATALYST"

Introduction

The invention relates to a silver electrode catalyst and uses thereof.

In on aspect the invention relates to catalysing the decomposition and electrochemical reduction of hydrogen peroxide. The electrocatalytic reduction of hydrogen peroxide is important for a wide range of applications including chemical sensors, biosensors, fuel cells and batteries, chemical synthesis, and decomposition processes.

Hydrogen peroxide is an extremely widely used raw material due to its oxygen content and its electron-donating properties. The catalytic reduction of hydrogen peroxide can be used in a wide variety of applications. Often, this process is coupled electrochemically either for analytical purposes or to use hydrogen peroxide as an oxidant source in fuel cells and batteries. Many catalysts are available for the decomposition and reduction of hydrogen peroxide, most notably metallic silver and platinum. However, precious metal catalysts such as these are extremely expensive, can easily become poisoned and are relatively inefficient compared to biological catalysts such as enzymes (e.g., peroxidase and catalase).

There are only a few commercial non-enzymatic devices available for the reduction and decomposition of hydrogen peroxide. However, there is huge demand for such technologies in a number of markets. Although the decomposition and reduction of hydrogen peroxide reduction are thermodynamically favourable, these processes are relatively kinetically unfavourable and thus tend to require catalysts. This is also the case for the reduction of hydrogen peroxide taking place at an interface such as an electrode at which a large electrical over-potential must be applied to bring about the reduction process which severely limits its application. Biological catalysts such as enzymes (peroxidase and catalase) are also used at electrode interfaces which allow reduction of hydrogen peroxide at significantly lower over-potentials than would otherwise be required without the use of the biological catalyst. Biological catalysts have many drawbacks in that they are difficult and expensive to purify and are unstable in many environments and applications. Employing a more effective non-biological catalyst that could reduce the over-potential required for electrocatalysis would be extremely useful.

To date significant electroreduction of hydrogen peroxide in the absence of biological catalysts has not been demonstrated. Hydrogen peroxide electroreduction does occur on precious metals; however no significant reports have been published stating that the reaction becomes kinetically useful for sensor applications when using precious metal catalysts. The main problem addressed by the present invention is to reduce the activation energy required to bring about the reductive decomposition of hydrogen peroxide at an electrode surface allowing significant levels of catalytic reduction at low applied potentials, thus making it a very useful device for applications in electrochemical measurement and detection and as a fuel cell/battery oxidant supply. We have demonstrated that by employing a silver/organic composite material (i.e., specifically a screen printed silver paste), and combining it with certain surfactants and metal ions, results in a dramatic increase in the catalytic behaviour of the bulk material towards hydrogen peroxide.

A solution to the creation of suitable catalytic systems would be a material that had good environmental stability such as precious metal catalysts, but with minimal cost implications. Silver is a precious metal that is approximately 100 times cheaper than its platinum counterpart. It is a well-known catalyst used for example, in the production of formaldehyde from methanol and air. Silver is the only catalyst available today to convert ethylene to ethylene oxide.

To date, there have only been a few reports on the use of liquid hydrogen peroxide as the oxidant for a fuel cell. Typically, platinum or lead sulphate have been reported as the cathode material. Silver has not been reported as a cathodic material in a fuel cell for hydrogen peroxide reduction as its efficiency, in its pure state for this reduction process is simply not high enough. To our knowledge, no one has reported pure silver, or silver composites for hydrogen peroxide catalysis for fuel cell applications. Our approach, to modify a silver/organic composite to bring about catalytic enhancements that could be useful as a cathodic material for a direct hydrogen peroxide fuel cell, therefore, has not been reported and is not obvious to those working in the field.

The direct electroreduction of hydrogen peroxide to water has a formal electrode potential of 1.77 V vs. NHE and so requires the application of a significant overpotential to drive the process. This is the main limiting factor on its application as an oxidising agent in fuel cells. Several approaches have been taken to enhance the reduction process through catalytic means. These typically involve the use of the precious metal catalyst, platinum, which is increasingly being used in a nanoparticulate form. Often this is further embedded in conductive matrices to reduce

particle loadings and maintain electrical connectivity. One significant drawback with these materials is the cost of these precious metal catalysts, in particular platinum.

A type of Fuel Cell that does not employ noble-metal catalysts is the alkaline Fuel Cell. Because of facile oxygen reduction kinetics at a high pH, non-precious metals can be utilised. However, it suffers drawbacks due to problems with liquid electrolyte management and electrolyte degradation. In addition, this approach cannot be used for hydrogen peroxide reduction as the process requires an acidic medium.

Perhaps the most significant drive to overcome the use of non-platinum catalysts has been in the (bio)Fuel Cell, where enzymes or micro-organisms are used to drive the electrochemical reaction. However, currently, the power generated is low, and a clear disadvantage is the use of biological components which are sensitive to environmental conditions, and hence do not possess the robustness of other chemical systems.

Russell Mainstreams market a potentiometric hydrogen peroxide probe sensor (WP7 Hydrogen Peroxide Probe) suitable for water disinfection applications. Due to a special membrane system protecting the sensor, it is resistant to chemicals and surface agents. It has a sensitivity range of 0 to 2000 ppm hydrogen peroxide. However, its response Time is slow, with of T90 (time required to come to 90 % of final value) of approximately 4 minutes.

Another market that demands H_20_2 analysis is the clinical field, where exhaled breath is often monitored for H_20_2. Hydrogen peroxide in the breath is indicative of lung diseases such as asthma and chronic obstructive pulmonary diseases. Up to now, a common method to collect the exhaled breath condensate is to use a special cooling collector including a freezing cooling tube (usually cooled using ice or liquid nitrogen) and cooling machine, which has a refrigerator's circuit. Once collected, the condensate is analyzed off-line by techniques, such as spectroscopy, with assistance of peroxidase. H_20_2 is also the most valuable marker for oxidative stress, recognized as one of the major risk factors in progression of disease-related pathophysiological complications in diabetes, atherosclerosis, renal disease, cancer, aging and other condition. Hydrogen peroxide sensors are also needed for the development of biosensors based on enzyme oxidases. Universal Sensors market an amperometric peroxide electrode based on a platinum electrode for these types of applications.

Statements of Invention

According to the invention there is provided a catalyst comprising a silver electrode wherein the electrode has been modified with surfactant-salt solution.

In one embodiment the electrode comprises silver colloids, silver particles, or silver nanoparticles.

In one case the electrode is a silver paste electrode.

The electrode may be a screen printed electrode.

In one embodiment the surfactant is present at a concentration of from 0.01 to 0.1M.

In one embodiment the salt is present at a concentration of at least 0.001M.

The surfactant may, for example, be selected from:

dodecyl benzene sulphonic acid (DBSA)
sodium dodecyl sulphate (SDS)
cetyl trimethylammonium bromide (CTAB)
polyethylene glycol p-(l,l,3,3-tetramethylbutyl)-phenyl ether (Triton X-100)

Preferably the catalyst is selected from DBSA and SDS.

The salt solution may, for example be a solution selected from:

Potassium Chloride (KC1)
Sodium Chloride (NaCl)
Sodium Bromide (NaBr)

The molar ratio of surfactant and salt to achieve maximum catalysis may be approximately 1:3. This concentration ratio may optimise the formation of complex structures which are particularly suitable for deposition onto the silver electrode substrate.

In one case the surfactant-salt solution contains approximately 0.033M DBSA and approximately 0.1M KCI.

In another case the surfactant-salt solution contains approximately 0.033M SDS and approximately 0.1M NaCl.

In a further case the surfactant-salt solution contains approximately 0.0033 M CTAB and approximately 0.1M NaBr.

In another case the surfactant-salt solution contains approximately 0.033M Triton X-100 and approximately 0.0001 M KCI.

The electrode may be modified with the surfactant-salt solution for about 3 hours.

In one embodiment of the catalyst is coated with a coating such as nafion and/or chitosan and/or cellulose acetate.

The catalyst may be a non-enzymatic catalyst.

The catalyst may be a peroxide catalyst such as a hydrogen peroxide catalyst.

As well as hydrogen peroxide, many other inorganic (metal peroxides) such as lithium peroxide, sodium peroxide and potassium peroxide, as well as organic peroxides which have organic functional groups have a range of known and potential applications which relate to their catalytic reduction and/or decomposition. Such materials may also be amenable to similar catalytic processes exhibited by the invention.

In general terms, catalysts operate by reducing the activation energy required for a chemical transformation, increasing its kinetics. This is typically achieved by the formation of an energetically favourable transition state structure between the catalyst and the species being transformed. This is true of either homogeneous catalysts or heterogeneous (surface) catalyst such as that proposed here. However, the nature of heterogeneous catalysts has, in the past, been limited to a number of materials which exhibit good catalytic properties such as metals (e.g., platinum, gold, silver) as well as metallic oxides. A key feature of these is that they form highly

geometrically defined crystal structures which undergo precise interactions with chemical species being catalysed. However, this is less so of non-crystalline materials and has rarely been seen to be the case for organic materials or organic/inorganic hybrid materials. Thus, it is surprising that the combination of materials set out in this invention results in the enhanced catalytic activity towards hydrogen peroxide reduction and decomposition. In this regard, it may form the basis of a catalyst for a range of species as yet uncharacterised. This opens up the potential to be a catalyst for a vast array of chemical species which can undergo reduction, oxidation, or decomposition. Important species in this regard would include, but not be limited to a range of gasses such as hydrogen, oxygen, carbon dioxide, carbon monoxide, nitrogenous gasses, hydrogen sulphide, chlorine and other halogens, ammonia, phosgene, methane and other higher alkanes. It would also include, but not be limited to low molecular weight species including hydrocarbons, carbohydrates, organic and inorganic salts, transition metal complexes, fluorocarbons and related halogenated carbons, organophosphorous compounds and nitrogenous chemicals. It could also include catalytic reactions involving macromolecules including, but not limited to proteins, complex carbohydrates, lipids, phospholipids and derivatives thereof, supramolecular assemblies including, but not limited to species such as carbon nanotubes, fullerenes, graphenes and derivatives thereof.

The invention also provides a sensor system comprising a catalyst of the invention.

The sensor may be a biosensor, or a chemical sensor.

The invention further provides a cholesterol sensor comprising a catalyst of the invention.

The invention also provides a glucose sensor comprising a catalyst of the invention.

The invention also provides a fuel cell comprising a catalyst of the invention.

The invention further provides a cathode (such as a fuel cell cathode) comprising a catalyst of the invention.

In one embodiment the catalyst is provided in a gas diffusion layer. The silver may be provided in the gas diffusion layer which is then modified with a surfactant - salt solution.

The invention also provides a method for manufacturing a fuel cell cathode comprising providing silver in a gas diffusion layer, and subsequently modifying the silver with a surfactant - salt solution.

In one case a porous substrate (such as a carbon cloth material) is provided and the silver is applied to the porous substrate, for example by printing. The silver may be in the form of an ink for application to the substrate.

In a further aspect the invention provides the use of a catalyst of the invention in

- fuel cells;
- batteries;
- chemical synthesis; and/or
- decomposition processes.

In another aspect the invention provides a method of detecting hydrogen peroxide comprising the steps of:

- providing a silver electrode;
- modifying the electrode with a surfactant-salt solution; and
- rinsing the electrode with distilled water.

The method may comprise rinsing the electrode with water before exposing the electrode to the sample.

In the invention the rate at which the hydrogen peroxide molecule can be catalytically cleaved to hydroxy! radicals and hydroxide ions which can then be reduced electrochemically at an electrode at low applied reduction potentials is increased. Although the exact mechanism is not yet fully elucidated and we do not wish to be bound by theory, it is believed that catalytic structures composed of dodecyl benzene sulphonic acid (or other appropriate amphiphilic molecules) and metal halides (potassium bromide, sodium chloride or others) form at the surface of a silver electrode surface. It is believed that these structures catalyse the initial decomposition of the hydrogen peroxide which in turn oxidises the surface of the silver electrode. The oxidised

silver electrode surface is then returned to its neutral state via electrochemical reduction resulting from an applied cathodic potential to the electrode.

One application of the invention is demonstrated as a suitable platform for cholesterol detection. For this work, a modified screen printed electrode (SPE) is used (termed HyPer) to detect hydrogen peroxide that evolved from a cholesterol-cholesterol oxidase interaction in bulk solution. The HyPer electrode has been used to quantitatively detect 1- 5 mM cholesterol, which is the relevant clinical range for this analyte.

Another application of the invention is demonstrated as a suitable platform for glucose sensing.

Brief Description of the Drawings

The invention will be more clearly understood from the following description of some embodiments thereof, given by way of example only, with reference to the accompanying drawings, in which:-

Fig. 1 are cyclic voltammograms of Ag SPEs measured in PBS pH 6.g solution: (a) unmodified, in the absence of H_2O_2; (b) unmodified, $[H_2O_2]$ = 5-10^{-3} M; (c) 3.3-10^{-2} M DBSA/ 0.1 M KC1 modified, in the absence of H_2O_2; (d) 3.3-10^{-2} M DBSA/ 0.1 M KC1 modified, $[H_2O_2]$ = 5-10^{-3} M. Inset: magnified diagram of voltammograms (a) and (b);

Fig. 2 are amperometric i-t curves of Ag SPEs measured at - 0.1 V (vs Ag/AgCI) in PBS pH 6.8: (a) unmodified and (b) modified with 3.3$\cdot 10^{-2}$ M DBSA/ 0.1 M KC1 at H_2O_2 concentration from 1 to 5-10^{-3} M;

Fig. 3 are amperometric i-t curves of Ag SPEs measured at - 0.1 V (vs Ag/AgCI) in PBS pH 6.8: (a) unmodified; (b) 3.3$\cdot 10^{-2}$ M DBSA (c) 0.1 M KC1 and (d) 3.3$\cdot 10^{-2}$ M DBSA/ 0.1 M KCl modified electrodes, at H_2O_2 concentration ranges from 1 to 5-10^{-3} M;

Fig. 4 are plots of current vs log [DBSA] obtained during amperometric measurements of Ag SPEs at - 0.1 V (vs Ag/AgCI) at 5$\cdot 10^{-3}$ M H_2O_2. The electrodes were modified only with DBSA (a) or 0.1 M KC1 and DBSA (b);

Fig. 5 are plots of current vs log [KCl] obtained during amperometric measurements of Ag SPEs at - 0.1 V (vs Ag/AgCl) at 5-10^{-3} M H_20_2. The electrodes were modified only with KCl (a), 10^{-2} M DBSA/ KCl (b), 3.3·10^{-2} M DBSA/ KCl (c) and 0.1 M DBSA/ KCl (d). Value at log [salt] = - 10 corresponds to unmodified Ag SPEs;

Fig. 6 is a plot of current vs modification time obtained during amperometric measurements of Ag SPEs at - 0.1 V (vs Ag/AgCl) at 5-10^{-3} M H_20_2. Data at 0 s corresponds to unmodified electrode;

Fig. 7 are plots of i_{cat} vs electrolyte pH for Ag SPEs (a) with and (b) without DBSA/KC1 modification in 5-1 0^{-3} M H_20_2 at - 0.1 V vs Ag/AgCl.;

Fig. 8 are amperometric responses of the DBSA/KC1 modified electrodes in 20·10^{-6} M aliquots of H_20_2 (20 - 160 · 10^{-6} M) at -0.1 V (vs Ag/AgCl) in PBS pH 6.8. Input: Plot of cathodic current vs H_20_2 concentration at -0. 1 V (vs Ag/AgCl) in PBS pH 6.8;

Fig. 9 are illustration of reproducibility study using three different electrodes: (a) electrode 1; (b) electrode 2; (c) electrode 3. Amperometric responses of the DBSA/KCI modified electrodes in 20- 10^{-6} M aliquots of H_20_2 (20 - 160 -10^{-6} M) at - 0.1 V (vs Ag/AgCl) in PBS pH 6.8. Each electrode was measured three times: (·) repeat 1; **(A)** repeat 2; (■) repeat 3;

Fig. 10 are SEM images using secondary electron (SE) detection of Ag SPEs (a) unmodified; (b) DBSA/KCl-modified; (c) DBSA/KCI-modified after electrochemical reduction of 5-10^{-3} M H_20_2; (d) AgCl electrochemical ly deposited; (e) KCl modified. Accelerating voltage of 20 kV. (5.0k x magnification). Below, the respective EDX spectrum for each sample. Binding energies in keV;

Fig. 11 are XPS images of Ag SPEs (a) unmodified and (b) DBSA/KCI modified;

Fig. 12 are amperometric i-t curves of Ag SPEs measured at - 0.1 V (vs Ag/AgCl) in PBS pH 6.8: (a) unmodified; (b) AgCl electrodeposited and (c) DBSA/KCI modified electrodes, at H_20_2 concentrations from 1 to 5-10^{-3} M;

Fig. 13 is an illustration of the comparison of the surface hydrophilicity of an unmodified (on the right) and a DBSA/KC1 modified Ag SPE when $2 \cdot 10^{-6}$ $1H_20$ was deposited onto the surface (surface area = 0.126 cm^2);

Fig. 14 are plots of change in mass per unit area versus time of (a) unmodified and (b) modified Ag SPE in 2 ml 1M H_20_2;

Fig. 15 are plots of the change in mass per unit area versus time of (a) unmodified and (b) modified Ag SPE in 2ml 1M H_20_2 solution for 1 hour. Each electrode was measured three times and the number of the repetition is indicated besides each graph;

Fig. 16 are SEM images of unmodified Ag SPEs (A) before and (B) after the measurements in 1 M H_20_2 solution. SEM images of Ag SPEs modified with DBSA/KC1 (C) before and (D) after exposure to 1 M H_20_2 solution. Accelerating voltage of 20 kV. (5.0 k x magnification);

Fig. 17 are SEM images of Ag SPEs modified with DBSA/KC1 (A) before exposure to 1 M H_20_2; and after (B) 1 h, (C) 2 h and (D) 3 h exposure to 1 M H_20_2 solution. Accelerating voltage of 20 kV. (5.0 k x magnification);

Fig. 18 are plots of current vs log [SDS] obtained during amperometric measurements of Ag SPEs at - 0.1 V (vs Ag/AgCl) at $5\text{-}10^{-3}$ M H_20_2. The electrodes were modified (a) only with SDS or (b) SDS and 0.1 M NaCl;

Fig. 19 are plots of current vs log [salt] obtained during amperometric measurements of Ag SPEs at - 0.1 V (vs Ag/AgCl) at $5\text{-}10^{-3}$ M H_20_2. Electrodes were modified with (·) $3.3\text{-}10^{-2}$ M DBSA/KC1; (★) $3.3\text{-}10^{-2}$ M Triton X-100/ KC 1; (■) $3.3 \cdot 10^{-3}$ M CTAB/NaBr or **(A)** $3.3\text{-}10^{-2}$ M SDS/NaCl. Salt concentration ranged from 1.5 to 10^{-7} M. Value at log [salt] = - 10 corresponds to the unmodified Ag SPEs;

Fig. 20 are illustrations of (i). Simplified surfactant structure, (ii). Typical surfactant aggregates: (a) cylindrical structures, (b) lamellar structures and (c) spherical micelles;

Fig. 2 1 are plots of current vs log [XCl] obtained during amperometric measurements of Ag SPEs at - 0.1 V (vs Ag/AgCl) at $5 \cdot 10^{-3}$ M H_20_2. The electrodes were modified with mixtures of $3.3\text{-}10^{-2}$ M DBSA and different concentrations of: (·) LiCl ; (■) NaCI ; **(A)** KC1 or (*) CsCl. Salt concentration ranged from 1.5 to 10^{-7} M. Value at log [salt] = - 10 corresponds to the unmodified Ag SPEs;

Fig. 22 are amperometric i-t curves of metallic silver electrodes measured at - 0.1 V (vs Ag/AgCl) in PBS pH 6.8: (a) unmodified; (b) 3h; (c) 1 day DBSA/KCI modified, at H_20_2 concentrations from 1 to $5\text{-}10^{-3}$ M;

Fig. 23 are SEM images using SE detection of metallic Ag (99.9 %) electrodes (a) unmodified and (b) DBSA/KCI modified. Accelerating voltage of 20 kV. (5.0k x magnification);

Fig. 24 are amperometric i-t curves of Ag wire electrodes measured at - 0.1 V (vs Ag/AgCl) in PBS pH 6.8: (a) unmodified; (b) DBSA/KCI modified; (c) AgCI electrochemical formation after 2 s at + 1 V (vs Ag/AgCl) in 0.1 M HCl (d) AgCI electrochemical formation after 5 s at + 1 V (vs Ag/AgCl) in 0.1 M HCl three times, at H_20_2 concentrations from 1 to $5 \cdot 10^{-3}$ M.

Fig. 25 are plots of the change of mass per unit area versus time for (a) unmodified and (b) modified 92.5 % Ag electrodes upon repeated exposure to 1 M H_20_2 solution for 1 hour. The number of exposures is indicated besides each graph;

Fig. 26 are plots of the change of mass per unit area versus time for (a) unmodified and (b) modified 99.9 % metallic Ag electrodes upon exposure to 1 M H_20_2 solution for 1 hour;

Fig. 27 are plots of the change in mass per unit area versus time for (a) unmodified and (b) modified (circle) 92.5 %, (triangle) SPE and (square) 99.9 % Ag electrodes when exposed to 1 M H_20_2 solution for 1 hour. These data correspond to the first repetition of each electrode;

Fig. 28 are SEM images of unmodified sterling 92.5 % Ag electrodes (A) before and (B) after being exposed to 1 M H_2O_2 solution and 99.9 % Ag metallic electrodes (C) before and (D) after H_2O_2 decomposition measurements. Accelerating voltage of 20 kV. (5.0 k x magnification);

Fig. 29 are SEM images of modified sterling 92.5 % Ag electrodes (A) before and (B) after exposure to 1 M H_2O_2 solution and 99.9 % Ag (C) before and (D) after H_2O_2 decomposition measurements. Accelerating voltage of 20 kV. (5.0 k x magnification);

Fig. 30 are amperometric i-t curves of metallic Au (99.9 %) electrodes measured at - 0.1 V (vs Ag/AgCI) in PBS pH 6.8: (a) unmodified and (b) DBSA/KCI modified, at H_2O_2 concentrations from 1 to $5 \cdot 10^{-3}$ M;

Fig. 31 are plots of change in mass per unit area versus time for (a) unmodified and (b) modified metallic Au (99.9 %) electrodes upon repeated exposure to 1 M H_2O_2 solution for 1 hour. The number of exposures is indicated besides each graph;

Fig. 32 are plots of change in mass per unit area versus time for (a) unmodified and (b) modified Au SPEs after exposure to 1 M H_2O_2 solution for 1 hour. The number of exposure is indicated besides each graph;

Fig. 33 are plots of change in mass per unit area versus time for (a) unmodified and (b) modified (square) Au (99.9 %) metallic electrodes and (circle) Au SPEs upon exposure to 1 M H_2O_2 solution for 1 hour. These data correspond to the first repetition of each electrode;

Fig. 34 are plots of change in mass per unit area versus time for (a) unmodified and (b) modified Pt SPEs upon repeated exposure to 1 M H_2O_2 solution for 1 hour. The number of exposures is indicated besides each graph;

Fig. 35 is a plot $-\ln [H_2O_2]/[H_2O_2]_0$ versus time for (a) unmodified and (b) modified Ag SPEs after exposure to 1 M H_2O_2 solution for 1 hour;

Fig. 36 is a plot of the kinetics of H_20_2 decomposition on (a) unmodified and (b) modified Ag SPEs;

Fig. 37 is a calibration curve of cathodic current increase against cholesterol concentration. Working Electrode: HyPer. Buffer solution: Made up according to Audit Diagnostics protocol with 200-fold increase in cholesterol oxidase concentration. Inset: Signal based on increase in amperometric current from trough to peak;

Fig. 38 is a plot of the effect of addition of various solutions to BSA to monitor the current drop Working Electrode: HyPer. (a) 3.2 mM Cholesterol in Deionised Water (500 µL); (b) Buffer, pH 7 (500 µL); (c) Deionised Water (500 µL). A current decrease is observed when cholesterol was added to the system. Negligible, if any oxidation current was observed for buffer or H_20 additions to the system;

Fig. 39 is a calibration graph of maximum amperometric cathodic response of HyPer electrode to additions of lyophilised cholesterol over the concentration range 0.5 - 3.2 mM;

Fig. 40 is a calibration graph of the slope of the amperometric cathodic response of HyPer electrode to additions of lyophilised cholesterol over the concentration range 0.5 - 3.2 mM. (Slopes measured by approximating response as straight line and by dividing net response from net time taken to reach that response);

Fig. 41 is a calibration graph of the time taken to reach the maximum amperometric cathodic response of HyPer electrode to additions of leophilised cholesterol over the concentration range 0.5 - 3.2 mM;

Fig. 42 is a graph of the response of HyPer electrode to 10 mL H_20_2 injections (each addition was equivalent to 0.5 mM H_20_2). Bulk solutions: (a) PBS with Choi Ox and Lipo-lipase, (b) Pipes/$MgCl_2$ with no enzyme, (c) PiPes/$MgCl_2$ with Choi Ox and Lipo-lipase;

Fig. 43 are amperometric responses of the Nafion-coated HyPer electrodes (A) and bare HyPer electrodes (B) to H_20_2 (0.5 mM) in the presence of varying amounts of BSA in

bulk solution: (a) 0.5% BSA, (b) 0.25% and (c) 0.125%. The effect of Nafion or of increasing the amount of BSA in the solution does not affect the sensor response to hydrogen peroxide;

Fig. 44 is a graph of the response of HyPer electrode to H_20_2 injections (each addition was equivalent to 0.5 mM H_20_2) in the presence of: (a) PBS (0.13813 g/10 ml), (b) $MgCl_2$ (0.005 g/10 ml), (c) PIPES (0.13813 g/10 ml) and (d) PIPES/$MgCl_2$ (as per AD Buffer);

Fig. 45 are amperometric responses to hydrogen peroxide (0.5 mM additions) of: (a) Nafion-coated and (b) unmodified HyPer electrode in AD PIPES buffer. It can be observed that there is no significant effect on the initial response of the electrode to hydrogen peroxide when a Nafion membrane is employed;

Fig. 46 are amperograms showing electrode responses to injections of H_20_2 in buffers: (a) PBS (HyPer electrode) and Pipes/$MgCl_2$ (b) Chitosan-coated and (c) unmodified HyPer electrode. It can be seen that the HyPer electrodes response could be improved in Pipes buffer by employing the chitosan membrane;

Fig. 47 is a graph of the effect of the amount of chitosan (1%) used to modify the electrode: (a) 3 μï, (b) 5 μï and (c) 7 μl. 3 μï chitosan dropped onto the surface of the electrode results in the highest response and fastest response time (750 s approx. from initial addition of cholesterol at t = 500 s. (1.6 mM concentration);

Fig. 48 is a graph of the addition of cholesterol (1.6 mM) at time = 500 s. (a) Amperometric response from a chitosan-coated HyPer electrode. (b) Amperometric response from a bare HyPer electrode. Response time from the chitosan- HyPer is 700 s, while the response time of the bare HyPer electrode was approx. 1500s;

Fig. 49 is a graph of the addition of cholesterol (1.6 mM)) at time = 400 - 500 s. Pipes $MgCl_2$/ Cholesterol Oxidase AD Buffer with various electrode barriers. (a) Amperometric response from a chitosan HyPer electrode. (b) Amperometric response from a HyPer electrode. (c) Amperometric response from a cellulose acetate—coated HyPer electrode

Response time from the chitosan-modified electrode is 750 s, while the response time of the bare electrode was approx. 1500s;

Fig. 50 is a graph of the addition of cholesterol (1.6 mM) at time = 500 s using Bis-Tris $MgCl_2$/ cholesterol oxidase buffer with various electrode membranes. (a) Amperometric response from a HyPer electrode. (b) Amperometric response from a chitosan-coated HyPer electrode. (c) Amperometric response from a cellulose acetate—coated HyPer electrode Response time from the chitosan-modified electrode is 700 s, while the response time of the bare electrode was approx. 1500s;

Fig. 51 are amperometric i-t curves of Ag_DBSA/KCl SPEs measured at - 0.1 V (vs Ag/AgCl) in PBS pH 6.8: (a) H_20_2 sensing (b) glucose sensing, with lmg/ml GOx in solution and (c) H_20_2 sensing after glucose sensing, at H_20_2 and glucose concentration from 1 to $5 \cdot 10^{-3}$ M;

Fig. 52 are amperometric i-t curves of Ag_DBSA/KCI SPEs measured at - 0.1 V (vs Ag/AgCl) in PBS pH 6.8: (a) without and (b) with a cellulose acetate film, at H_20_2 concentration from 1 to $5\text{-}10^{-3}$ M;

Fig. 53 are amperometric responses of the DBSA/KCl_CA_GOx modified Ag SPEs in $1 \cdot 10^{-3}$ M aliquots of glucose ($1\text{-}5 \cdot 10^{-3}$ M) at - 0.1 V (vs Ag/AgCI) in PBS pH 6.8. Input: Plot of the cathodic current vs glucose concentration at - 0.1 V (vs Ag/AgCl) in PBS pH 6.8;

Fig. 54 is an illustration of a hydrogen peroxide fuel cell;

Fig. 55 is an illustration of the gas diffusion layer and its modification with the catalyst;

Fig. 56 is a typical current voltage diagram for a fuel cell indicating the points on the I-V curves that correspond to different losses;

Fig. 57 is a graph of test results of fuel cells;

Fig. 58 is a photomicrograph of a gas diffusion layer material before modification;

Fig. 69 are photomicrographs of gas diffusion layer material after modification with the hydrogen peroxide catalyst; and

Fig. 60 are profilometry images after modification with the hydrogen peroxide catalyst.

Detailed Description

Materials

Dodecylbenzenesulfonic acid (DBSA-D0989) was purchased from TCI Europe. Poly(vinylsulfonic acid) (PVS), sodium dodecyl sulphate (SDS), cetyl trimethylammonium bromide (CTAB), Triton X-100, lithium, sodium, potassium and caesium chloride (LiCI, NaCI, KCI, CsCl), sodium bromide (NaBr) and potassium dihydrogen phosphate (KH_2PO_4) were purchased from Sigma-Aldrich. Di-sodium hydrogen phosphate (Na_2HPO_4) was purchased from Riedel-de Haen. 30% (v/v) hydrogen peroxide solution was purchased from Merck. Sterling silver (92.5%, 300 μηι-thick) was purchased from NN Enterprises (Dublin, Ireland) and it was cut into 0.6 cm^2 substrates (unless otherwise is stated). 0.5 mm diameter silver wire (99.9 %) was purchased from Sigma-Aldrich and 1.1 cm long electrode were prepared as working electrodes using isolating tape. Silver (CHI 103, 99.9 %, A =0.031 cm^2) and gold (CHI 101, 99.9 %, A = 0.031 cm^2) metallic electrodes were purchased from IJ Cambria Scientific Ltd. (Carms, UK). Gold and platinum screen-printed electrodes (A = 0.1 cm^2) were purchased from DuPont (Delaware, US). Gold and platinum screen-printed electrodes (4 mm diameter) were purchased from Dropsens (Asturias, Spain). Silver conductive ink (Electrodag ® PF-410) was purchased from Henkel (Scheemda, The Netherlands). Poly(ethylene) terephthalate substrates were Melinex ® (pre-shrunk) films obtained from HiFi Industrial Film Ltd. (Dublin, Ireland). All the solutions were prepared using 18 MΩ Milli-Q water.

Buffers and solutions

Unless otherwise stated, all electrochemical measurements were carried out in phosphate buffered saline solution (PBS). The buffer solution is 0.1 M phosphate, 0.137 M NaCI and 0.0027 M KCI. This was prepared by mixing solution 1 (0.1 M Na_2HPO_4, 0.137 M NaCI and 0.0027 M KCI) and solution 2 (0.1 M KH_2PO_4, 0.137 M NaCI and 0.0027 M KCI) to a pH of 6.8.

Cholesterol oxidase/Pipes buffer was prepared as follows, according to an AD protocol unless otherwise stated: 0.13813g Pipes Di-sodium Salt and 0.00526 g of magnesium chloride 6-hydrate were diluted with water and the pH adjusted to between 6.9 - 7.0, the enzymes cholesterol oxidase (-20 mg) and lipoprotein lipase (~1 1 mg) and the entire solution total volume was 10 ml, unless otherwise stated.

Phosphate buffered saline (PBS), was prepared to pH 6.8 and used to the same concentration as the Pipes. (-0.13813 g/10 ml). Bis-Tris was also investigated at the same concentration (-0.13813 g/10 ml).

Hydrogen peroxide was prepared to a concentration of 50 mM by diluting 0.5 ml to 5 ml with deionised water. 10 µl was added to 1 ml of the appropriate enzyme/buffer or buffer solution to give an overall concentration of 0.5 mM in order to examine the electrode response.

Lyophilised cholesterol samples were diluted with 2.5 ml deionised water and added to the buffer to a final concentration of 1.6 mM, unless otherwise stated.

1% (w/v) Nafion solution was prepared by diluting 100 µl into 10 ml deionised water. 1% (w/v) Chitosan solution was prepared by dissolving of 0.1 mg into 10 ml of 10% Acetic Acid. Cellulose Acetate 1% (w/v) suspension was prepared by diluting 0.1 mg into 10 ml deionised water.

Instrumentation

Silver screen-printed electrodes (Ag SPE) were fabricated using an automated DEK 248 machine (Weymouth, UK). Briefly, a layer of silver paste was deposited onto PET substrate and cured in a convectional oven at 120°C for 5 minutes. Then, an isolating tape layer was deposited to define the working electrode area (0.126 cm^2).

All electrochemical measurements were performed in a three-electrode electrochemical batch cell, using a Ag/AgCl/NaCl (saturated) electrode and a platinum mesh electrode as reference and auxiliary electrodes, respectively. Cyclic voltammetry and time-based amperometric measurements were carried out with a CHI601C electrochemical analyzer with CHI60IC software (IJ Cambria Scientific Ltd., UK). Measurements were performed at room temperature,

18 ± 2 °C. Unless otherwise stated, all potential values are referred to the Ag/AgCl/NaCl (saturated) electrode.

Scanning Electron Microscopy (SEM) using Secondary Electron (SE) and Energy Dispersive X-ray (EDX) detection was carried out with a Hitachi S-3400N. An acceleration voltage of 20 kV was used to obtain the surface images.

A Sartorius CP225D analytical balance was employed to register the mass differences during H_2O_2 decomposition.

Electrode modification with surfactant-based solutions

Screen-printed (Au, Pt, Ag) and sterling 92.5 % Ag electrodes were dipped into a freshly-prepared solution of a surfactant (DBSA, CTAB, Triton X-100, SDS) and a salt (LiCI, NaCl, KCl, CsCl) at a range of concentrations (modification solution) for 3 hours. The electrodes were then rinsed with water to remove the excess of modification solution on it and measured directly. Au and Ag metallic (99.9 %) electrodes were initially polished using 0.3 and 0.05 μm alumina. They were then sonicated for 5 min in distilled water and subsequently dipped into the modification solution for 3 hours, following the same procedure used for SPEs.

Electrochemical characterisation

All the electrochemical measurements were carried out in a stirred batch system with a three-electrode configuration. Unless otherwise stated, the electrodes were measured in 10 ml PBS pH 6.8. Cyclic voltammograms were obtained in the potential range from -0.200 to 0.025 V (vs Ag/AgCI) at a scan rate of 0.1 V/s whereas the amperometric i-t curves were performed at -0.1 V (vs Ag/AgCI). 1 M stock solution of hydrogen peroxide was prepared daily and then aliquots from this solution were added to the working cell during both cyclic voltammetry and amperometric measurements in order to characterize the sensor parameters.

Measurement of H_2O_2 decomposition

H_2O_2 decomposition was assessed by the decrease in mass registered when the electrodes were placed in 2 ml of 1 M H_2O_2. The electrodes were dipped into the H_2O_2 solution and the vials were covered with parafilm to avoid losses due to water evaporation. In order to allow the O_2 formed during the decomposition to release from the devices, a small hole was made in the

parafilm. The mass data were registered every minute for 1 hour and each electrode was measured three times, with a resting time of 10-15 minutes between measurements.

HyPer Electrode Preparation for cholesterol biosensing

Silver electrodes were prepared by a screen printing method using the DEK 248 printing system. The electrodes were conditioned by placing them in a solution of 0.1 M KG and 0.033 M DBSA for at least 2 hours followed by a washing step with deionised water before using them as sensors. These electrodes are referred to throughout the text as HyPer electrodes.

RESULTS AND DISCUSSION

A catalytic effect on **H2O2** decomposition and electrochemical reduction was observed when Ag SPEs were modified with a surfactant/salt combination solution. This finding led to the assessment of the catalysis by varying different modification parameters such as surfactant and salt concentrations, modification times as well as the type of surfactant and salt. The motivations of using these modified SPEs are their low cost, rapid fabrication and ease of use, which would allow the rapid manufacture of H_20_2 sensor devices. These data were also compared to those obtained by using other silver-based and noble material electrodes such as Au and Pt.

Optimisation and characterisation of the catalytic and electrocatalvtic enhancement to H_2O_2 at silver screen-printed electrodes (Ag SPEs)

Electrochemical characterization

Cyclic voltammetry and time-based amperometry were carried out in order to assess the catalytic effect observed when Ag SPEs had been modified with surfactant-based solutions. Cyclic voltammetry and amperometry were performed on the unmodified home-made electrodes in PBS pH 6.8 as controls. Subsequently, Ag SPEs were dipped into a solution of $3.3\cdot 10^{-2}$ M DBSA/ 0.1 M KC1 for 3 h and rinsed with distilled water to remove any excess of modifying solution on the surface and they were also subjected to cyclic voltammetry and amperometry in PBS pH 6.8. For the latter, volume (μï) aliquots of 1 M **H2O2** were sequentially added to the bulk so H_20_2 concentration in the solution increased from H O^3 to $5\cdot 10^{-3}$ M. One of the main requirements of a substrate to be used as a platform in an electrochemical sensing process is that it be electrochemical ly inert in the selected range of potential. Here, a narrow window of potential was chosen for the voltammetric measurements (-0.2 to + 0.025 V vs. Ag/AgCl), as a wider potential range would lead to the oxidation of Ag (at more positive potentials) or 0_2

interferences (at more negative potentials), distorting H_20_2 responses. Fig. 1 shows the cyclic voltammograms for unmodified and DBSA/KCI modified Ag SPEs in the presence and absence of $5\text{-}10^{-3}$ M H_20_2. As can be seen, the non-faradaic or charging current from the cyclic voltammograms in the absence of H_20_2, is up to ten times higher for the modified electrodes than that for the unmodified ones. This indicates that Ag SPE surface has undergone a modification after being dipped into surfactant-based solutions. Moreover, the cathodic current in the presence of $5\text{-}10^{-3}$ M H_20_2 was more than 100 times higher for electrodes after being modified with $3.3\text{-}10^{-2}$ M DBSA/ 0.1 M KC1 when compared to unmodified electrodes. Thus, the cathodic current at -0.1 V from the cyclic voltammograms in the presence of $5\text{-}10^{-3}$ M H_20_2 was approx. $4.4\cdot 10^{-5}$ A for the modified electrode, after subtracting the background current, whereas the modified one exhibited only a $3.8\cdot 10^{-7}$ A current at the same potential.

Fig. 1 are cyclic voltammograms of Ag SPEs measured in PBS pH 6.8 solution: (a) unmodified, in the absence of H_20_2; (b) unmodified, $[H_20_2] = 5\text{-}10^{-3}$ M; (c) $3.3\cdot 10^{-2}$ M DBSA/ 0.1 M KCI modified, in the absence of H_20_2; (d) $3.3\text{-}10^{-2}$ M DBSA/ 0.1 M KCI modified, $[H_20_2] = 5\cdot 10^{-3}$ M. Inset: magnified diagram of voltammograms (a) and (b).

This catalytic effect for the surfactant-based pre-treated electrodes is also presented in Fig. 2, where the amperometric i-t curves for the unmodified and DBSA/KCI modified electrodes when H_20_2 ($0\text{-}5\cdot 10^{-3}$ M) is added to the solution are shown. These were performed at - 0.1 V (vs Ag/AgCl). Although a catalytic effect is seen by the modified electrodes from + 0.025 V in Fig. 1, the current increased quite linearly within the cathodic potential window with a discernible peak between - 0.1 and - 0.15 V. Given the significant current increases at these potentials, the narrow potential window of the Ag paste electrodes and the desire to avoid interferences at lower potentials, -0.1 V seemed to be a suitable potential to study the catalytic effect of the surfactant-based modification on Ag SPEs towards H_20_2 reduction. Typical applied potentials used for the amperometric determination of H_20_2 reduction in the literature range from - 0.7 V (GC/PABS-modified electrodes),[1, 2] - 0.5 V (Ag nanoparticles in a polyvinyl alcohol film on a Pt electrode)[3], - 0.1 V commonly applied in enzymatic biosensors (such as a HRP-modified electrodes)[4, 5] and up to 0 V with Prussian Blue.[6] The fact that H_20_2 reduction can be detected at this potential in the absence of enzymes represents a unique advantage because it avoids the tiresome experimental conditions of temperature, concentration and pH required by the enzymatic compounds and broadens its application field.

Figure 2. Amperometric i-t curves of Ag SPEs measured at - 0.1 V (vs Ag/AgCI) in PBS pH 6.8: (a) unmodified and (b) modified with 3.3-10^{-2} M DBSA/ 0.1 M KC1 at H_20_2 concentration from 1 to 5· 10^{-3} M

The current decays observed in some of the steps of the amperometric response shown in Fig. 2 e.g. at 210 s, might be the result of a mixing problem when analyte is added to the solution. Although amperometric measurements were performed under stirring conditions, a human error might be possible during the addition of the H_20_2 aliquots to the solution. It would lead to a temporary false reading of the cathodic current, which would reach the steady state response after some seconds of homogenization of the bulk solution.

Modified Ag SPEs showed cathodic currents of approx. 3.60-10^{-5} A at - 0.1 V in the presence of 5-1 0^{-3} M H_20_2 whereas the current obtained with the unmodified ones reached approx. 4.2- 10^{-7} A. This difference of almost two orders of magnitude was previously observed in the cyclic voltammograms in Fig. 1. Moreover, the greater steady state background current exhibited by the modified amperometric curve (approx. 1.6-1 0^{-6} A) compared to the unmodified one (approx. 9.0-10^{-8} A) makes it evident that the Ag SPE surface undergoes a modification following the exposure to DBSA/KCI solution.

Further controls employing DBSA or KCI alone were performed. Figure 3 shows the amperometric curves of an unmodified Ag SPE and with DBSA (0.033 M) and KCI (0.1 M) together and separately. As can be seen, there was no a notable enhancement in the cathodic current corresponding to the DBSA modified electrode compared to the unmodified one. Thus, the latter showed a cathodic current in the presence of 5·10^{-3} M H_20_2 of 4.2- 10^{-7} A, which was only five-fold lower than that exhibited by the DBSA modified electrode, 2.4- 10^{-6} A. However, enhanced responses were obtained when the Ag SPE electrode had been exposed to KCI, showing 9.4· 10^{-6} A as cathodic current at 5-10^{-3} M H_20_2. However, the highest cathodic current was obtained when the Ag SPE was modified with a mixture of both DBSA and KCI. Such pre-treated electrodes provided cathodic responses of 3.6-10^{-5} A, which represented a more than eighty-fold greater response to H_20_2 than those without any modification. Therefore, the relative order of the modified Ag SPEs regarding the catalytic response to 5· 10^{-3} M H_20_2 is the following:

Unmodified < 3.3-10^{-2} M DBSA modified < 0.1 M KCI modified < 3.3-10^{-2} M DBSA/ 0.1 M KCI modified

The same relative order was observed with respect to the steady state background current of the amperometric responses, where unmodified electrodes showed the lowest value (4.8-10^{-8} A) whereas the DBSA/KC1 modified showed the greatest (approx. $1.6 \cdot 10^{-6}$ A). Once again, the background or charging current was proportional to the catalytic effect shown by the electrodes and, therefore, the modification rate of the electrode surfaces.

Figure 3. Amperometric i-t curves of Ag SPEs measured at - 0.1 V (vs Ag/AgCl) in PBS pH 6.8: (a) unmodified; (b) $3.3 \cdot 10^{-2}$ M DBSA (c) 0.1 M KCI and (d) $3.3 \cdot 10^{-2}$ M DBSA/ 0.1 M KCI modified electrodes, at H_2O_2 concentration ranges from 1 to 5-10^{-3} M.

Having established that both DBSA and KCI were necessary for full catalytic effect, the concentrations of DBSA and KCI were optimised. Cyclic voltammetry and amperometry were performed using first 0.1 M KCI over a range of DBSA concentrations followed by $3.3 \cdot 10^{-2}$ M DBSA over a range of KCI concentrations. The cathodic responses to 5-10^{-3} M H_2O_2 were correlated with DBSA or KCI concentrations. Fig. 4 shows the responses of Ag SPEs after dipping into several DBSA concentration solutions for 3h, in the absence and the presence of 0.1 M KCI in the modifying solutions. At low DBSA concentrations, the presence of KCI provided approx. six-fold higher responses, being $5.5 \cdot 10^{-6}$ A the cathodic current at 5-10^{-3} M H_2O_2 whereas the electrode modified in the absence of KCI showed only 9-10^{-7} A. However, from 10^{-4} M DBSA and above, the difference between the reduction currents obtained from the electrodes without and with KCI in their modification solution increased to more than 20 fold. Thus, at 10^{-3} M DBSA the cathodic current exhibited by the electrode modified in the absence of KCI was approx. 1.4-10^{-6} A whereas the current from the electrode modified with DBSA/KC1 rose to 3.1-10^{-5} A. Even at 10^{-2} M DBSA, where the electrode modified in the absence of KCI showed the highest response, the cathodic current of the electrode modified with the DBSA/KC1 mixture was still six-fold greater than the former. This confirmed that the presence of both DBSA and KCI reagents in the pre-treatment solution was essential for the full catalytic reduction effect of H_2O_2 observed on the Ag SPEs.

Figure 4. Plot of current vs log [DBSA] obtained during amperometric measurements of Ag SPEs at - 0.1 V (vs Ag/AgCl) at 5-10^{-3} M H_2O_2. The electrodes were modified only with DBSA (a) or 0.1 M KCI and DBSA (b).

Fig. 5 shows the results of a similar study, using three DBSA concentrations and a range of KCI concentrations. Fig. 4 highlighted that the optimum DBSA concentration in the modification solution was between 0.1 and 0.01 M. Therefore, DBSA concentrations of 0.1, 3.3-10^{-2} and 10^{-2} M were studied. Fig. 5 presents the results for these experiments and compares them to those obtained using KCI alone. The catalytic effect on H_2O_2 reduction was again observed for those electrodes modified with both DBSA and KCI reagents whereas those electrodes pre-treated only with KCI displayed a small catalytic increase at 0.1 M, which was also seen with amperometry in Fig. 3. The enhancement of the H_2O_2 reduction current was shown to be dependent on KCI concentrations greater than 10^{-4} M. Thus, at 10^{-4} M KCI the cathodic currents observed for the unmodified, 10^{-2} M DBSA/KC1, $3.3 \cdot 10^{-2}$ M DBSA/KC1 and 0.1 M DBSA/KC1 modified electrodes were $1.4 \cdot 10^{-6}$ A, $2.1 \cdot 10^{-6}$ A, $5.0 \cdot 10^{-6}$ A and $2.2 \cdot 10^{-5}$ A, respectively, whereas at 10^{-3} M KCI the reduction currents were 1.3-10^{-6} A, 1.5-10^{-5} A, 2.8-10^{-5} A and 3.2-10^{-5} A, respectively. The optimum KCI concentration in the modification solution was found to be approx. 0.1 M, where the cathodic currents for the studied electrodes reached values of $8.7 \cdot 10^{-6}$ A, $3.1 \cdot 10^{-5}$ A, $3.5 \cdot 10^{-5}$ A and $3.5 \cdot 10^{-5}$ A, respectively. Further increases in KCI concentration in the modification solutions led to a decrease in the reduction current, as can be seen in Fig. 5 for 1 M KCI. The onset of the enhanced catalysis was also dependent on DBSA concentration, as is shown by the above-mentioned cathodic current data at 10^{-4} M KCI. At this value, the catalytic ratio shown by the modified electrodes went along the following relative order: unmodified < 10^{-2} M DBSA/KC1 < $3.3 \cdot 10^{-2}$ M DBSA/KC1 < 0.1 M DBSA/KC1. Electrodes exhibited enhanced catalysis at lower KCI concentrations when DBSA concentrations were increased. Electrodes modified with 0.1 M DBSA/KC1 solutions showed catalytic activity from approx. 10^{-4} M KCI concentrations whereas the onset of the catalysis occurred from 10^{-3} M KCI for the electrodes modified in 3.3-10^{-2} M DBSA/KC1 or 10^{-2} M DBSA/KCI solutions. As will be commented upon later in this section, surfactants are well-known to form organized structures when they are in aqueous solution.[7,8] At low concentrations but above the critical micelle concentration (CMC), typical surfactant aggregations are in the form of spheroidal micelles. As the concentration of surfactant in solution increases, greater aggregations such as hexagonal or lamellar structures are observed. The addition of a salt or cosurfactant to the solution allows the formation of these high-aggregation structures at lower surfactant concentrations. This was observed by Sein et al.[9]

with sodium dodecylbenzenesulfonate (NaDoBS) in the presence of several chloride salts. The CMC for DBSA is approx. 1.6-2-1 0^{-3} M,[9, 10] so at least a micellar level should be observed in all the modification solutions used. The fact that greater catalytic responses are obtained when both the surfactant and salt concentrations in the modification solution are increased might be directly related with the early formation of hexagonal or lamellar structures in the solution, which may bring about the modification of the Ag SPE surface in some way. Hence, a solution of 3.3- 10^{-2} M DBSA and 0.1 M KC1 was established as the optimum modification solution, which provided the highest electrocatalysis of H_20_2 reduction on Ag SPEs and this was used in subsequent experiments. Thus, the optimum molar concentration and ratio of surfactant and salt to achieve maximum catalysis was found to be approx. 3.3 x 10^{-2} M/0.1 M or 1:3. This concentration ratio may relate to the optimum molecular ratios to form complex micellar or lamellar structures and their subsequent ability to become deposited onto the silver electrode substrate.

Figure 5. Plot of current vs log [KCI] obtained during amperometric measurements of Ag SPEs at - 0.1 V (vs Ag/AgCl) at 5-10^{-3} M H_20_2. The electrodes were modified only with KCI (a), 10^{-2} M DBSA/ KCI (b), 3.3· 10^{-2} M DBSA/ KCI (c) and 0.1 M DBSA/ KCI (d). Value at log [salt] = -10 corresponds to unmodified Ag SPEs.

Another parameter of the deposition process which needed to be optimized and studied was the modification time, i.e. the time Ag SPEs were deposited in the DBSA/KCl solution before their application in H_20_2 detection. Several Ag SPEs were submerged into 3.3· 10^{-2} M DBSA/ 0.1 M KCI solutions for different periods of time, from a few seconds to one day. Then, the electrodes were rinsed thoroughly with distilled water to remove any non-adherent species which might remain on the surface and these were measured amperometrically in 5-10^{-3} M H_20_2 in PBS pH 6.8. Fig. 6 shows the plot of these data vs modification time. As can be seen, the catalytic effect on H_20_2 reduction was noticeable even when the electrodes had been immersed for a very short period of time (2-10 s) into the DBSA/KCl solution. These electrodes exhibited approx. 2.2-10^{-5} A response, more than twenty times higher reduction currents when they were measured in the presence of 5-10^{-3} M H_20_2 compared to unmodified electrodes, which only exhibited 7.5T0 $^{-7}$ A. This suggested that whatever process was taking place between the electrodes and the DBSA/KCl was extremely rapid. The catalytic reduction current increased with modification time but quickly reached a plateau where the current rise was not as marked as before. The cathodic currents displayed by Ag SPEs after 60, 300 and 600 s modification time were all approx. 2.9· 10^{-5} A. The highest cathodic current value of 3.4-1 0^{-5} A was obtained with electrodes

following exposure to DBSA/KCI modification solution for 2 hours. Further exposure times such as 1 day or 1 week did not improved the response; on the contrary, the catalytic current started to decrease. To ensure that the highest catalytic currents were obtained, 3 hours was chosen as the optimum modification time for the experiments. This was used for all subsequent experiments.

Figure 6. Plot of current vs modification time obtained during amperometric measurements of Ag SPEs at - 0.1 V (vs Ag/AgCl) at $5\text{-}10^{-3}$ M H_20_2. Data at 0 s corresponds to unmodified electrode.

Influence of pH on the catalytic process. The influence of the pH of the bulk electrolyte solution during the reduction of $5\text{-}10^{-3}$ M H_20_2 was investigated for both unmodified and DBSA/KCI modified Ag SPEs. Amperometric measurements at - 0.1 V were performed (Fig. 7) using the same electrode while changing the pH. H_20_2 reduction at the unmodified Ag SPE showed little catalytic response in the pH range from 2 to 10, unlike a DBSA/KCI modified one. Thus, the cathodic currents of the unmodified electrodes ranged from $3.4\cdot10^{-7}$ A at pH 2 to $3.6\cdot10^{-6}$ A at pH 10, with a maximum value of $4.4\text{-}10^{-6}$ A at pH 6.8. The DBSA/KCI modified electrode showed no catalytic activity at very acidic solutions (pH = 2), $6.0\cdot10^{-7}$ A, whereas the cathodic current increased approx. 50-fold up to $3.3T0^{-5}$ A as the bulk solution pH increased up to 10. This suggests that the catalytic mechanism by which H_20_2 is reduced is enhanced significantly in basic solution. This pH-dependence of H_20_2 reduction has been observed previously and explained by the effect of the pH on the reduction potential. At high concentrations of H^+ in solution, H_20_2 reduction occurs at more negative potentials than when the concentration is lower. This behaviour is typical of a mechanism of reaction in which H^+ appears as a reactant or OH^- as a product of the reaction, which agrees with many of the proposed mechanisms for H_20_2 reduction," [15] as for example the following:

$$H_20_2 + e^- \leftrightarrow OH_{(ads)} + OH^-$$
$$OH_{(ads)} + e^- \leftrightarrow OH^-$$
$$2OH^- + 2H^+ \leftrightarrow 2H_20$$

Therefore, at - 0.1 V the rate of H_20_2 reduction was higher when the reaction took place in more basic solution rather than in more acidic ones.[16] pH 6.8 was selected for the electrolyte measurement solutions in further work as it exhibited more than thirty-fold higher catalytic

currents and is a suitable pH for the study of biological systems, such as enzyme-based biosensors, for which this system will form a platform.

Figure 7. Plot i_{cat} vs electrolyte pH for Ag SPEs (a) with and (b) without DBSA/KCl modification in $5 \cdot 10^{-3}$ M H_2O_2 at - 0.1 V vs Ag/AgCl.

Analytical parameters for a H_2O_2 sensor. Subsequently, the feasibility of Ag SPEs electrodes modified with $3.3 \cdot 10^{-2}$ M DBSA/ 0.1 M KCl to be used as H_2O_2 sensors was assessed and limit of detection (LOD) and reproducibility studies were carried out. Three Ag SPEs were modified in $3.3 \cdot 10^{-2}$ M DBSA/ 0.1 M KCl solutions for 3 h, according to the adopted standard protocol. After rinsing, they were measured in PBS pH 6.8. Amperometric responses to H_2O_2 from 2 to $16 \cdot 10^{-5}$ M are shown in Fig. 8. Experiments were repeated three times with each electrode and the data were compared to check the intra- and inter- electrode reproducibility. Although the lowest concentration measured was $2T0^{-5}$ M, the lowest theoretical LOD of the sensor devices was found to be $10.8\text{-}10^{-6}$ M, with a signal-to-noise ratio of 3. The LOD was calculated from the regression line obtained from the plot of the cathodic currents vs H_2O_2 concentration. These data are presented in the inset of Fig. 8. The response across this range of concentrations was non-linear. The upward curvature observed here is different from the downward curvature found for substrate limitation at enzyme electrodes and might be explained by an autocatalytic process during the H_2O_2 reduction. The autocatalytic reduction of H_2O_2 on Ag electrodes has been previously reported by Flatgen et al." They observed two mechanisms of H_2O_2 reduction operating at different overvoltages. At potentials more negative than - 0.45 V (vs Ag/AgCl) the "normal" reduction took place whereas a second mechanism was operative at E > - 0.35 V. They proposed that the rate of H_2O_2 reduction in this second case was increased by the presence of the adsorbate $(OH)_{ad}$ formed during the reduction process on the Ag surface, leading to an autocatalytic reaction on the electrode. Moreover, the catalytic activity of the modified Ag SPEs seemed to improve with the number of repeat measurements. This behaviour was not observed at H_2O_2 concentrations > 10^{-3} M, where the catalytic responses decreased with the number of repeats. Moreover, the shape of the curvature adopted a downward trend at H_2O_2 concentrations in the range 10^{-2} - 10^{-1} M, which might be explained by the saturation of the electrode at such high analyte concentrations. Fig. 9 shows the three data point collection obtained for each of the electrodes in the range of H_2O_2 concentrations 2 to $16\text{-}10^{-5}$ M. In the three cases, the highest catalytic responses for H_2O_2 reduction were obtained in the last repeat.

Figure 8. Amperometric responses of the DBSA/KC1 modified electrodes in $20 \cdot 10^{-6}$ M aliquots of H_2O_2 (20 - 160 $\cdot 10^{-6}$ M) at -0.1 V (vs Ag/AgCl) in PBS pH 6.8. Input: Plot of cathodic current vs H_20_2 concentration at -0.1 V (vs Ag/AgCl) in PBS pH 6.8.

Figure 9. Reproducibility study using three different electrodes: (a) electrode 1; (b) electrode 2; (c) electrode 3. Amperometric responses of the DBSA/KC1 modified electrodes in $20 \cdot 10^{-6}$ M aliquots of H_20_2 (20 - 160 -10^{-6} M) at - 0.1 V (vs Ag/AgCl) in PBS pH 6.8. Each electrode was measured three times: (·) repeat 1; (A) repeat 2; (■) repeat 3.

Surface characterization

Scanning electron micrographs and EDX spectra of Ag SPE before and after DBSA/KCl modification and following electrocatalytic reduction of H_20_2 are shown in Fig. 10. Then, SEM images using Secondary electron (SE) for the detection were performed. Due to the conductive character of the silver-based ink, no gold-sputtering was required on these surfaces. KCI-modified electrodes and AgCI-modified electrodes are also shown as controls. The unmodified screen-printed electrode (Fig. 10a) shows the typical morphology of a metallic silver paste. It is known that the ink used contains metallic Ag particles, an organic binder and solvent.[17] Thus, SEM shows amorphous metallic Ag suspended in an organic paste. Following exposure to the DBSA/KCI solution, spheroidal structures became visible on the DBSA/KCI modified electrodes. These structures were not present on the KCI-modified surfaces, although these electrodes did show some structural differences to controls - they also showed some catalysis. The spheroidal structures varied in size with typical diameters of approx. 1 μηι. These modifications were observed on electrodes which exhibited the catalytic effect on H_20_2 reduction. In addition, the morphology of the structures appeared to change following the electrodes when these were used to reduce H_20_2, which might be explained by the interaction between H_20_2 and the structures during the reduction process.

With EDX, Ag was shown to be the major component in the unmodified electrodes, where C was also detected, as one might expect due to the metallic/organic binder composition required to obtain the rheological and curing characteristics for the printing process. When DBSA/KCI modified electrodes were analysed, CI was detected as well as Ag, which was more significant in the areas with greater numbers of spheroidal structures. However, no CI could be identified in the spectrum corresponding to DBSA/KCI modified electrodes following exposure to H_20_2

reduction. Therefore, the spheroidal structures formed after DBSA/KCl pre-treatment appear to result from or result in an increase in surface CI levels and may be involved in the catalytic process of H_20_2 reduction.

Figure 10. SEM images using secondary electron (SE) detection of Ag SPEs (a) unmodified; (b) DBSA/KCl-modified; (c) DBSA/KCl-modified after electrochemical reduction of 5-10° M H_20_2; (d) AgCl electrochemically deposited; (e) KC1 modified. Accelerating voltage of 20 kV. (5.0k x magnification). Below, the respective EDX spectrum for each sample. Binding energies in keV.

X-Ray Photoelectron Spectroscopy (XPS) measurements were performed using a Kratos AXIS 165 spectrometer (University of Limerick). The samples analysed were unmodified and DBSA/KCl modified Ag SPEs. Spectra and concentration percentages are presented in Fig. 1] and Table 1, respectively. As might be expected, Ag SPE surfaces showed the presence of CI, K and S after the modification in DBSA/KCl solutions. However, a higher proportion of CI (4.3 %) over K (0.6%) was detected on the electrode surface, which is approx. 7.5-fold greater than that which would be expected on an equimolar basis. This fact could be explained by the formation of AgCl on the substrates during the modification which, unlike K would remain on the surface after the electrodes were rinsed.

Table 1. XPS data for unmodified and DBSA/KCl modified Ag SPEs

Unmodified Ag SPE			DBSA/KCl modified Ag SPE		
Name	**Position (eV)**	**% Conc.**	**Name**	**Position (eV)**	**% Conc.**
O 1s	533.3	12.9	**O 1s**	531.4	11.7
Ag 3d	368.2	24.5	**Ag 3d**	367.7	26.1
C 1s	284.5	62.5	**C 1s**	284.6	55.8
--	--	--	**K 2p**	291.8	0.6
--	--	--	**Cl 2p**	197.5	4.3
--	--	--	**S 2p**	167.5	1.6

Figure 11. XPS images of Ag SPEs (a) unmodified and (b) DBSA/KCl modified.

Consequently, to check if the catalysis observed on modified Ag SPEs was due to the effect of CI⁻ ions and the formation of AgCl on the surface, Ag SPEs were dipped into 0.1 M HC1 and a

potential of 1 V was applied for 5 s.[18] Such conditions are usually applied to coat Ag electrodes with AgCl during the fabrication of Ag/AgCl references electrodes. Ag SPEs after this pre-treatment blackened due to the formation of the AgCl salt on the surface. Then, the electrodes were rinsed and placed in PBS pH 6.8 to the electrochemical analysis. Aliquots of H_2O_2 were added to the solution during the amperometric curves performed at -0.1 V, so **H2O2** concentration in solution raised to $5\text{-}10^{-3}$ M. The amperometric curves for these electrodes were compared to those obtained for the unmodified and DBSA/KC1 modified ones (Fig. 12).

Figure 12. Amperometric i-t curves of Ag SPEs measured at - 0.1 V (vs Ag/AgCl) in PBS pH 6.8: (a) unmodified; (b) AgCl electrodeposited and (c) DBSA/KC1 modified electrodes, at **H2O2** concentrations from 1 to $5\text{-}10^{-3}$ M.

The reduction current corresponding to $5\text{-}10^{-3}$ M **H2O2** solution obtained with the AgCl modified SPE was about 4 times higher than that shown by the unmodified electrode, whereas for the DBSA/KC1 modified one, this was about thirty times greater. The slight catalytic effect of the AgCl modified electrode could be explained as the response expected due to an increase of the Ag metallic area available to H_20_2. However, it is clear that the catalysis is not solely due to the formation of AgCl at the electrode, although this may play a role in the process. Lian et a!.[19] recently reported the increasing roughness of Ag electrodes by electrochemical oxidation-reduction cycles (ORC) in a KC1 solution and their application to the quantitative determination of **H2O2.** The process began with the stripping of Ag to form Ag-Cl complex and the subsequent cathodic electrodeposition of Ag^+ to form Ag nanoparticles on the Ag substrate. The Ag-Cl complex decreased the diffusion rate of Ag^+ and made the reduction of Ag^+ more difficult, which was helpful in the formation of small Ag nanoparticles. The activity of the roughed electrodes towards H_2O_2 reduction was assessed as a function of the number of cycles, KC1 concentration and scan rate during the cyclic voltammetry. The catalytic current due to **H2O2** reduction increased with cycle number and, therefore, Ag surface area of the electrodes.[1, 20-21]

The extreme conditions (1 V for 5 s) required for the electrochemical formation of AgCl on the electrodes in the present work could also generate the decomposition of the organic compounds which bind the metallic particles of Ag in the paste, rendering more Ag sites free to perform the reduction of H_2O_2. With regard to the chemical analysis of the surface, EDX data in Fig. 10d showed the presence of Ag and CI as predominant components in the AgCl modified Ag SPEs. However, unlike the DBSA/KC1 modified electrodes, the spherical structures formed on the

surfaces were smaller for the Ag/AgCl SPE, as is shown in the SEM images for both substrates. Such differences in the morphology could be expected as the modification procedures were very unalike. The electrochemical deposition of Ag/AgCl was the result of intense conditions by the application of a very high oxidising potential, whereas the DBSA/KC1 modification was performed under much milder conditions. The formation of the larger spheroidal aggregates on the surface of Ag SPEs seemed to be favoured by the presence of the surfactants at certain concentrations in the modification solution. Such structures may be implicated in the catalytic process for the electrochemical reduction of H_20_2, providing responses up to eighty times higher than those obtained with the unmodified electrodes. One possible explanation could be that micellar, hexagonal or lamellar structures often formed by the surfactants when they are in solution may have become deposited onto the Ag SPE in some way, creating an enhanced surface for the catalytic process. These structures or processes appear to create the appropriate environment for the subsequent formation of AgCl due to the presence of Cl^- in the modification solution. This would explain the presence of a higher concentration of AgCl on the electrode surface following DBSA/KCI modification. Another explanation for the catalytic process could be that the interactions of DBSA/KCI with the electrode surface may have changed the Ag morphology by creating a nanostructured surface. This would provide nanoparticulate silver structures, increasing the active surface area available to perform the H_20_2 reduction.

The fact that no surfactants were detected on the substrates (i.e. no S from DBSA) using EDX analysis may be an artefact of the EM imaging process. When Ag SPEs are modified, rinsed and used directly in the cell to carry out the electrochemical techniques, these hexagonal or lamellar structures may be present on the surface because it always remains wet. However, the SEM technique requires dry surfaces to take images of the substrates, or else the detector could be damaged. Therefore, once the surface is dried, the possible structures responsible for the surface modification would be broken down, making their detection more difficult. In fact, XPS data showed the presence of S on the DBSA/KCI modified Ag SPE, which was not detected on the unmodified one. Although its concentration (1.6 %) was not so high as Cl concentration (4.3 %), its presence can not be ignored and further studies should be performed to conclude if the presence of S on the modified electrode surface is due to either the real surface modification or the remaining modification solution which has not been rinsed thoroughly enough. This would require more sophisticated preparation of samples for SEM, such as cryo-field emission scanning electrode microscopy (cryo-FESEM), which has been already used to characterize water/oil microemulsion structures.[22, 23] Other techniques already applied for the characterization of

surfactant deposited on surfaces is atomic force microscopy (AFM), which has been used to image surfaces coated with different surfactants to determine their aggregate morphology.[24-26]

DBSA/KC1 modified Ag SPEs were shown by contact angle measurements in water to be more hydrophilic compared to the unmodified electrodes, as is shown in Fig. 13. This increase in hydrophilicity and surface energy would be consistent with modification with an amphiphile in a "head-up" orientation. Dominguez et al.[27] have already reported the difference in contact angle for unmodified and surfactant modified surfaces. They performed contact angle measurements on graphite surfaces modified with SDS in the presence and the absence of different NaCI concentrations to show the different characteristics of the aggregates on the electrode surface. They found that the contact angle decreased as the salt concentration was increased. This indicated that the SDS aggregates wet the surface more thoroughly as the salt concentration increased. This agreed with a more dense surface coverage with less hydrophic graphite exposed to solution reported by Wanless et al.[25] for the same system. They proposed that a decrease in SDS aggregate separation on the surface occurred when the salt concentration was increased because the electrolyte screened the interactions between charged head groups.

Figure 13. Comparison of the surface hydrophilicity of an unmodified (on the right) and a DBSA/KC1 modified Ag SPE when $2 \cdot 10^{-6}$ $1 H_2 0$ was deposited onto the surface (surface area = 0.126 cm^2)

Effect of DBSA/KC1 modification of Ag SPEs on H_2O_2 decomposition

During studies on the electrochemical reduction of $H_2 0_2$ on the DBSA/KCI modified electrodes, it was observed that there was also an increase in 0_2 evolution as a result of accelerated decomposition. Therefore, the surface shared both increased catalytic and coupled electrocatalytic reduction of $H_2 0_2$. As a consequence of this observation, the catalytic effect on the chemical decomposition of $H_2 0_2$ was also assessed. Gravimetric measurements of $H_2 0_2$ decomposition on Ag SPEs were carried out before and after modification of the substrates in freshly prepared $3.3 \cdot 10^{-2}$ M DBSA/ 0.1 M KC1 solutions. The mass differences due to 0_2 releases after the break-down of $H_2 0_2$ were plotted versus time to compare the effect that the surfactant-based solution had on the decomposition process. Figure 15 shows the different behaviour of a Ag SPE before and after the modification. As can be observed, the modified electrode showed faster $H_2 0_2$ decomposition (and therefore greater loss of 0_2) than the

unmodified one. This could also be observed visually by the formation of gas bubbles at the electrode surface. The amount of 0_2 evolved from the solution was approx. eight times higher for the modified electrode after a 1 hour reaction. The degradation showed significant non-linearity of the responses with time exhibited by the modified electrodes. These electrodes showed a linear dependence with time during the first 5-6 minutes, after which the amount of 0_2 released per unit time seemed to decrease drastically. This effect, which appears only with modified electrodes, was further analysed.

Figure 14. Plot of change in mass per unit area versus time of (a) unmodified and (b) modified Ag SPE in 2 ml 1M H_20_2.

Each electrode was tested three times in order to analyze the stability and reproducibility of the measurements in fresh H_20_2 solutions (Figure 15). Both modified and unmodified Ag SPEs showed decreasing responses as the number of repetition increases. Significant decreases were observed for the modified SPE as compared to the unmodified one and this may suggest that the decomposition process is not truly catalytic as the surface may lose its catalytic properties over time.

Therefore, the use of DBSA/KC1 solution as a modification agent for Ag SPEs resulted in the acceleration of the decomposition process when the electrodes were placed in H_20_2, resulting in faster 0_2 release compared to the unmodified ones.

Figure 15. Change in mass per unit area versus time of (a) unmodified and (b) modified Ag SPE in 2ml 1M H_20_2 solution for 1 hour. Each electrode was measured three times and the number of the repetition is indicated besides each graph.

Scanning electron microscopic images of the unmodified and DBSA/KCI modified Ag SPEs were obtained before and after exposure to 1 M H_20_2 solution (Figure 16). As can be observed, Ag SPE electrodes presented very rough surfaces. Ag paste ink used to manufacture these electrodes consists of metallic Ag as well as an organic solvent and a vinyl or epoxy-based polymeric binder to maintain the structure of the ink and make it printable.[17] The purpose of the binder is to ensure the ink's affinity for the substrate in terms of adhesion properties. After screen-printing, the fresh electrodes are cured in the oven so the organic solvent from the ink is evaporated. Moreover, as Grennan et al. (2001) reported using carbon-paste screen-printed

electrodes,[28] as the temperature of curing is increased, the surface roughness increases because the microparticulate nature of the Ag ink is consequently increased. Regarding the SEM images after H_20_2 measurements, rougher surfaces of both types of electrodes were observed after the reaction either due to the formation of a reaction product on the surfaces or because something on the electrode surface reacts with H_20_2, provoking its decomposition and increasing the amount of holes on the surface. This increase of the surface roughness during H_20_2 decomposition process was already reported by Schmidt et al.[29] They observed a micro-roughening effect occurred on hydrophobic silicon wafers after being immersed into H_20_2/NH_4OH (SCI) cleaning solutions. They believed that small 0_2 bubbles were stuck on the initially hydrophobic silicon surfaces preventing them from the etching action of the SCI chemistry and making them responsible of the micro-masking effect.

It should be noted, however, that although unmodified Ag SPEs underwent a morphological change upon exposure to H_20_2, this was not associated with an increase in catalytic decomposition.

Before the reaction, the DBSA/KC1 modification appeared to produce some structural alteration on Ag SPEs (Fig.l6C) which didn't appear on the unmodified electrodes (Fig. 16A). Moreover, Ag SPEs after modification did exhibit greater increases in levels of 0_2 evolution from the solution due to H_20_2 decomposition than those observed with the same electrodes without modification. The appearance of smaller structures in the same place as those formed prior to modification after the reaction with H_20_2 seems to indicate that these surfactant-based structures formed on the electrode surfaces after the modification are in some way responsible for, or are a result of the catalytic effect on H_20_2 decomposition observed on the modified Ag electrodes. In addition, the two structural morphologies exhibited for unmodified electrodes following H_20_2 exposure and modified electrodes prior to H_20_2 exposure cannot be equated and do not result in similar catalytic behaviours.

Figure 16. SEM images of unmodified Ag SPEs (A) before and (B) after the measurements in 1 M H_20_2 solution. SEM images of Ag SPEs modified with DBSA/KCI (C) before and (D) after exposure to 1 M H_20_2 solution. Accelerating voltage of 20 kV. (5.0 k x magnification).

The progressive alteration of the surface of the DBSA/KCI modified Ag SPE following repeated exposures to H_20_2 is shown in Fig. 17. After 1 h exposure to H_20_2 there were still many of the

spheroidal structures formed following DBSA/KCl modification remaining on the electrode surface, as can be seen in Fig. 17b. However, when the electrode was further exposed to H_20_2, the size of these structures diminished from approx. 1 μηι after 1 h exposure to 100 - 300 nm after 3h, as can be observed from Fig. 17b-d. This enforces the notion of the involvement of the spheroidal structures created on the electrode surface after DBSA/KCl modification in the H_20_2 decomposition reaction, and also that the change in their morphology over time is associated with a decrease in catalytic activity.

Study of the effect of surfactant type and Group 1 metal chloride salt in the modification solutions on electroreduction and decomposition of H_2O_2

Given the catalytic effect that had been observed towards H_20_2 reduction when Ag SPEs were modified with DBSA/KCl solutions, several other surfactants were studied to see what effect this would have on the catalytic process. Initially, sodium dodecyl sulphate (SDS) was assessed. This surfactant showed physical characteristics similar to DBSA: both of them possess a long hydrophobic alkyl chain and a hydrophilic anionic head. The salt used as a co-partner for SDS modifying solutions was NaCl as opposed to KC1 with DBSA. The aim was to check if catalysis towards H_20_2 reduction was observed when Ag SPEs are pre-treated with SDS solutions and to evaluate the role of the salt in this effect. Therefore, Ag SPEs were dipped into solutions with different concentrations of SDS (0.5 - 10^{-7} M), with and without 0.1 M NaCl for 3 h. Once rinsed, the electrodes were placed in the working cell (containing 10 ml PBS pH 6.8) and amperometry was performed. Cathodic current data from the amperometric responses to $5\text{-}10^{-3}$ M H_20_2 were correlated with SDS concentration. Fig. 18 shows the comparison between modification with and without NaCl.

Figure 18. Plot of current vs log [SDS] obtained during amperometric measurements of Ag SPEs at - 0.1 V (vs Ag/AgCI) at $5\text{-}10^{-3}$ M H_20_2. The electrodes were modified (a) only with SDS or (b) SDS and 0.1 M NaCl.

As with DBSA, Ag SPEs modified solely with SDS solutions showed little catalytic effect towards H_20_2 reduction, even though SDS concentration was increased to 1.5 M. However, the presence of NaCl in the modification solutions caused a noticeable enhancement in the cathodic current when Ag SPEs were measured in the presence of $5\cdot10^{-3}$ M H_20_2. At 0.1 M NaCl a significant rise in cathodic current was observed from 10^{-4} to 10^{-2} M SDS, where it plateued.

Consequently, the SDS concentration was fixed at 3.3-1 0^{-2} M, to enable comparison with earlier DBSA data, and to investigate the effect of different concentrations of NaCl. At the same time, other surfactants were assessed in combination with an appropriate salt in the modification solution. Surfactant concentration used to pre-treat Ag SPEs was kept constant at $3.3 \cdot 10^{-2}$ M and the salt concentrations were varied. However, CTAB was used with a final concentration of $3.3 \cdot 10^{-3}$ M as at higher concentrations, insoluble aggregates were formed.

Table 2. Structure and characteristics of several surfactants.

Surfactant	Type[a]	CMC[b] / mM	Structure	Salt
Dodecyl Benzene Sulphonic Acid (DBSA)	A	1.6-2[9, 10]	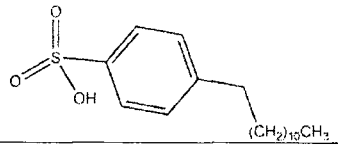	KCl
Sodium Dodecyl Sulphate (SDS)	A	8-9[7, 8]	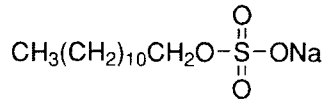	NaCl
Cetyl Trimethylammonium Bromide (CTAB)	C	0.9-1[7, 8]	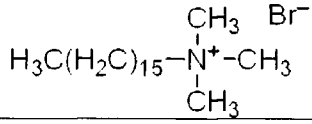	NaBr
Triton X-100	N	0.2-0.3[7, 8]	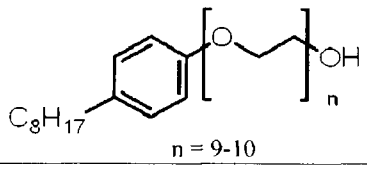	KCl

[a] A, anionic; C, cationic; N, non-ionic.
[b] CMC - Critical Micelle Concentration.

Table 2 shows the structures and main characteristics of the surfactants under study. The Group I halogen salt used with the surfactants in the modification solutions are also presented in Table 2. Cathodic current data from amperometric measurements using $5 \cdot 10^{-3}$ M **H2O2** are shown in Fig. 19. Ag SPEs exposed to the different surfactant solutions showed enhanced catalysis in a manner similar to that seen with DBSA/KC1 and SDS/NaCl. No remarkable enhancement effect was noticed when the concentration of the respective salt in the modification solutions remained below 10^{-5} M. However, above this concentration, a significant catalytic effect towards H_20_2 reduction was observed, providing the highest reduction current values at salt concentrations in the modifying solutions of 10^{-2} to 1.5 M.

Figure 19. Plot of current vs log [salt] obtained during amperometric measurements of Ag SPEs at - 0.1 V (vs Ag/AgCl) at 5-10^{-3} M H_20_2. Electrodes were modified with (·) 3.3· 10^{-2} M DBSA/KC1; (*) 3.3-10^{-2} M Triton X-100/ KC1; (■) 3.3-10^{-3} M CTAB/NaBr or (▲) 3.3-10^{-2} M SDS/NaCl. Salt concentration ranged from 1.5 to 10^{-7} M. Value at log [salt] = - 10 corresponds to the unmodified Ag SPEs.

Although the overall behaviour of all the surfactant solutions was the same, there were some distinctions. One of these was the salt concentration at which H_20_2 catalytic effect was observed. Triton X-100 required the lowest salt concentration to induce enhanced catalysis, being 10^{-4} M KC1, whereas SDS required the highest concentration of 0.1 M NaCl. DBSA required at least 10^{-3} M KC1 to show a noticeable increase in catalysis, whereas CTAB showed a slight catalytic effect at very low NaBr concentrations in the modification solutions (10^{-7} M), although 0.1 M was required to obtain the most significant effect. Therefore, the surfactants under study in this work could be ordered from the lowest to the highest salt concentration required in the modification solution to show enhanced catalysis towards H_20_2 reduction as reported below:

Triton X-100 < DBSA < CTAB < SDS

With the exception of CTAB, surfactants followed the same relative order as their respective critical micelle concentrations (CMC):

Triton X-100 (0.2-0.24) < CTAB (0.9-1) < DBSA (2) < SDS (7-10)

The different behaviour observed with CTAB could be explained as a result of the lower concentration of CTAB (3.3· 10^{-3} M) employed for the modification solutions, which was ten times lower than that for the other surfactants (3.3T0 $^{-2}$ M). The reason for this is that the CTAB was not soluble at 3.3 x 10^{-2} M. It is also worth noting that this is the only one with Br as counterion, which might lead to alterations or different behaviours during the formation of surfactant aggregates.

As is well-known, surfactants can form several types of organized structures in aqueous solutions as a function of concentration and/or experimental conditions. [7-9-27] Typical surfactant aggregate structures are shown in Fig. 20.

Figure 20. (i). Simplified surfactant structure. (ii). Typical surfactant aggregates: (a) cylindrical structures, (b) lamellar structures and (c) spherical micelles.

Spheroidal micelles are the simplest aggregates formed by surfactants at low concentrations. When the surfactant concentration increases, cylindrical structures are observed, and above 30-40 % (w/v) of surfactant, liquid crystalline phases are formed. These structures result from the aggregation of surfactant molecules into large domains, often of hexagonal or lamellar structures. However, surfactant concentration is not the only cause of changes in shape and structure. There are also other methods of inducing aggregate growth, which includes the addition of a salt such as NaCI, the addition of cosurfactants, changes in the counterions and the use of surfactant mixtures. Moreover, whereas solutions containing spherical micelles have low viscosity, the liquid crystalline phase (especially the hexagonal phase) exhibit very high viscosity values. [7]

The transition of micelles of the anionic surfactant sodium dodecylbenzenesulfonate (NaDBS) into lamellar aggregates by the addition of alkali metal chlorides was studied in dilute aqueous solution by Sein et al.[9] The behaviour of NaDBS was described as a function of salt concentration, where the salt was varied along the lyotropic series (LiCI to CsCI). The cation hydration changes dramatically along this series, from highly hydrated for Li^+ to weakly hydrated for Cs^+. On a molecular level, an increase in alkali metal cation concentration induced the packing of molecules into lamellar structures, which was facilitated by the increase in counterion binding and by the dehydration of the headgroup due to the addition of a salting-out electrolyte. Both effects would encourage a closer packing of the surfactant headgroups, which produced the rearrangement from micelles into lamellae. Less hydrated ions led to an increase in counterion binding, i.e. a decreasing electrolyte concentration from LiCI to CsCI was required to induce the packing in a lamellar array.

In the present work, both DBSA and SDS modification of, or exposure to Ag SPEs, in the presence of an alkali chloride salt (KC1 and NaCI, respectively) produced similar catalytic responses when H_20_2 reduction currents were plotted versus salt concentration. The catalytic effect of the modified electrodes was only significant above a certain salt concentration. Moreover, the highest cathodic currents were detected when the viscosity from the modification solutions was increased, with the formation of precipitates in the bulk solution being noted. Therefore, the catalytic effect observed by Ag SPEs on H_20_2 reduction following pre-treatment

with these surfactant-based solutions could be related to the formation of micelles or lamellar arrays by the surfactants in the presence of increasing salt concentration. Such structures would be formed in the solution and might become subsequently deposited or assembled at the electrode surfaces. Baryla et al.[24] recently studied the adsorption mechanisms and aggregation properties of CTAB and used atomic force microscopy (AFM) to image and determine the aggregate morphology of the surfactant on coated surfaces. They also reported the surfactant concentration dependence of the micellar coating on fused silica substrates as well as the effect of ionic strength on the surface assembly of CTAB. At low phosphate buffer ionic strength, CTAB formed spherical aggregates on the substrates whereas at higher ionic strength (0.1 M) a combination of short rods and spherical aggregates was observed. As has been shown previously, surfactant monomers form aggregates in aqueous solution because of the hydrophobic interactions between the long hydrocarbon chains which seek to minimise their interaction with water, and the hydrophilic head groups which favour interactions with water. The favourable interactions of adjacent amphiphiles are limited by the unfavourable electrostatic repulsion between the polar headgroups. Increasing the ionic strength of the buffer minimizes this repulsion by ionic screening, which leads to the formation of different morphologies such as lamellae. Therefore, surfactants in such a conformation are likely to be deposited onto a surface in different morphologies depending on the salt concentration in the solution.[24-30, 31] This effect could explain the dependence of the catalytic reduction current (i_{cat}) with [XCI] observed in the present work. To a certain extent, increasing the salt concentration in the surfactant-based modification solution would favour the formation of micelles or other highly packed aggregates, which are subsequently deposited on, or in some other way interact with the Ag SPE surface. Whatever the process, this appears to provide an appropriate environment to perform the significantly enhanced H_2O_2 reduction observed.

Chloride salts with different Group I cations. In order to study the effect of the counter-cation size from the chloride salts used in the modification solution on catalysis, Ag SPEs were dipped into solutions containing $3.3\text{-}10^{-2}$ M DBSA with a range of concentrations of the respective chloride salts (XCI, X = Li, Na, K or Cs). Then, the electrodes were rinsed and placed in PBS pH 6.8, where amperometric measurements were performed at - 0.1 V (vs Ag/AgCl) in $5\text{-}10^{-3}$ M H_2O_2 (Fig. 21).

Ag SPEs modified with different alkaline salts combined with $3.3\text{-}10^{-2}$ M DBSA showed similar patterns of catalysis with an onset above approx. 10^{-4} M salt and peaking at 10^{-1} M, except

DBSA/CsCl peaking at 1 M salt concentration. At 10^{-3} M, the cathodic currents obtained for all DBSA/salt modification solutions were similar and ranged between 1.4-1 .7-10^{-5} A. When the salt concentration in the modification solution increased, the cathodic current interval was spread, showing significant differences depending on the salt type in the modification solution. At 10^{-2} M, the highest catalytic activity was shown by the electrode exposed to DBSA/NaCl, with 2.2-10^{-5} A, followed by KCl (1.9-10^{-5} A), LiCI (1.7-10^{-5} A) and CsCl (1.3-10^{-5} A). The greatest cathodic current were obtained at 10^{-1} M salt concentration, with $2.4 \cdot 10^{-5}$ A for NaCl, $2.2 \cdot 10^{-5}$ A for KCl and $2.0 \cdot 10^{-5}$ A for CsCl whereas the maximum value for LiCI, $2.1 \cdot 10^{-5}$ A, was obtained at 1 M concentration. Therefore, although all the peak catalytic currents were in the same order of magnitude, the electrodes modified with DBSA/NaCl seemed to have the better responses in the concentration range under study.

Figure 21. Plot of current vs log [XC1] obtained during amperometric measurements of Ag SPEs at - 0.1 V (vs Ag/AgCI) at $5\text{-}10^{-3}$ M H_2O_2. The electrodes were modified with mixtures of 3.3-10^{-2} M DBSA and different concentrations of: (·) LiCI ; (■) NaCl ; (▲) KCl or (★) CsCl. Salt concentration ranged from 1.5 to 10^{-7} M. Value at log [salt] = - 10 corresponds to the unmodified Ag SPEs.

Moreover, the fact that all the salts resulted in catalytic activity in the same concentration range in the modification solution might be related again to the formation of surfactant aggregation in the solution. As was mentioned earlier, Sein et al.[9] studied the transition of surfactant micelles into lamellar structures when the concentration of alkali chloride in solution was increased. They observed that in the concentration range of approx. $0.05 \cdot 10^{-3}$ M for CsCl to 1.1-10^{-3} M for LiCI, surfactant aggregates changed from micelles to unilamellar or flocculated multilamellar structures. This salt concentration range agrees with that of the enhanced H_2O_2 reduction process observed in the present study and shown in Fig. 2 1. At $3.3 \cdot 10^{-2}$ M DBSA, more than ten times the DBSA CMC, surfactant is found as micelle aggregates in the modification solution. Dominguez et al.[27] have also recently reported the formation of hemicylindrical aggregates of SDS molecules on graphite surfaces at different salt (NaCl)/water solutions. They performed a molecular dynamics simulation study and the results were compared to those obtained experimentally by atomic force microscopy (AFM). Again, the aggregates exhibited different structures as the salt concentration was increased. Without salt, the hemicylindrical aggregates showed only two well-defined layers due to the adsorbtion of the SDS tails on the graphite surface. At low NaCl concentration, a third layer was observed, which vanished at high salt

concentration. Any change in solution properties which causes a reduction in the effective size of hydrophilic head groups, i.e. the addition of an electrolyte, will change the aggregate size and shape of the micelle structures.[32] When a salt is added to the modification solution, unilamellar or multilamellar structures are formed, which interact with the Ag SPE electrodes providing an enhanced ability for **H2O2** reduction. The higher the salt concentration, the greater the catalytic activity shown by the Ag SPEs. At [salt] > 1 M, the catalytic currents decreased, which might be explained by the breaking-down of the surfactant aggregates in the modification solution or the decreasing interaction between the latter and the electrode surface.[27]

Investigation of the effect of other metallic electrodes on the catalytic decomposition and electrocatalytic reduction of H_2O_2 following surface modification with surfactant/salt

After the study of DBSA/KC1 modification of Ag SPEs and their catalytic activity towards H_2O_2 decomposition and electrochemical reaction, the same effect on other metallic electrodes was subsequently investigated. Other silver-based electrodes such as metallic Ag (99.9 %) or sterling Ag (92.5 %) ones as well as gold and platinum-based electrodes were assessed and their catalytic activity on H_2O_2 reactions was compared to Ag SPEs.

Silver-based electrodes

A). Electrochemical characterization. Planar Ag (99.9 %) metallic electrodes were used to study the catalytic effect on **H2O2** previously observed with Ag SPEs. The electrodes were polished using 0.3 μηι first and 0.05 μη then, and sonicated in distilled water for 5 min to remove any possible impurity on the surface. Next, they were dipped into $3.3 \cdot 10^{-2}$ M DBSA/ 0.1 M KC1 solutions for 3 h, rinsed copiously with distilled water and placed in a working cell containing 10 ml PBS pH 6.8. Cyclic voltammograms and amperometric time-based measurements were performed in $0\text{-}5 \cdot 10^{-3}$ M **H2O2.** The measurements obtained with the modified electrodes were compared to those from the unmodified ones (Fig. 22).

Figure 22. Amperometric i-t curves of metallic silver electrodes measured at - 0.1 V (vs Ag/AgCl) in PBS pH 6.8: (a) unmodified; (b) 3h; (c) 1 day DBSA/KC1 modified, at H_20_2 concentrations from 1 to $5\text{-}10^{-3}$ M.

As no enhancement was observed following the modification, the experiment was repeated leaving the metallic Ag (99.9 %) electrode exposed to the surfactant-based solution for 1 day (Fig. 22c). The longer pre-treatment time seemed to provide greater catalysis of H_20_2 reduction. However, in comparing the amperometric responses from the metallic Ag (99.9 %) electrode before and after the modification, approximately ten-fold higher reduction currents were obtained with 1 day modification whereas the cathodic current was eighty times higher for the modified Ag SPEs in only 3 h, as was shown in Fig. 2. The metallic silver (99.9 %) electrodes were also pre-treated in HCI at + 1 V (vs Ag/AgCl) for 2 s to electrochemically form AgCI on the electrode surface,[18] but no enhancement of the amperometric responses was obtained.

SEM imaging of metallic Ag (99.9 %) electrodes before and after DBSA/KCI modification was performed. Metallic Ag (99.9 %) did not show the formation of any surface structures or increasing roughness after the pre-treatment in DBSA/KCI, as is observed by comparing Fig. 23a and 23b. This data was in agreement with the lack of catalytic effect on H_20_2 reduction. It reinforces the fact that the creation of the spheroidal structures on the Ag SPE surface after DBSA/KCI modification is related to the enhancement of H_20_2 reduction.

Figure 23. SEM images using SE detection of metallic Ag (99.9 %) electrodes (a) unmodified and (b) DBSA/KCI modified. Accelerating voltage of 20 kV. (5.0k x magnification).

The same procedure performed with Ag SPEs and planar metallic Ag (99.9 %) electrodes was also applied to other available silver-based substrates, such as 0.5 mm diameter Ag wire (99.9 %) and sterling Ag (92.5 %). The electrodes were modified in DBSA/KCI for 3 h and then placed in a working cell containing 10 ml PBS pH 6.8, where amperometric measurements were made at - 0.1 V. Cathodic currents from $5\text{-}10^{-3}$ M H_20_2 were recorded and compared to those obtained for Ag SPEs and planar metallic Ag (99.9 %) electrodes. As with planar metallic Ag (99.9 %) electrode substrates, little enhancement in the reduction currents were observed with the DBSA/KCI modified Ag wire and sterling Ag (92.5 %) electrodes with respect to the unmodified ones. Thus, the unmodified Ag wire exhibited a cathodic current of $4.7\cdot 10^{-8}$ A at $5\cdot 10^{-3}$ M H_20_2 whereas the DBSA/KCI modified one showed $4.1\cdot 10^{-8}$ A (Fig. 21).

AgCI was also electrochemically formed onto the Ag wire electrodes by applying the same conditions as those above mentioned in section 3.1.2.[18] and the electrodes were subsequently tested in the presence of H_20_2 (Fig. 24). The increased deposition of AgCI on the Ag wire

electrode did lead to an increase in the catalytic current. Thus, the cathodic current at $5\text{-}10^{-3}$ M H_2O_2 was $1.0 \cdot 10^{-6}$ A for a Ag wire electrode after 2 s in 0.1 M HCl and reached $2.3 \cdot 10^{-6}$ A after 3 x 5 s exposures in 0.1 M HCl. The formation of AgCl on the surface also led to an increase in the background noise and current. For the latter, $4.6\text{-}10^{-8}$ A was observed for the unmodified electrode whereas $2.7 \cdot 10^{-6}$ A was exhibited by the electrode modified 5 s in 0.1 M HCl three times, which reflected the increasing level of surface modification.

Figure 24. Amperometric i-t curves of Ag wire electrodes measured at - 0.1 V (vs Ag/AgCl) in PBS pH 6.8: (a) unmodified; (b) DBSA/KCl modified; (c) AgCl electrochemical formation after 2 s at + 1 V (vs Ag/AgCl) in 0.1 M HCl (d) AgCl electrochemical formation after 5 s at + 1 V (vs Ag/AgCl) in 0.1 M HCl three times, at H_2O_2 concentrations from 1 to $5\text{-}10^{-3}$ M.

This catalytic effect on H_2O_2 reduction after the electrochemical formation of AgCl on the surface could be due to the increase of the electrode surface area, as have been previously reported. [19] However, there is no direct evidences that relates the AgCl formed on the electrode surfaces following DBSA/KCl exposure to the catalytic activity towards H_2O_2 decomposition and electrochemical reduction shown in Section 3.1 .2.

H_2O_2 decomposition. H_2O_2 decomposition was then analysed on Ag metallic electrodes (92.5 % and 99.9 %) using the same conditions as for the Ag SPEs. The initial aim was to check if the catalytic effect was also observed on these substrates and to assess the influence of Ag surface on the H_2O_2 decomposition process. The mass differences were expressed per unit area (g/cm^2). The area values used in the experiments were the geometric areas because the narrow potential range in which Ag is not electroactive has so far prevented the accurate calculations of their electroactive areas.

The measurements of the metallic electrodes, before and after modification, are shown in Fig. 25 and 26. Unlike SPEs, the metallic Ag electrodes did not show decreased responses after multiple H_2O_2 exposures. On the contrary, higher mass decreases were observed on the unmodified 92.5 % Ag electrodes as the number of exposures increased and a steady-state was shown by the same electrodes after DBSA/KCl modification. The 99.9 % metallic Ag electrodes also showed a stable response after being exposed to H_2O_2 solution for 1 hour, either in the modified or unmodified state.

Overall, the 99.9 % Ag electrodes showed significantly higher mass reductions than the 92.5 % Ag, irrespective of the state of modification. These differences were approximately ten-fold after 1 hour of exposure to **H2O2.** Again, the non-linearity of the modified 92.5 % electrode seems significant - in instances where modification has enhanced the catalysis, this seems to be non-linear in nature.

Figure 27 shows the compiled responses of SPE and metallic 92.5 % and 99.9 % Ag electrodes, before and after the DBSA/KC1 modification. The data correspond only to the first of the measurements for each electrode. The catalytic effect observed after surfactant-base modification of Ag SPEs was partially shown by the 92.5 % Ag electrodes. However, the catalytic responses after modification were only three times higher than before for the 92.5 % Ag electrodes, whereas this was about eight times better in the case of SPEs. No enhancement in H_20_2 decomposition was observed on the 99.9 % Ag electrode after surfactant-based modification.

Figure 27. Change in mass per unit area versus time for (a) unmodified and (b) modified (circle) 92.5 %, (triangle) SPE and (square) 99.9 % Ag electrodes when exposed to 1 M H_20_2 solution for 1 hour. These data correspond to the first repetition of each electrode.

Therefore, DBSA/KC1 modification seemed to enhance H_20_2 decomposition only on Ag SPE and metallic 92.5 % Ag electrodes whereas no improved catalytic process was observed on metallic 99.9 % Ag electrodes.

Scanning electron microscopic images of the unmodified metallic 92.5 and 99.9 % Ag electrodes were obtained before and after exposure to 1 M H_20_2 solution (Fig. 28). As can be observed, the 92.5 and 99.9 % Ag metallic electrodes presented smoother surfaces than the SPE electrodes (Fig. 16). Between these two electrodes, the 99.9 % Ag metallic seemed to be the smoothest one and only some scratches were shown on its surface possibly due to the polishing process whereas the 92.5 % Ag metallic surface showed many surface defects, pitting, etc. Following exposure to H_20_2, the formation of reaction products which increased surface roughness were again observed. However, the 92.5 % Ag metallic surface seems to be less affected by H_20_2, which agrees with the low differences of mass obtained with this electrode. On the other hand, 99.9 % Ag electrode shows the roughest surface after H_20_2 decomposition as well as the highest differences of mass observed for that process.

Figure 28. SEM images of unmodified sterling 92.5 % Ag electrodes (A) before and (B) after being exposed to 1 M H_2O_2 solution and 99.9 % Ag metallic electrodes (C) before and (D) after H_2O_2 decomposition measurements. Accelerating voltage of 20 kV. (5.0 k x magnification)

SEM images of the two types of electrodes after the modification with DBSA/KCI were carried out, and the changes before and after exposure to H_2O_2 were compared. These images are shown in Fig. 29. As with Ag SPEs, spheroidal structures were observed on sterling 92.5 % Ag electrodes after DBSA/KCI modification, which were associated with the surface defects of the Ag whereas 99.9 % Ag electrode surfaces didn't show any such structures after the surfactant-based modification. Again the formation of rougher surfaces after the reaction with H_2O_2 was observed in all the Ag electrodes with the difference that either the formation of holes or the creation of reaction products on sterling 92.5 % Ag electrodes was more pronounced (Fig. 28b and 29b) whereas no noticeable changes relative to the unmodified substrates were shown by metallic 99.9 % Ag electrodes (Fig. 28d and 29d). Moreover, sterling 92.5 % Ag electrodes did show greater levels of O_2 evolution during H_2O_2 decomposition reaction after DBSA/KCI modification whereas 99.9 % Ag electrode showed no differences in the amount of O_2 released before and after the DBSA/KCI treatment.

Figure 29. SEM images of modified sterling 92.5 % Ag electrodes (A) before and (B) after exposure to 1 M H_2O_2 solution and 99.9 % Ag (C) before and (D) after H_2O_2 decomposition measurements. Accelerating voltage of 20 kV. (5.0 k x magnification)

Therefore, as was observed before for Ag SPEs, the formation of the spheroidal structures on the electrode surface following DBSA/KCI treatment seemed to be directly implicated in the enhancement of the H_2O_2 decomposition reaction.

Gold-based electrodes

Electrochemical characterization. Other noble metallic substrates were assessed in order to check if it was an isolated effect from Ag surfaces or a general behaviour from this group of metallic elements. Several gold-based electrodes were evaluated and their responses compared to those obtained with silver-based electrodes. In addition, the relationship between metallic Au electrodes and Au paste electrodes was also assessed.

Gold screen-printed electrodes (Au SPEs) were directly exposed to $3.3 \cdot 10^{-2}$ M DBSA/ 0.1 M KC1 for 3 h without any prior pre-treatment, rinsed with distilled water and placed in a working

cell containing 10 ml PBS pH 6.8, where cyclic voltammetry and amperometry were performed. Three types of Au SPEs with different surface areas were assessed. The current densities of these electrodes to $5 \cdot 10^{-3}$ M H_2O_2 at - 0.1 V (vs. Ag/AgCl) are shown in Table 3, before and after DBSA/KC1 modification. Au SPEs showed some enhancement of the H_2O_2 reduction current after the modification with DBSA/KC1, although this effect was not so marked as that shown by Ag SPEs. Thus, the highest ratio of cathodic density current obtained for a modified Au SPE compared to an unmodified one was approx. 12, whereas almost 90 was the ratio obtained with Ag SPEs. Regarding the Au electrodes from Dropsens, Au SPE AT (cured at high temperature) showed a more noticeable catalytic effect after DBSA/KC1 pre-treatment, with approx. $8.03 \cdot 10^{-6}$ A/cm^2, than Au SPE BT (cured at low temperatures), on which the cathodic current was only $0.51 \cdot 10^{-6}$ A/cm^2. Although there was already a three-fold difference between their cathodic currents in the unmodified state, this contrast was more remarkable after the modification, with a sixteen-fold difference. The variation between both electrodes could be a consequence of the different surface roughness.

Table 3. Cathodic current densities of Au SPEs to $5 \cdot 10^{-3}$ M H_2O_2 at - 0.1 V (vs. Ag/AgCl) before and after DBSA/KC1 treatment.

Electrode	Area (cm^2)	i_{unmod}/A (μA/cm^2)	i_{mod}/A (μA/cm^2)	i_{mod}/i_{unmod}
Au SPE AT (Dropsens)	0.126	0.66	8.03	12.17
Au SPE BT (Dropsens)	0.126	0.27	0.51	1.89
Au SPE (DuPont)	0.045 (unmod)/ 0.040 (mod)	1.69	11.21	6.63
Ag SPE	0.126	3.08	273.57	88.82

Generally, electrodes cured at higher temperature show rougher surfaces because the organic compounds presented in the printable ink are evaporated from the substrates when the temperature increases.[28] Thus, Au SPEs AT may be more prone to DBSA/KCl modification because they would present a higher surface area than Au SPEs BT and this would increase the amount of H_2O_2 able to be reduced on them. However, differences in organic binder composition cannot be excluded. In any case, the catalytic effect obtained by the gold-based SPEs was very low in comparison to that of Ag SPEs. One possible explanation is the higher tendency of Cl^- in the modification solution to form AgCl rather than AuCI (standard enthalpies of formation of AgCI and AuCI are 97 and 189 kJ/mole, respectively),[33] which was previously observed as a likely important step in the subsequent enhancement of H_2O_2 reduction.

Planar metallic Au (99.9 %) electrodes (A = 0.031 cm^2) were also assessed. They were polished using first 0.3 μm and later 0.05 μη alumina. Then, they were rinsed and sonicated in distilled water. Once cleaned, they were exposed to $3.3 \cdot 10^{-2}$ M DBSA/ 0.1 M KC1 for 3 h. The amperometric responses at - 0.1 V (vs Ag/AgCl) obtained in PBS pH 6.8 before and after DBSA/KCl modification are shown in Fig. 30.

Figure 30. Amperometric i-t curves of metallic Au (99.9 %) electrodes measured at - 0.1 V (vs Ag/AgCl) in PBS pH 6.8: (a) unmodified and (b) DBSA/KCl modified, at H_20_2 concentrations from 1 to $5 \cdot 10^{-3}$ M.

DBSA/KCl modification did not seem to improve the catalytic features of metallic Au (99.9 %) electrodes, as can be observed by comparing the amperometric responses from the unmodified and DBSA/KCl modified electrodes. While 41.11 μA/cm^2 was shown by the unmodified Au metallic electrode in the presence of $5 \cdot 10^{-3}$ M H_20_2, only 31.72 μA/cm^2 was obtained with the DBSA/KCl modified one. Furthermore, comparing these data to those presented for Ag SPEs, metallic Au (99.9 %) showed higher reduction current values, which is probably due to the available metallic surface area of conductivity. However, the Ag SPEs showed greater increases in catalytic currents when treated with DBSA/KCl than did metallic Au. This may relate to availability of surface defects or the deposition/modification sites not available on planar metallic Au (99.9 %).

B). H_20_2 decomposition. Following the study of the catalytic effect of H_20_2 decomposition on silver-based electrodes, the same effect was studied on gold-based electrodes. Metallic Au (99.9 %) electrodes were polished using 0.3 and 0.05 μηι alumina, and subsequently rinsed with distilled water and sonicated for 5 min in order to clean the surfaces before the modification. Then, they were immersed in fresh $3.3 \cdot 10^{-2}$ M DBSA/ 0.1 M KC1 solution for 3 hours. Au SPEs were directly dipped into the surfactant-based solution without any pre-treatment. Subsequently, H_20_2 decomposition was analyzed by submerging the electrodes in 1 M H_20_2 solution for 1 h. Mass differences were registered every minute and compared to the previously obtained decomposition data for silver-based electrodes. The data from the metallic Au and SPEs are presented in Fig. 31 and Fig. 32, respectively. Both gold-based electrodes did not show remarkable differences over H_20_2 decomposition before and after DBSA/KCl modification. Thus, unmodified metallic Au (99.9 %) electrode showed a change in mass per unit area of 0.026

g/cm^2 after a 1 h reaction in 1 M H_2O_2 whereas the same electrode after the modification showed only 0.023 g/cm^2 for the first measurement. Subsequent exposures resulted in changes of 0.01 5 and 0.018 g/cm^2, respectively. This indicated that the modification did not enhance the catalytic behaviour of this type of Au electrodes towards H_2O_2 decomposition. Similarly, unmodified Au SPEs exhibited changes of 0.006 g/cm^2 after H_2O_2 reaction whereas the modified ones showed 0.008 and 0.007 g/cm^2 after the first and second exposure to H_2O_2, respectively.

Figure 32. Change in mass per unit area versus time for (a) unmodified and (b) modified Au SPEs after exposure to 1 M H_2O_2 solution for 1 hour. The number of exposure is indicated besides each graph.

Both types of electrodes did not exhibit improved catalytic effect on H_2O_2 decomposition after the modification or noticeable changes in mass per unit area after subsequent measurements. However, greater mass decreases were obtained using the metallic Au (99.9 %) electrodes compared to the Au SPEs, as was commented on before and is shown in Fig. 33. This behaviour was already observed for the silver-based electrodes, where the differences of masses obtained for the metallic electrode were higher than those obtained for the SPE or sterling 92.5 % Ag ones. In that case, an approx. 20 times greater difference of mass was obtained with the unmodified metallic 99.9 % Ag electrode, reaching a total loss of 0.414 g/cm^2, whereas only 0.026 g/cm^2 loss resulted by using the metallic Au electrode. These results were expected because Ag is a known catalyst of H_2O_2 decomposition whereas no similar behaviour has been reported for gold-based materials.

Figure 33. Change in mass per unit area versus time for (a) unmodified and (b) modified (square) Au (99.9 %) metallic electrodes and (circle) Au SPEs upon exposure to 1 M H_2O_2 solution for 1 hour. These data correspond to the first repetition of each electrode.

Platinum-based electrodes

A). Electrochemical characterization. Platinum screen-printed electrodes (Pt SPEs) from two different sources were modified following the same procedure as that used for Ag and Au SPE pre-treatment. After the modification in $3.3 \cdot 10^{-2}$ M DBSA/ 0.1 M KC1 solution, amperometric measurements were performed and the cathodic currents obtained for $5\text{-}10^{-3}$ M H_2O_2 are shown in Table 4. Pt is the best known catalyst for H_2O_2 reduction, and this fact is supported by the cathodic current data obtained even with unmodified Pt SPEs. Comparing the values obtained for

the different metallic substrates before any modification, Pt SPEs presented up to three orders of magnitude higher responses to H_2O_2 than Au SPEs and up to two orders of magnitude higher than Ag SPEs, as is shown in Table 3 and 4. Thus, cathodic current of the unmodified Pt SPE (Dropsens) at $5\text{-}10^{-3}$ M H_2O_2 was $480.95 \cdot 10^{-6}$ A whereas the responses for Au AT and Ag SPEs were $0.66 \cdot 10^{-6}$ and $3.08 \cdot 10^{-6}$ A, respectively.

Table 4. Cathodic current of Pt SPEs at $5\text{-}10^{-3}$ M H_2O_2, - 0.1 V vs Ag/AgCl, before and after DBSA/KC1 treatment.

Electrode	Area (cm^2)	i_{unmod}/A ($\mu A/cm^2$)	i_{mod}/A ($\mu A/cm^2$)
Pt SPE (Dropsens)	0.126	480.95	956.27
Pt SPE (Dupont)	0.035	959.43	910.00

However, after DBSA/KCI modification, Ag SPEs presented reduction currents of $273.57 \cdot 10^{-6}$ A, in the same order of magnitude than Pt SPEs, $956.27 \cdot 10^{-6}$ A (only a 3.5-fold difference). This showed the marked catalytic effect of DBSA/KCI on this kind of substrate. Thus, Pt showed almost no enhancement in H_2O_2 reduction after the surfactant-based pre-treatment, and gold-based electrodes only presented a moderate effect, as was shown earlier. Only silver-based electrodes, and particularly Ag SPEs, seemed to be highly improved by DBSA/KCI modification, which again enforces the theory of AgCl formation as an intermediate in the catalytic process.

B). H_2O_2 decomposition. Despite the fact that Pt is a well known catalyst for H_2O_2 decomposition, Pt SPEs were modified with DBSA/KCI in order to analyze if the catalytic effect observed with the silver-based electrodes was also exhibited by this material. The electrodes were modified following the same procedure previously reported for Ag and Au SPEs and were subsequently submerged in 1 M H_2O_2 (2 ml) for 1 h. The results for the unmodified and modified substrates are presented in Fig. 34. Pt SPEs modified with the DBSA/KCI solution showed at least ten-fold greater rates of catalytic decomposition when they were exposed to 1 M H_2O_2 than those registered for the unmodified substrates. Thus, changes in mass per unit area of 0.005 g/cm^2 were registered by the unmodified electrodes whereas 0.046 g/cm^2 were reported by the modified ones. Moreover, it seemed that the decomposition process was enhanced over time because the data obtained during the second measurement, 0.093 g/cm^2 change in mass after 1 h

in 1 M H_2O_2, were significantly greater than those obtained during the first measurement. This phenomenon is not only reflected by the differences in mass after 1 h reaction, but also by the increasing slopes of the plots at the first stages of the decomposition, which is proportional to the initial rate of the reaction and will be discussed in the next section.

Figure 34. Change in mass per unit area versus time for (a) unmodified and (b) modified Pt SPEs upon repeated exposure to 1 M H_2O_2 solution for 1 hour. The number of exposures is indicated besides each graph.

Comparing the data obtained for different metal SPEs, both Ag and Pt showed an enhancement in the H_2O_2 decomposition process after being treated with DBSA/KCl solutions. The losses of mass per area after 1 hour reaction were approx. 8 and 10 times higher than those obtained by the same unmodified Ag and Pt electrodes, respectively. However, Au SPEs did not show any catalytic effect after the above mentioned modification, presenting the same behaviour before and after dipping into DBSA/KCl solution.

Kinetic study of $H^{\wedge}O_2$ decomposition on unmodified and DBSA/KCl modified metallic surfaces

As is well-known, a catalyst is a substance that participates in a chemical reaction by increasing the rate of reaction. In order to compare the catalytic effect on H_2O_2 decomposition of the above-studied metallic electrodes before and after the modification, rate constants of the decomposition reactions were calculated.

The reaction rate is defined as the change in the advancement of the reaction with time, i.e. the change in the number of moles of a given species (reactant or product) with time:

$$R = \frac{1}{v_i}\frac{d[i]}{dt} \qquad \text{(Equation 1)}$$

where R is the intensive reaction rate, v, is related to the stoichiometric coefficient of species i and [i] is the molarity of species i. The rate of a reaction will generally depend on the temperature, pressure and concentrations of species involved in the reaction as well as the phase or phases in which the reaction occurs. The empirical relationship between reactant concentrations and the rate of a chemical reaction is know as a rate law, and it is written as:

$R = k [A]^{\alpha} [B]^{\beta} \ldots$ (Equation 2)

where [A] is the concentration of reactant A, [B] is the concentration of reactant B, and so forth. The constants a and β are the reaction orders with respect to A and B, respectively, and k is referred to as the rate constant for the reaction. The rate constant is independent of concentration, but dependent on pressure and temperature. [34]

The rate constant of H_20_2 decomposition was determined by measuring the mass of 0_2 liberated as a function of time at room temperature. The mass data were rearranged to be expressed as the H_20_2 concentration remaining in the vial versus time to study the kinetics of the reaction. All obtained results revealed that such decomposition followed pseudo first-order kinetics:

$$-\frac{d[H_2O_2]}{dt} = k_{app}[H_20_2] \quad \text{(Equation 3)}$$

and thus,

$$\ln\frac{[H_2O_2]_t}{[H_2O_2]_0} = -*_{app}t \quad \text{(Equation 4)}$$

where k_{app} is the apparent first-order H_20_2 decomposition rate constant, and $[H_20_2]$, and $[H_20_2]_0$ are the concentrations of H_20_2 in the solution at time t and time zero, respectively. The data from Ag SPEs before and after modification with DBSA/KCI are shown in Fig. 35.

Figure 35. Plot -In $[H_2O_2]/[H_2O_2]_0$ versus time for (a) unmodified and (b) modified Ag SPEs after exposure to 1 M H_20_2 solution for 1 hour.

As was mentioned above, the data appears to be linear during the first ten minutes, after which it deviates from linearity. This observation could be as a result of the formation of a diffusion layer at the surface, which could become a limitation of the reaction, or as a result of bulk substrate limitation (mass transport). As the measurements with the unmodified and modified Ag SPEs were performed in a vial containing 2 ml 1 M H_20_2, the maximum mass of 0_2 which could be released was 0.034 g. After 1 hour reaction, the difference of mass observed with the modified electrode was approx. 0.010, which means that almost a third of the H_20_2 in the solution had

been broken down. The fast disappearance of H_2O_2 in the vicinity of the electrode surface could provoke the shape observed in the plots as H_2O_2 does not diffuse as fast towards the surface as it decomposes. Changes or losses of the surface catalytic activity over time could also lead to deviations from the linear behaviour. More precise and detailed determination of the heterogeneous rate constant would require treatment of the diffusion processes at the heterogeneous interface. For simplicity, however, further analysis was based on initial constants using the initial linear portion of the responses. Initial rates for Ag SPEs are shown in Fig. 36.

The same study was carried out using 92.5 % and 99.9 % Ag as well as SPE and metallic Au electrodes and Pt SPE. The apparent rate constants obtained with each electrode are summarized in Table 5.

Table 5. Apparent initial rate constants k_{app} for H_2O_2 decomposition on different metallic catalysts.

		Ag			Au		Pt
		SPE ($A=0.126cm^2$)	**92.5 %** ($A=0.6cm^2$)	**99.9 %** ($A=0.031cm^2$)	**SPE** ($A=0.1cm^2$)	**Metallic** ($A=0.031cm^2$)	**SPE** ($A=0.1cm^2$)
Unmod. k_{app} ($x10^{-5}$ s^{-1})	R1	1.52	0.68	1.04	0.40	0.05	0.43
	R2	2.96	2.94	1.06	--	--	--
	R3	1.41	5.66	--	--	--	--
DBSA/KCl k_{app} ($x10^{-5}$ s^{-1})	R1	19.70	29.2	1.08	0.64	0.04	3.91
	R2	8.12	53.7	0.97	1.20/5.2	0.03	9.95
	R3	4.11	57.8	--	--	0.03	--

R1 - repeat 1; R2 - repeat 2; R3 - repeat 3

The apparent initial H_2O_2 decomposition rate constants obtained for Ag SPEs after the modification with DBSA/KCI were ten times (for the first measurement) and four times (for the second and third repeats) higher than those obtained for the same electrodes without any modification, respectively. Thus, apparent rate constants of 1.52, 2.96 and 1.41 s^{-1} were obtained by the unmodified Ag SPEs after the first, second and third exposure to 1 M H_2O_2, respectively whereas 19.7, 8.12 and 4.11 s^{-1} were obtained by the modified ones under the same measurement conditions. The decrease in the catalytic responses observed for the modified electrodes as a function of the repeat could be explained as a loss of the surface modification or surface inactivation with the time, even though, H_2O_2 decomposition was up to four times faster than the same process carried out on the unmodified electrodes. More remarkable is the catalytic effect observed on the sterling 92.5 % Ag electrodes after the modification. The unmodified electrode

showed an increase of decomposition rate as the substrate was re-measured. Thus, this electrode exhibited an initial rate constant of 0.68 s^{-1} for the first measurement and 2.94 and 5.66 s^{-1} for the subsequent exposures to 1 M H_2O_2. A similar growth trend was observed for the modified electrodes, although in this case the apparent rate constants of 29.2, 53.7 and 57.8 s^{-1} respectively were thirty times higher than those obtained with the unmodified electrodes. Unlike SPEs and sterling 92.5 % Ag electrodes, no differences in the kinetic data were observed using metallic 99.9% Ag electrodes before and after the modification. Apparent rate constants of 1.04 and 1.06 s^{-1} were obtained by the unmodified electrodes after the first and second exposure to H_2O_2, respectively, whereas 1.08 and 0.97 s^{-1} were obtained for the modified electrodes. The apparent rate constant for the unmodified electrode was approx. the same order of magnitude as those obtained from the unmodified **SPE** and 92.5 % Ag and this did not change after exposure to the **DBSA /KC1** solution. With regard to the gold-based electrodes, they did not show any enhancement on H_2O_2 decomposition after **DBSA /KC1** modification. Moreover, the apparent rate constants obtained using metallic 99.9 % Au electrodes (0.05 s^{-1}) were quite low relative to those exhibited by Ag electrodes. This agrees with the fact that silver is a known catalyst for H_2O_2 decomposition [35] whereas no similar data have been reported for Au up to know. On the other hand, Pt SPEs also showed a catalytic effect on H_2O_2 decomposition after their treatment with DBSA/KC1, leading to ten times higher $\mathbf{k_{app}}$ on the modified surfaces relative to the same unmodified substrates.

To compare accurately the catalytic activity of the different metallic substrates, the apparent rate constants must be normalized to the surface area of the catalysts. Falcon and Carbonio showed that the heterogeneous reaction for peroxide decomposition is a slow process and the transport to the surface would therefore be diffusion controlled. Under these conditions, the heterogeneous rate constant can be expressed as:

$$\mathbf{k_s\ (Cm\ S^{-1}) = Vijqkapp/Acat}$$

where $\mathbf{Vi_{,q}}$ is the volume of solution (in ml), and $\mathbf{A_{ca}t}$ the surface area of the catalyst (cm^2).[36, 37]

The heterogeneous rate constants of the studied metallic substrates are reported in Table 6.

Table 6. Heterogeneous rate constants k_s for H_2O_2 decomposition on different metallic catalysts.

		Ag			Au		Pt
		SPE ($A=0.126cm^2$) $V_{liq}=2ml$	**92.5 %** ($A=0.6cm^2$) $V_{liq}=2ml$	**99.9 %** ($A=0.031cm^2$) $V_{liq}=27ml$	**SPE** ($A=0.1cm^2$) $V_{liq}=2ml$	**Metallic** ($A=0.031cm^2$) $V_{liq}=27ml$	**SPE** ($A=0.1cm^2$) $V_{liq}=2ml$
Unmod. k_s ($x10^{-4}$ $cm \cdot s^{-1}$)	R1	2.4	0.2	90.0	0.8	4.3	0.9
	R2	4.7	1.0	92.0	--	--	--
	R3	2.2	1.9	--	--	--	--
DBSA/KCl k_s ($x10^{-4}$ $cm \cdot s^{-1}$)	R1	31.0	9.7	94.0	1.3	3.9	7.8
	R2	13.0	18.0	84.0	2.4/1.0	2.2	20.0
	R3	6.5	19.0	--	--	2.7	--

R1 – repeat 1; R2 – repeat 2; R3 – repeat 3

Unmodified metallic 99.9 % Ag showed the highest heterogeneous rate constant for H_2O_2 decomposition and it did not change after its treatment with DBSA/KCl. Unlike metallic 99.9 % Ag and SPE, sterling 92.5 % Ag electrodes improved their H_20_2 decomposition responses up to 10 times after exposure to the surfactant-based solution. Similar enhancement was presented by Pt SPEs after being modified with DBSA/KCl. The responses obtained with unmodified gold-based electrodes were close to those shown by the other metallic electrodes under study, except for metallic 99.9 % Ag. However, no improvements were observed after the surfactant-based modification, as is shown by no change in the heterogeneous rate constants before and after the modification. The overall data from the unmodified electrodes were of the same order of magnitude than those previously reported.[37]

SUMMARY

Hydrogen peroxide reduction has been shown to be enhanced on Ag SPEs after their modification with DBSA/KCl solutions. $3.3 \cdot 10^{-2}$ M DBSA and 0.1 M KC1 as well as 3 h modification time have been presented as the optimum conditions in order to obtain the highest cathodic current, assessed in the presence of $5\text{-}10^{-3}$ M H_20_2. Moreover, the reduction process was highly favoured in basic solutions for the modified electrodes. SEM images presented the formation of spheroidal structures on the modified surfaces, which consisted of Ag and CI, which were affected after the electrochemical H_20_2 reduction on them, remaining as only Ag-based structures, as was evidenced by EDX. Two possible explanations to the catalytic effect shown by DBSA/KCl modified Ag SPEs have been suggested. On one hand, the surfactant/salt combination may undergo changes on the Ag morphology with the subsequent formation of nanostructures, which would increase the active surface area available to perform the electrochemical H_20_2 reduction. On the other hand, the micellar or lamellar structures possibly formed by the DBSA/KCl in solution may have become deposited onto the Ag SPE in some

way, creating an enhanced surface for the catalytic processes. The effect of the surfactant/salt modification on other metallic electrodes and their catalytic activity towards the electrochemical **H2O2** reduction has been also studied.

The surfactant-based modification on several metallic-based electrodes also seemed to induce an enhancement on **H2O2** decomposition. The greater differences of mass due to the release of O_2 during **H2O2** decomposition after the electrodes were treated with DBSA/KCl showed the surfactant-based solution produced an improvement in the catalytic process. Such an enhancement was proven by the increase of the heterogeneous rate constants obtained after the kinetics study carried out on both unmodified and modified electrodes. It showed that DBSA/KCl modification on the metallic surfaces provided an easier mechanism for H_20_2 decomposition. On the other hand, Au and Pt substrates did not show as high a catalytic effect on both electrochemical H_20_2 reduction and **H2O2** decomposition after DBSA/KCl modification as Ag electrodes.

Ag SPEs after the modification with DBSA/KCl resulted into an effective alternative to electrochemical ly quantify **H2O2** concentration. The easy and low cost manufacture makes this non-enzymatic device a unique platform for ¾ O_2 sensing.

APPLICATION OF Ag SPEs AS HyPer SENSOR FOR CHOLESTEROL BIOSENS1NG

HyPer sensors (modified Ag SPEs) were used as described in Materials and Methods for cholesterol sensing. The electrochemical cell was filled with 1 ml enzyme buffer solution (buffer according to Audit Diagnostics protocol where cholesterol oxidase concentration was increased 200-fold). By addition of cholesterol solution (lyophilized sample), a three-point calibration curve over the concentration range of 1-5 mM was constructed where the change in current on addition of the cholesterol solution was monitored. Cholesterol concentrations used were 4.8 mM, 3.2 mM and 0.86 mM. (Note: these cholesterol concentrations were achieved by adding different volumes of lyophilised cholesterol solution, as opposed to prior preparation of a dilution series of varying concentrations. Therefore, the enzyme concentration was different for each cholesterol concentration used (the rates therefore of the catalysis varied over the range, but the absolute response could still be measured.)

A three-point calibration curve, monitoring the increase of the current after addition of cholesterol solution, was constructed and is shown below in Fig. 37.

Figure 37: Calibration curve of cathodic current increase against cholesterol concentration. Working Electrode: HyPer. Buffer solution: Made up according to Audit Diagnostics protocol with 200-fold increase in cholesterol oxidase concentration. Inset: Signal based on increase in amperometric current from trough to peak.

Specificity of the response

As the cholesterol was added in different volumes in order to vary the cholesterol concentration, it was considered that the initial drop in current that was observed (See Fig. 37 inset) could have been due to a change in ionic strength of the solution rather than the amount of cholesterol added. In order to investigate if the change in ionic strength was contributing to the signal, a range of solutions with differing ionic strengths were added to the electrochemical cell, (where the control electrolyte in this instance was PBS containing 0.138 mg L^{-1} of BSA protein) and the response monitored. Fig. 38 shows the effect of the addition of cholesterol sample (overall concentration: 3.2 mM) (Red), control buffer (AD buffer with cholesterol oxidase increased 200-fold) (purple) and deionised water (green) to a buffer solution containing of Bovine Serum Albumin (BSA) (0.138 mg L^{-1}).

Figure 38: Effect of addition of various solutions to BSA to monitor the current drop. Working Electrode: HyPer. A current decrease is observed when cholesterol was added to the system. Negligible, if any oxidation current was observed for buffer or H_20 additions to the system.

The addition of cholesterol to the system resulted in a significant current drop (anodic response). This is a non-specific response which may result from a change in conductivity of the solution due to cholesterol itself being non conductive cholesterol micelles are also known to form in aqueous solution (Biophys.J. 1992, 63, 1455-1461). It is also possible that there may be some direct redox activity associated with the cholesterol that is resulting in this initial electrode response.

Although this initial response is not ideal or fully understood, it is clear that it is due to an interaction of the cholesterol with the solution or the electrode but that it doesn't affect the

specific cathodic response that is observed which is due to the catalytic breakdown of the in-situ generated hydrogen peroxide. In addition, it may be possible to offset these signals by employing appropriate potential steps in the final assay protocol to eradicate the electrode discharge current completely.

The calibration experiments were repeated using cholesterol standard solutions in the range of 0.2 to 3.2 mM by preparing a dilution series of a 3.2 mM cholesterol stock solution. For each of experiment, 500 μL of the appropriate cholesterol solution was added to 1000 μL of enzyme buffer.

For each of the experiments, the current increase, the slope of the increase and the length of time from initial addition to the maximum response was monitored. The calibration curves obtained are shown in Fig.s 39-41.

Dilution	Concentration, mM
Stock	3.2
1/2	1.6
1/4	0.8
1/8	0.4
1/16	0.2

Table 1: Dilution series of the lyophilized cholesterol used for the calibration curve

Figure 4 1: Calibration graph of the time taken to reach the maximum amperometric cathodic response of HyPer electrode to additions of leophilised cholesterol over the concentration range 0.5 - 3.2 mM.

All parameters examined (current increase, slope and response time) could be used to quantify the amount of cholesterol in the system. However, a time-based assay (Fig. 41) is inappropriate and the time taken to reach maximum current response is too long to be suitable for a rapid

assay. Therefore, using the response rate (Fig. 40) may be a viable way of obtaining a reliable and rapid response...

Having established that calibration in cholesterol/cholesterol oxidase was possible, further optimization of the sensor system was undertaken, particularly with respect to the speed of response and the impact of assay constituents such as the enzyme and buffer on the speed and amplitude of the amperometric signal. Experiments were performed to show that in the presence of the AD Pipes buffer, the electrode's direct response to hydrogen peroxide decreased, indicating that the electrode was being affected by a component of the buffer system. The buffer and constituents, the presence of protein were all investigated and one strategy which was used to overcome this issue was to examine some membranes to isolate the electrode from the bulk solution components but which would still allow hydrogen peroxide generated to permeate through to be electroreduced at the HyPer surface.

The effect of buffer

The effect of the enzyme buffer on the electrochemistry of H_20_2 at the electrode surface was determined by analysing the response of a HyPer electrode to the addition of a 10 L aliquot of 50 mM H_20_2. Buffers examined were PBS (pH 7.0) and Pipes (with and without enzyme) (Fig. 42).

Figure 42: Response of HyPer electrode to 10 mL H_20_2 injections (each addition was equivalent to 0.5 mM H_20_2).

The buffer of PBS containing cholesterol oxidase and lipo-lipase showed much more significant response to H_20_2 than compared to the Pipes/$MgCl_2$. The Pipes/$MgCI_2$ buffer with and without enzyme showed comparable responses again illustrating that the presence of the enzyme was not the source of the deleterious effect on the sensor's response to H_20_2.

The effect of enzyme/protein

To further rule out that the reduction in response was not due to the cholesterol oxidase enzyme/protein in the sample, e.g., by non-specific adsorption, BSA was used in place of cholesterol oxidase enzyme in varying concentrations and the sensor's response to H_20_2

investigated. Modification of the electrode with a Nafion membrane was also investigated to see would this have any beneficial effect. The amperograms are shown below in Fig. 43. The performance of the electrode was monitored by adding 10 µL of a 50mM H_2O_2 solution at 100 s intervals.

The results show that the large concentrations of BSA used had no effect on sensor response to H_2O_2 and so it is likely that adsorption of protein directly to the surface of the electrode does not occur, or at least does not affect the response of the electrode to hydrogen peroxide (Fig. 43a). The results also demonstrated that using a Nafion layer did increase the sensor response (Fig. 43b).

Figure 43: Amperometric responses of the Nafion-coated HyPer electrodes (A) and bare HyPer electrodes (B) to H_2O_2 (0.5 mM) in the presence of varying amounts of BSA in bulk solution. The effect of Nafion or of increasing the amount of BSA in the solution does not affect the sensor response to hydrogen peroxide.

From this and the previous experiments it was determined that the buffer constituents and not the enzyme were the cause in the reduction of the system response to H_2O_2 and that if these effects could be reduced or removed, then the sensor should perform well as a cholesterol sensor.

Investigation of buffer constituents

The effect of the buffer components was examined in more detail by looking at the direct electrochemistry of H_2O_2 reduction in the presence of the individual components of the AD buffer solution. Fig. 44 shows the amperograms with H_2O_2 additions where the effect of the presence of PBS, Pipes/MgCI, $MgCI_2$ and Pipes was monitored. The Pipes/$MgCl_2$ containing buffer showed much lower initial responses to H_2O_2. Pipes buffer or $MgCl_2$ alone, gave higher responses to that of the Pipes/$MgCl_2$ buffer indicating that they appear to have a combined effect.

Figure 44: Response of HyPer electrode to H_2O_2 injections (each addition was equivalent to 0.5 mM H_2O_2) in the presence of PBS (0.13813 g/10 ml), PIPES/$MgCI_2$ (as per AD Buffer), $MgCl_2$ (0.005 g/10 ml) and PIPES (0.13813 g/10 ml).

Investigation of the addition of membrane layers

Nafion and Chitosan were both examined as membrane layers to reduce the impact of buffer effects. Nafion solution (3 μL, 1% w/v) was drop-coated onto the HyPer electrode and allowed to dry. The performance of the electrode was monitored by adding 10 μL of a 50mM H_2O_2 solution (overall concentration: 0.5 mM) to a BSA protein buffer solution at 100 s intervals (BSA was employed as a non-specific control protein). Chitosan-coated HyPer electrodes were prepared similarly (according to Section 2.1) and similar responses were observed. Neither chitosan nor Nafion were shown to have any negative effects on the electrode, and so were proved as potentially a valid approach for protecting the electrode surface.

Figure 45: Amperometric responses to hydrogen peroxide (0.5 mM additions) of the Nafion-coated HyPer electrode in AD PIPES buffer. It can be observed that there is no significant effect on the initial response of the electrode to hydrogen peroxide when a Nafion membrane is employed.

The Nafion-coated electrode showed increased amperometric responses to H_2O_2 as compared to an equivalent HyPer electrode (Fig. 45).

Chitosan, a linear polysaccharide, which is present in the shells of shellfish, was also looked at as a potential membrane modification for the electrode. With injections of 10 μL 50 mM H_2O_2, the response was monitored (Fig. 46). Using a HyPer electrode, it was again evident that the Pipes/MgCh electrolyte buffer was the cause of the reduction of the electrochemical response, as indicated by the purple line in Fig. 46. The red line shows a HyPer electrode in PBS buffer, which has an initial response of more than double that of the electrode in Pipes.

A HyPer electrode coated with 3 μL 1% solution of chitosan was also examined for its response to H_2O_2. This electrode was placed in the Pipes/$MgCl_2$ solution and the initial response for the first injection of H_2O_2 was greater than that of the bare HyPer electrode in PBS. It was evident that the chitosan barrier has a beneficial effect on the detection of H_2O_2 using the HyPer electrode in Pipes/$MgCl_2$.

Figure 46: Amperograms showing electrode responses to injections of H_2O_2 in buffers PBS and Pipes. It can be seen that the HyPer electrodes response could be improved in Pipes buffer by employing the chitosan membrane.

In order to further optimise the chitosan modification, the HyPer sensors were fabricated with a range of volumes of chitosan (1% w/v) dropped onto the surface of the HyPer electrode and tested with cholesterol oxidase and cholesterol at 1.6 mM. In the range of deposited volumes studied it appears that smaller volumes led to more rapid and larger response times, consistent with reductions in the thickness of the diffusional barrier (Fig. 47). Further optimisation of this layer will need to be investigated to further reduce its thickness and impact on diffusion, while also maintaining an effective barrier to the buffer constituents.

Figure 47: Effect of the amount of chitosan (1%) used to modify the electrode. 3 ul chitosan dropped onto the surface of the electrode results in the highest response and fastest response time (750 s approx. from initial addition of cholesterol at t = 500 s. (1.6 mM concentration).

The chitosan-modified electrode was further compared to that of a bare HyPer electrode. Fig. 48 shows the amperometric response of the electrodes to cholesterol (500 mL of Cholesterol - overall concentration 1.6 mM) in the presence of AD buffer containing cholesterol oxidase comparing the HyPer electrode with a 1% chitosan-coated HyPer electrode. This does appear to show that the slope of the response for the chitosan-modified electrode is greater than the unmodified electrode (response time of 750 s as compared to 1480 s).

Figure 48: Addition of cholesterol (1.6 mM) at time = 500 s. Red line is the amperometric response from a chitosan-coated HyPer electrode. Black line is the amperometric response from a bare HyPer electrode. Response time from the chitosan- HyPer is 700 s, while the response time of the bare HyPer electrode was approx. 1500s.

Enzymatic Cholesterol Responses in Different Buffers

To look at the effect of buffer on sensor performance, the Pipes/$MgCl_2$ buffer and an alternative buffer system based on Bis-Tris/$MgCI_2$ were both investigated. In addition, sensors were also modified with the chitosan membrane as before and also a cellulose acetate membrane layer. In the case of the Pipes/$MgCl_2$ buffer (Fig. 49) the results show that chitosan-coated HyPer

electrode has the most rapid response and was quickest to reach its peak value (750 s) compared to bare HyPer electrode which had a time of 1228 s. The cellulose acetate-coated HyPer electrode had an even longer response time of 1823 s.

Figure 49: Addition of cholesterol (1.6 mM)) at time = 400 - 500 s. Pipes $MgCl_2$/ Cholesterol Oxidase AD Buffer with various electrode barriers. Dark blue line is the amperometric response from a chitosan HyPer electrode. Red line is the amperometric response from a HyPer electrode. Blue line is the amperometric response from a cellulose acetate—coated HyPer electrode Response time from the chitosan-modified electrode is 750 s, while the response time of the bare electrode was approx. 1500s.

Table 2: Pipes/$MgCl_2$ Cholesterol oxidase buffer for cholesterol response with various electrode barriers.

	Current increase (A)	Slope (A/s)	Time (s)
Unmodified	8.4×10^{-7}	5.4×10^{-10}	1228
Chitosan	7.2×10^{-7}	1.1×10^{-9}	715
Cellulose acetate	1.4×10^{-6}	4.1×10^{-10}	1823

In the case of the Bis-Tris buffer, however, overall amperometric responses were poor compared to Pipes/$MgCl_2$. In this case, the bare HyPer electrode had the fastest and highest response for the injection of cholesterol, followed by the chitosan HyPer electrode and then the cellulose acetate HyPer electrode (Fig. 50). Bis-Tris did not improve the responses of any of the electrodes and should not be used in place of Pipes buffer.

Figure 50: Addition of cholesterol (1.6 mM) at time = 500 s using Bis-Tris $MgCl_2$/ cholesterol oxidase buffer with various electrode membranes. Red line is the amperometric response from a HyPer electrode. Purple line is the amperometric response from a chitosan-coated HyPer electrode. Blue line is the amperometric response from a cellulose acetate—coated HyPer electrode Response time from the chitosan-modified electrode is 700 s, while the response time of the bare electrode was approx. 1500s.

Table 3: Bis-Tris/$MgCl_2$ buffer for cholesterol response with various electrode barriers

	Current increase (A)	Slope (A/s)	Time (s)
Unmodified	5.5×10^{-7}	3.9×10^{-10}	778
Chitosan	5.2×10^{-7}	3.0×10^{-9}	1043
Cellulose acetate	9.5×10^{-6}	2.2×10^{-10}	1621

HyPer technology developed to date

This research was commenced on the basis that there was preliminary data showing that the HyPer electrode responded to enzymatically generated hydrogen peroxide. However, the main issue with the system was that the response times were prohibitively long (1300 s approx.) and so was not suitable in that form for the AD assay. This feasibility study involved looking into the reasons behind the long response times as well as strategies to reduce the response time of the sensors to less than 600 s. It was found that the co-factor $MgCI_2$ as well as the PIPES buffer appeared to have negative effects on the electrode response. The actual interaction is not fully understood, however several strategies were looked at over the study to overcome these effects. Membranes were examined as potential materials that could isolate the electrode from the negative effects of the buffer solution - Nafion, chitosan and cellulose acetate were examined. Both Nafion and Chitosan were shown to be promising materials as membranes. It was shown that using chitosan, the response time was decreased approximately 2-fold, reducing the peak response time to 750 s approximately in the PIPES buffer.

Alternate buffer systems were also examined: PBS and Bis-Tris. Bis-Tris was found not to be a suitable buffer for the cholesterol response. More work would be required to see if PBS or indeed any other system could replace the PIPES in order to eliminate the inhibitory effect on the sensor.

Currently, the platform in place can detect cholesterol (1.6 mM) within 700 s over the concentration range - 0 - 5 mM. However, further work is required to generate solid analytical calibration data to show the improvements that the chitosan layer has on the system when compared to the bare electrode.

Example of Ag DBSA/KC1 Application as a Glucose Sensor

1. Materials and Methods

1.1. Materials

Dodecylbenzenesulfonic acid (DBSA-D0989) was purchased from TCI Europe. Sodium and potassium chloride (NaCl, KC1), potassium dihydrogen phosphate (KH_2P0_4), alpha-D-(+)-glucose, cellulose acetate (CA), hexamethylenediamine (HMDA) and glucose oxidase (Type II-S: from Aspergillus niger, 20% protein) were purchased from Sigma-Aldrich. Di-sodium

hydrogen phosphate (Na_2HP0_4) was purchased from Riedel-de Haen. 30% (v/v) hydrogen peroxide solution was purchased from Merck. Glutaraldehyde (GA) was purchased from Fluka Chemika. Acetic acid glacial was purchased from Fisher Scientific. Silver conductive ink (Electrodag® PF-410) was purchased from Henkel (Scheemda, The Netherlands). Poly(ethylene) terephthalate substrates were Melinex® (pre-shrunk) films obtained from HiFi Industrial Film Ltd. (Dublin, Ireland). All the solutions were prepared using 18 MΩ Milli-Q water.

1.2. Buffers and solutions

Unless otherwise stated, all electrochemical measurements were carried out in phosphate buffered saline solution (PBS). The buffer solution is 0.1 M phosphate, 0.137 M NaCl and 0.0027 M KCl. This was prepared by mixing solution 1 (0.1 M Na_2HP0_4, 0.137 M NaCl and 0.0027 M KCl) and solution 2 (0.1 M KH_2P0_4, 0.137 M NaCl and 0.0027 M KCl) to a pH of 6.8.

Hydrogen peroxide was prepared to a concentration of 1 M by diluting 0.5 ml to 5 ml with deionised water. 10 μï was added to 1 ml of the appropriate enzyme/buffer or buffer solution to give an overall concentration of 1 mM in order to examine the electrode response.

A 0.2 M glucose solution was prepared and aliquots of 50 μl were added to the bulk to obtain a final concentration of 1 mM, unless otherwise stated.

0.02 % (w/v) cellulose acetate solution was prepared by dissolving Img into 5 ml of glacial acetic acid.

5 % (w/v) hexamethylenediamine solution was prepared by dissolving 0.1 5 g into 3 ml deionised water.

2.5 % glutaraldehyde solution was prepared by diluting 0.3 ml into 2.7 ml deionised water.

25 mg/ml glucose oxidase solution was prepared by dissolving 50 mg into 0.4 ml PBS pH 5.

1.3. Instrumentation

Silver screen-printed electrodes (Ag SPE) were fabricated using an automated DEK 248 machine (Weymouth, UK). Briefly, a layer of silver paste was deposited onto PET substrate and cured in a convectional oven at 120°C for 5 minutes. Then, an isolating tape layer was deposited to define the working electrode area (0.126 cm^2).

All electrochemical measurements were performed in a three-electrode electrochemical batch cell, using a Ag/AgCl/NaCl (saturated) electrode and a platinum mesh electrode as reference and auxiliary electrodes, respectively. Cyclic voltammetry and time-based amperometric measurements were carried out with a CHI601C electrochemical analyzer with CHI601C software (IJ Cambria Scientific Ltd., UK). Measurements were performed at room temperature, 18 ± 2 °C. Unless otherwise stated, all potential values are referred to the Ag/AgCl/NaCl (saturated) electrode.

1.4. Electrode modification with surfactant-based solutions

Silver screen-printed electrodes were dipped into a freshly-prepared solution of DBSA/KC1 for 3 hours. The electrodes were then rinsed with water to remove the excess of modification solution on it and measured directly.

1.5. Electrochemical characterisation

All the electrochemical measurements were carried out in a stirred batch system with a three-electrode configuration. Unless otherwise stated, the electrodes were measured in 10 ml PBS pH 6.8. Cyclic voltammograms were obtained in the potential range from -0.200 to 0.025 V (vs Ag/AgCl) at a scan rate of 0.1 V/s whereas the amperometric i-t curves were performed at -0.1 V (vs Ag/AgCl). 1 M stock solution of hydrogen peroxide was prepared daily. 0.2 M stock solution of glucose was prepared and left overnight to get beta-D-glucose by mutarotation. Aliquots from these solutions were added to the working cell during both cyclic voltammetry and amperometric measurements in order to characterize the sensor parameters.

1.6. Electrode Preparation for glucose biosensing

Silver electrodes were prepared by a screen printing method using the DEK 248 printing system. The electrodes were conditioned by placing them in a solution of 0.1 M KC1 and 0.033 M DBSA for 3 hours followed by a washing step with deionised water before using them as sensors. These electrodes were used as hydrogen peroxide sensors.

Glucose biosensors were prepared by immersing the DBSA/KC1 modified electrodes in a cellulose acetate solution (20% cellulose acetate in glacial acetic acid) for 3 s to create a thin and uniform layer of the polymer on the electrode. After the immersion, the electrode was placed for ten minutes in cold deionised water to accelerate the polymer solidification phase. Activation of the cellulose acetate layer was carried out by immersing the electrode into a 5% HMDA aqueous solution for 20 min. After washing in deionised water, the electrode was immersed for 20 min in 2.5% GA aqueous solution. After further washing with deionised water, the electrode was kept overnight at 4 °C in a 25 mg/ml of GOx in PBS pH 5 for enzyme immobilization. The whole process of covalent binding of glucose oxidase to the cellulose acetate layer is shown below: [38]

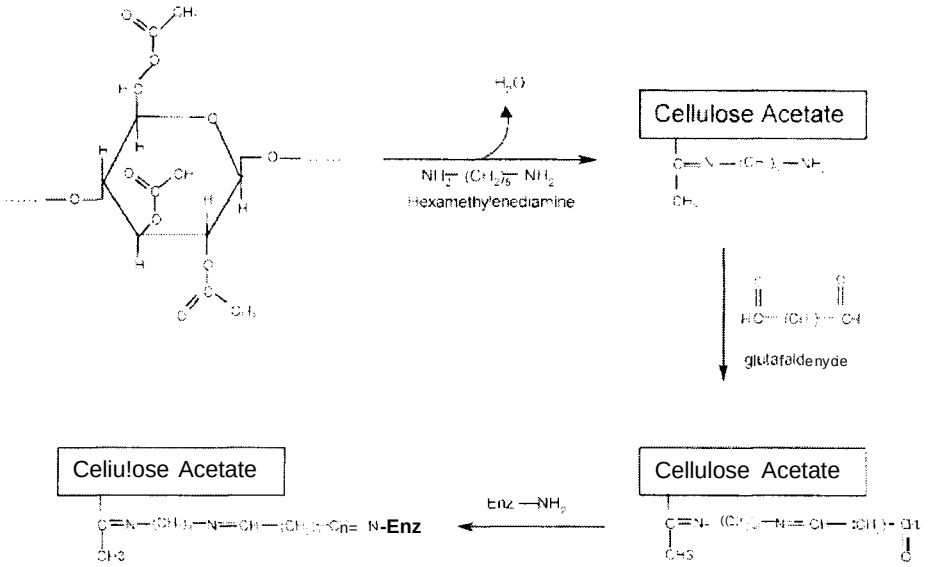

Results and Discussion

After the development of DBSA/KCl modified Ag SPEs as H_2O_2 sensors, those devices were used as a platform in the manufacture of a glucose biosensor. First, Ag_DBSA/KCl electrodes were checked as glucose sensors when the glucose oxidase enzyme was in solution. The modified electrode was first used to detect H_2O_2 by amperometric i-t curve at -O.l V (vs Ag/AgCl) in order to assess if it worked properly (Fig. 5la). Then, the electrode was placed in a cell containing 1mg/ml GOx in PBS pH 6.8 with compressed air passing through the solution and an amperometric i-t curve was performed at -0.1 V (vs Ag/AgCl). Aliquots from 0.2 M glucose solution were added to the cell in order glucose concentration to increase from 1 to 5 mM (Fig. 51b). The increases of the catalytic current at -0.1 V were proportional to the glucose

additions although those responses were quite slow compared to those from **H2O2** sensing. After glucose sensing, the electrode was again used as a **H2O2** sensor to evaluate the effect of the glucose detection. The catalytic response from the DBSA/KCI modified electrode after glucose sensing was approximately half of the initial response (Fig 51c). Therefore, glucose sensing seemed to affect negatively over the surfactant/salt modification of Ag SPEs. During the development of the glucose biosensor, a cellulose acetate film was deposited onto the Ag_DBSA/KCl electrodes to prevent both the activity loss from the surfactant modification and the enzyme denaturalization by metallic silver.[39]

The catalytic activity towards H_20_2 reduction of Ag_DBSA/KCl with a cellulose acetate film (Ag_DBSA/KCl_CA) was first assessed. A decrease in the catalytic current of approx. 20% was obtained with the modified electrode after the deposition of the cellulose acetate layer, as is shown in Fig. 52. However, the response was high enough to use the electrodes in the glucose sensor manufacture.

The glucose oxidase enzyme was then deposited onto the surface after the activation of the cellulose acetate film by hexamethyldiamine and glutaraldehyde. Once the electrode was rinsed, its catalytic activity towards glucose was assessed by amperometry at -0.1 V (vs Ag/AgCl). The electrode was placed in a batch cell containing 10 ml PBS pH6.8 and aliquots of 0.2 M glucose solution were added so glucose concentration ranged from 1 to 5 mM. The response of the glucose sensor is shown in Fig. 53. A calibration curve with the catalytic response of the sensor versus glucose concentration was built and the limit of detection and sensitivity of the device were calculated. The sensitivity was found to be 0.77 $\mu A\,cm^{-2}mM^{-1}$. The LOD was calculated from the regression line obtained from the plot of the cathodic currents versus glucose concentration. These data are presented in the inset of Fig. 53. Although the lowest concentration measured was $1T0^{-3}$ M, the lowest theoretical LOD of the sensor devices was found to be $3.6\text{-}10^{-4}$ M. The range of LOD and sensitivity calculated for glucose sensor and found in the literature is very wide and depending on the modification and enzyme immobilization method. Thus, a LOD of $2\text{-}10^{-5}$ M and sensitivity of 8.4 $\mu Acm^{-2}mM^{-1}$ was obtained when a platinum electrode was modified with a mixture of GOx and gold nanorods cross-linked with a cellulose acetate (CA) medium by glutaraldehyde. The glucose detection was performed at 0.4 V (vs Ag/AgCl) in phosphate buffer pH 6.8.[40] A glassy carbon electrode was modified using dispersed Pt nanoparticles supported on sulfonated multiwalled carbon nanotubes and then GOx was deposited on top to construct a glucose biosensor. Glucose was electrochemically detected at 0.5

Fuel Cell

This section describes the use of the hydrogen peroxide catalyst material in a direct hydrogen peroxide fuel cell for stable and efficient production of electric current by the electro-catalytic reduction of the hydrogen peroxide, via a cathode comprising of the hydrogen peroxide catalyst, coupled with the oxidation of a hydrogen containing fuel by means of proton transfer across a proton conducting electrolyte.

The hydrogen peroxide fuel cell consists of a proton conducting electrolyte, a porous electrical conducting substrate that supports the hydrogen peroxide catalyst and two porous or channelled flow manifolds that allow flow of the hydrogen peroxide (H202) to the cathode and a hydrogen containing fuel to the anode (Fig. 54).

The proton conducting electrolyte 1, such as an ion-conducting polymer comprising of a perfluorinated polymer containing sulfonic or carboxylic ionic functional groups of suitable type, durability and thickness as to allow efficient operation of the hydrogen peroxide fuel cell.

The cathode porous electrical conducting substrate or Gas Diffusion Layer (GDL) contains a hydrophobic agent 2. The silver-based ink composite, consisting of metallic component, binder components and solvent components is deposited by any suitable painting, deposition, coating process, on at least one side of the substrate. The application of the inks should not block the porous electrical conducting substrate. The porous electrical conducting substrate is then modified with the catalytic modification layer, again using any suitable means such as dip-coating or printing methods. The porous electrical conducting substrate, with the hydrogen peroxide catalyst layer is allowed to dry.

The anode porous electrical conducting substrate contains a hydrophobic agent 3. A suitable anode electro-catalyst, for a hydrogen containing fuel, is deposited by any suitable painting, deposition, coating process, on at least one side of the substrate. The application of the anode electro-catalyst should not block the porous electrical conducting substrate.

The porous or channelled flow manifold or flow plate 4, 5, that allows flow of the hydrogen peroxide to the cathode and a hydrogen containing fuel to the anode, has at least one input orifice and at least one output orifice. The design of the flow manifold is such that it allows effective

flow of the fluids to the electro-catalysts of the anode or cathode, supports the cell and enables a conductive path to the external circuit.

The anode and cathode porous electrical conducting substrate or Gas Diffusion Layer (GDL) 2, 3 can be incorporated onto the flow manifold if the flow manifold is constructed of suitable metallic or conductive porous matrix. This would negate the use of a porous electrical conducting substrate or GDL and the anode and cathode catalysts would then be coated directly to the conductive porous matrix of the anode and cathode flow manifolds 4, 5.

To assemble a hydrogen peroxide fuel cell, the cathode porous electrical conducting substrate or GDL with the hydrogen peroxide catalyst 1 is laid onto the proton conducting electrolyte 2, so that the catalyst-coated side faces the proton conducting electrolyte. The cathode porous or channelled flow manifold 4 is placed onto the cathode porous electrical conducting substrate and secured into position. The same procedure is completed for the anode side of the hydrogen peroxide fuel cell. The anode porous electrical conducting substrate or GDL with a suitable anode electro-catalyst, for a hydrogen containing fuel 3, is laid onto the other side of the proton conducting electrolyte 2, so that the coated anode electro-catalyst side faces the proton conducting electrolyte. The anode porous or channelled flow manifold is placed 5 onto the anode porous electrical conducting substrate and secured into position.

In operation, hydrogen peroxide in a water solution is allowed to flow through the cathode flow manifold. The hydrogen containing fuel is then allowed to flow through the anode flow manifold. When the anode and cathode are connected to an electrical circuit, electricity is produced [47-51]. Various fuel cells are described in US7344799; US7781083; US6485851 ; US7241521; and US78 16041 [47-51], the entire contents off which are all incorporated herein by reference.

In this configuration the reactant flow to the catalyst layer is predominantly achieved by molecular diffusion through the gas diffusion layer (GDL). This can lead to large concentration gradients across the GDL and mass transfer limitations because of the small channel dimensions, laminar gas flow and the inherent slow molecular diffusion process as illustrated in Fig. 55.

Proton Exchange Membrane ΓPEM) FUEL CELL_VOLTAGE& EFFICIENCY

If the PEM fuel cell was perfect at transferring chemical energy into electrical energy, the ideal cell voltage (thermodynamic reversible cell potential) of the hydrogen fuel cell would be 1.23 volts, at 25°C and one atmosphere [43]. However this is not the case for a practical cell, the formation of water from hydrogen and oxygen gases is an exothermic reaction, which has an enthalpy of -286 kilojoules of energy per mole of water formed. The free energy available to perform work decreases as a function of temperature. At 25°C and one atmosphere the free energy available to perform work is about -237 kilojoules per mole. This energy is observed as electricity and heat. As the fuel cell heats up to operating temperature, around 80°C the ideal cell voltage drops to about 1.1 8 volts. However there are many limiting factors that reduce the fuel cell voltage further. The voltage out of the cell is a good measure of electrical efficiency; the lower the voltage, the lower the electrical efficiency and the more chemical energy is released in the formation of water and transferred into heat [43]. . The fuel cell's performance is summarised with the graph of its current and voltage characteristics, polarisation curve (I-V curve) shown in Fig. 56.

Energy losses in PEM fuel cells

The losses in fuel cells are related to the power produced by the cells. The more current that is drawn from a cell, the higher the losses from the cell would be. This is the reason why the voltage of the cell reduces as more current is drawn from the cell. This ideal cell voltage (E_{rev}) of a fuel cell can be calculated from the available free energy, AG [43]. .This equation is shown below in equation 1:

$$E_{rev} = AG/nF \qquad \textit{Eqn. (1)}$$

Where AG is the free Gibbs energy, n is number of electrons transferred in the electrochemical reaction and F is the Faraday constant (94685 C/mole) [43]. The E_{rev} is also dependent on operating conditions like temperature, pressure and concentration of reactants.

The term overvoltage refers to the difference between the ideal cell voltage and the operating cell voltage. This, in due course, represents the losses in the cell. The relationship between the theoretical E_{rev} and the actual operating voltage (**E_{ce}ii),** expressed in equation 2, is a more correct way to express the efficiency (η) of a fuel cell [43].

$$\eta = E_{cell} / E_{rev} \qquad \textit{Eqn. (2)}$$

In general there are four main sources of potential drop in PEM fuel cells:

- Activation over potential
- Ohmic over potential
- Mass transport (concentration) over potential
- Fuel crossover and internal currents losses

Activation over potential

Activation losses are a result of the energy required to initiate the reaction and losses due to the slowness of the electrochemical reactions taking place on the surface of the electrodes. This is a result of the catalyst. The better the catalyst the less activation energy required. Platinum forms an excellent catalyst however there is much research underway for cheaper materials. A limiting factor to power density available from a fuel cell is the speed at which the reactions can take place. The cathode reaction, (e.g., the reduction of oxygen or hydrogen peroxide) is about 100 times slower than that of the reaction at the anode, thus it is the cathode reaction that limits power density. The losses depend on factors such as electrode material properties, ion intersection and electrolyte characteristics. These losses can be reduced by increasing the operating temperatures however increasing the temperature may cause other losses. Electrochemical reaction kinetics cause the voltage to decrease and these losses can mainly be seen in an I-V curve as the cell begins to produce current, as seen on the left-hand side of 2. The Tafel equation is used to model the losses, it is simplified as:

$$\tau_{|act} = A\ln(i/b) \qquad \textit{Eqn. (3)}$$

where, i is the current density, $A = A_a + A_c$, which are constants depending on the electrodes (slope of the Tafel equations) and $b = i_{oa}^{Aa/A} + i_{0C}^{Ac/A}$ where, i_0 is the exchange current density [43].

Ohmic over potential

Ohmic losses are a result of the combined electrical resistances of the various fuel cell components that produce heat. These include the electrode material resistance, the electrolyte membrane resistance and the various interconnection resistances. The major proportion of the losses within a fuel cell occur as more current is drawn from the cell, as seen in Fig. 56 (middle

V (vs Ag/AgCl) providing a sensitivity of 0.56 μAηιM^{-1} and a linear range from 0.01 to 6.4 mM.[41] A higher sensitivity (30.64 ¸uAcm^{-2}mM$^{-'}$) and LOD (2.5·10^{-6} M) was obtained with an amperometric glucose biosensor based on layer-by-layer (LbL) electrostatic adsorption of GOx and dendrimer-encapsulated Pt nanoparticles (Pt-DENs) on multiwalled carbon nanotubes (CNTs). Glucose was detected by amperometric measurements at 0 V (vs Ag/AgCl) in PBS pH 6.8.[42] Therefore, the device from the present work, Ag_DBSA/KCl_CA_GOx, has shown to be feasible as a glucose sensor, although further studies should be performed to improve its sensitivity and LOD.

A high through-put fabrication approach of printing could be adopted to fabricate the cathodic electrodes, aligning it with potential in the printed electronics area.

Much proprietary technology surrounds the catalysis and electrocatalysis of suitable oxidants for fuel cell applications, so a novel platform such as the one suggested here, based on modified silver, provides potentially improved catalytic performance.

The invention provides:

- Novel catalytic/electrocatalytic mechanism not demonstrated previously
- Highly efficient non-biological catalyst for hydrogen peroxide
- Highly processable form of silver/organic composite that is catalytically active towards hydrogen peroxide
- Low cost catalytic material, compared to other catalytic materials such as pure platinum and silver allowing for its use in a broader range of applications
- Wide range of operating conditions not available to organic catalysts including pH, temperature.
- Aqueous chemistry requiring no hazardous solvents

part of the plot). The voltage drop is linearly proportional to current density (or the current taken from the cell) therefore the loss can be modelled using [44]. :

$$\eta_{ohmic} = iR \qquad \textit{Eqn. (4)}$$

where, i is the current density given in Acm^{-2} and R is the specific resistance given by:

$$R = L/A\sigma\ \Omega cm^2 \qquad \textit{Eqn. (5)}$$

where L is the length of the electrode, A is the area of electrode and σ is the conductivity. The resistance can be reduced by using electrodes with a high conductivity, appropriate flow plate material and making the electrolytes as thin as possible [45].

Mass transport over potential

Mass transport (concentration) losses result from the reduction of the concentration of hydrogen and oxygen gases at the electrodes. For example, following the reaction new gases must be made immediately available at the catalyst sites. With the build up of water at the cathode, particularly at high currents, catalyst sites can become clogged, restricting oxygen access. This is responsible for the sharp decline in the potential at high current densities and can be seen at the tail end of the I-V curve in Fig. 57. Using the Nernst Equation, the loss can be modelled by the following equation [44].:

$$\eta_{conc} = (RT/2F)\ln(1-i/i,) \qquad \textit{Eqn. (6)}$$

where R is the specific gas constant for hydrogen, T is the operating temperature ii is the limiting current density. If R and T are known, equation 2.3.7 is further simplified to:

$$\eta_{conc} = m\exp(ni) \qquad \textit{Eqn. (7)}$$

where m is $3e^{-5}V$ and n is $8e^{-3}\ cm^2mA^{-1}$ [46].

Fuel cross over and internal currents

This loss is typically small compared to others therefore its effect can be negligible in correctly sealed and supported cells [45] It is the energy loss due to the waste of fuel passing through the electrolyte and from electron conduction through the electrolyte. The electrolyte is only supposed to transport ions; however a certain amount of fuel diffusion and electron transfer will always be possible.

Combining PEM fuel cell losses

It is these combined losses that characterise the I-V graphs and indicate the performance of the PEM fuel cell. The real voltage output of the cell can therefore be obtained by starting with the thermodynamically predicted voltage (1.23V) and then subtracting the voltage losses:

$$E_{cell} = V = E_{rev} - \eta_{act} - \eta_{ohmic} - \eta_{conc} \qquad \textit{Eqn. (8)}$$

therefore

$$V = E_{rev} - A\ln(i/b) - iR - m\exp(ni) \qquad \textit{Eqn. (9)}$$

E_{rev} is the reversible OCV given by {1.23 V}

A is the slope of the Tafel line {0.03V}

R is the area-specific resistance {2.45 e-4}

m {3e-5V} and n {8e-3 $cm^2 mA^{-1}$} are the constants in the mass-transfer overvoltage. These values are taken from Ballard Inc. [46].

Gas diffusion layer and hydrogen peroxide catalyst

H2Q2 catalyst Operational Conditions :

- Flow plate type: Double serpentine
- Membrane Type: Nafion 2 12

- Hydrogen side (Anode):
  - Flow Rate Hydrogen: 50 ml/min
  - GDL:
    - Carbon paper
    - Pt Content: 0.5 mg/cm2 60 wt% Pt
    - Active area: 3.8x3.8cm

- H202 side (Cathode):
  - Flow Rate H202: 0.1 ml/min
  - H202 Concentration: 0.1 Mol

- GDL:
  - Carbon paper
  - Silver ink Content(original 1.3mg/ml): 1:50
  - Catalytic modification Constant

Active area: 3.8x3.8cm

The results presented in Fig. 58 are a batch of tests on 1 new hydrogen GDL run after each other in one day. The fuel cell showed open circuit potentials in excess of 1 V, which shows excellent performance in this preliminary fuel cell application example. Many improved configurations could be envisaged such as further optimisations of the design and fabrication of the cathode material, use of alternative fuel sources, alternative membrane types, the potential for use and application in biofuel cell systems and microbial fuel cell systems, use of the hydrogen peroxide catalyst as a support for standard platinum cathodes employing the oxygen reduction reaction.

Figs 58, 59 and 60 show microscopic analysis of the gas diffusion layer material before and after modification with the hydrogen peroxide catalyst showing deposition of high contrast ratio materials, most likely silver, onto the gas diffusion layer.

The invention is not limited to the embodiment hereinbefore described, with reference to the accompanying drawings, which may be varied in construction and detail.

References

1. C. M. Welch, C. E. Banks, A. O. Simm and R. G. Compton, *Analytical and Bioanalytical Chemistry,* 2005, **382,** 12-21.

2. S. A. Kumar and S.-M. Chen, *Journal of Molecular Catalysis A: Chemical,* 2007, **278,** 244-250.

3. M. R. Guascito, E. Filippo, C. Malitesta, D. Manno, A. Serra and A. Turco, *Biosensors & Bioelectronics,* 2008, **24,** 1057-1063.

4. A. E. Radi, X. Munoz-Berbel, M. Cortina-Ping and J. L. Marty, *Electroanalysis,* 2009, **21,** 696-700.

5. M. Yemini, P. Xu, D. L. Kaplan and J. Rishpon, *Electroanalysis,* 2006, **18,** 2049-2054.

6. A. Karyakin, *Electroanalysis,* 2001, **13,** 813-819.

7. E. P. Pramauro, E., , *Surfactants in Analytical Chemistry. Applications of organized amphiphilic media,* Elsevier, 1996.

8. M. J. Rosen, *Surfactants and interfacial phenomena,* 2nd edn., John Wiley & Sons, 1989.

9. A. Sein and J. B. F. N. Engberts, *Langmuir,* 1995, **11,** 455-465.

10. V. Rumbau, J. A. Pomposo, J. A. Alduncin, H. Grande, D. Mecerreyes and E. Ochoteco, *Enzyme and Microbial Technology,* 2007, **40,** 1412-1421 .

11. G. Flatgen, S. Wasle, M. Lubke, C. Eickes, G. Radhakrishnan, K. Doblhofer and G. Ertl, *Electrochimica Acta,* **1999, 44**, 4499-4506.

12. K. Doblhofer, G. Flatgen, S. Horswell, B. Pettinger, S. Wasle and K. G. Weil, *Surface Science,* 2009, **603,** 1900-1903.

13. F. W. Campbell, S. R. Belding, R. Baron, L. Xiao and R. G. Compton, *The Journal of Physical Chemistry C,* 2009, **113,** 9053-9062.

14. M. Honda, T. Kodera and H. Kita, *Electrochimica Acta,* 1986, **31,** 377-383.

15. E. S. Brandt, *Journal of Electroanalytical Chemistry,* 1983, **150,** 97-109.

16. J. A. Cox and R. K. Jaworski, *Analytical Chemistry,* 1989, **61,** 2176-2178.

17. d. Tetrachim and c. A. (www.tetrachim.com) , *Electrodag PF-410 Product Datasheet.*

18. S. C. Hung, Y. L. Wang, B. Hicks, S. J. Pearton, D. M. Dennis, F. Ren, J. W. Johnson, P. Rajagopal, J. C. Roberts, E. L. Piner, K. J. Linthicum and G. C. Chi, *Applied Physics Letters,* 2008, **92,** 193903-193903.

19. W. Lian, L. Wang, Y. Song, H. Yuan, S. Zhao, P. Li and L. Chen, *Electrochimica Acta*, 2009, **54,** 4334-4339.

20. P. Kalimuthu and S. A. John, *Journal of Electroanalytical Chemistry*, 2008, **617,** 164-170.

21. F. F. Peng, Y. Zhang and N. Gu, *Chinese Chemical Letters*, 2008, **19,** 730-733.

22. K. K. Boonme P, Graf A, Rades T, Junyaprasert VB, *AAPS PharmSciTeck*, 2006, 7, 45.

23. M. Yamashita, K. Kameyama, R. Kobayashi, A. Asahina, S. Aita and K. Ogura, *J Electron Microsc (Tokyo)*, 1996, **45,** 461-462.

24. N. E. Baryla, J. E. Melanson, M. T. McDermott and C. A. Lucy, *Analytical Chemistry*, **2001, 73**, 4558-4565.

25. E. J. Wanless and W. A. Ducker, *The Journal of Physical Chemistry*, 1996, **100,** 3207-3214.

26. S. Manne and H. E. Gaub, *Science*, 1995, **270,** 1480-1482.

27. H. Domiinguez, *Langmuir*, 2009.

28. K. Grennan, A. J. Killard and M. R. Smyth, *Electroanalysis*, 2001, **13,** 745-750.

29. H. F. Schmidt, M. Meuris, P. W. Mertens, A. L. P. Rotondaro, M. M. Heyns, T. Q. Hurd and Z. Hatcher, 1994 International Conference on Solid State Devices and Materials (SSDM 94), Yokohama, Japan, 1994.

30. J.-F. Liu and W. A. Ducker, *The Journal of Physical Chemistry B*, 1999, **103,** 8558-8567.

31. V. Subramanian and W. A. Ducker, *Langmuir*, 2000, **16,** 4447-4454.

32. R. J. Farn, *Chemistry and technology of surfactants*, Wiley-Blackwell, 2006.

33. L. Pauling, *General Chemistry*, 3rd edn., Courier Dover Publications, 1988.

34. T. Engel and P. Reid, *Physical Chemistry*, 2006.

35. N. Kitajima, S. Fukuzumi and Y. Ono, *The Journal of Physical Chemistry*, 1978, **82,** 1505-1509.

36. H. Falcon and R. E. Carbonio, *Journal of Electroanalytical Chemistry*, 1992, **339,** 69-83.

37. R. Venkatachalapathy, G. P. Davila and J. Prakash, *Electrochemistry Communications*, 1999, **1,** 614-617.

38. M. Portaccio, D. Durante, A. Viggiano, S. Di Martino, P. De Luca, D. Di Tuoro, U. Bencivenga, S. Rossi, P. Canciglia, B. De Luca and D. G. Mita, *Electroanalysis*, 2007, **19,** 1787-1793.

39. C. C. Liu, F. M. Fryburg and A. K. Chen, *Bioelectrochemistry and Bioenergetics*, 1981, 8, 703-708.

40. X. Ren, D. Chen, X. Meng, F. Tang, A. Du and L. Zhang, *Colloids and Surfaces B: Biointerfaces*, 2009, 72, 188-192.

41. H. J. Wang, C. M. Zhou, F. Peng and H. Yu, *Int. J. Electrochem. Sci.*, 2007, 2, 508-516.

42. L. Xu, Y. Zhu, L. Tang, X. Yang and C. Li, *Electroanalysis*, 2007, **19**, 717-722.

43. O'Hayre R, Cha S, Colella W, Prinz FB. Fuel Cell Fundamentals. USA: John Wiley and Sons;0-471-74148-5, 2006.

44. EG&G Technical Services I. Fuel Cell Handbook. 7th ed. Virginia: U.S. Department of Energy; 2004.

45. Larminie J, Dicks A. Fuel Cell Systems Explained. Second edition ed. London: John Wiley & Sons Ltd; 2003.

46. Yu X, Zhou B, Sobiesiak A. Water and thermal management for Ballard PEM fuel cell stack. J.Power Sources 2005;147(1-2):184-195.

47. United States Patent 7344799

48. United States Patent 7781083

49. United States Patent 6485851

50. United States Patent 7241521

51. United States Patent 7816041

Claims

1. A catalyst comprising a silver electrode wherein the electrode has been modified with a surfactant-salt solution.

2. A catalyst as claimed in claim 1 wherein the electrode comprises silver colloids, silver particles, or silver nanoparticles.

3. A catalyst as claimed in claim 1 or 2 wherein the electrode is a silver paste electrode.

4. A catalyst as claimed in any of claims 1 to 3 wherein the electrode is a screen printed electrode.

5. A catalyst as claimed in any of claims 1 to 4 wherein the surfactant is present at a concentration of from 0.01 to 0.1M.

6. A catalyst as claimed in any of claims 1 to 5 wherein the salt is present at a concentration of at least 0.001M.

7. A catalyst as claimed in any of claims 1 to 6 wherein the surfactant is selected from:

dodecyl benzene sulphonic acid (DBSA);
sodium dodecyl sulphate (SDS);
cetyl trimethylammonium bromide (CTAB); and
polyethylene glycol p-(l,l,3,3-tetramethylbutyl)-phenyl ether (Triton X-100).

8. A catalyst as claimed in any of claims 1 to 6 wherein catalyst is selected from:

dodecyl benzene sulphonic acid (DBSA); and
sodium dodecyl sulphate (SDS).

9. A catalyst as claimed in any of claims 1 to 8 wherein the salt solution is a solution selected from:

Potassium Chloride (KC1)

Sodium Chloride (NaCl)

Sodium Bromide (NaBr)

10. A catalyst as claimed in any of claims 1 to 9 wherein the molar ratio of surfactant to salt is approximately 1:3.

11. A catalyst as claimed in any of claims 1 to 10 wherein the surfactant-salt solution contains approximately 0.033M DBSA and approximately 0.1M KC1.

12. A catalyst as claimed in any of claims 1 to 10 wherein the surfactant-salt solution contains approximately 0.033M SDS and approximately 0.1M NaCl.

13. A catalyst as claimed in any of claims 1 to 10 wherein the surfactant-salt solution contains approximately 0.0033 M CTAB and approximately 0.1M NaBr.

14. A catalyst as claimed in any of claims 1 to 9 wherein the surfactant-salt solution contains approximately 0.033M Triton X-100 and approximately 0.0001 M KC1.

15. A catalyst as claimed in any of claims 1 to 14 wherein the electrode is modified with the surfactant-salt solution for about 3 hours.

16. A catalyst as claimed in any of claims 1 to 15 wherein the electrode of the catalyst is coated with a coating such as nafion and/or chitosan and/or cellulose acetate.

17. A catalyst as claimed in any of claims 1 to 16 which is a non-enzymatic catalyst.

18. A catalyst as claimed in any of claims 1 to 17 wherein the catalyst is a peroxide catalyst.

19. A catalyst as claimed in any of claims 1 to 18 wherein the catalyst is a hydrogen peroxide catalyst.

20. A sensor system comprising the catalyst of any of claims 1 to 19.

21. A sensor as claimed in claim 20 comprising a biosensor.

22. A sensor as claimed in claim 20 comprising a chemical sensor.

23. A cholesterol sensor comprising a catalyst as claimed in any of claims 1 to 19.

24. A glucose sensor comprising a catalyst as claimed in any of claims 1 to 19.

25. A fuel cell comprising a catalyst as claimed in any one of claims 1 to 19.

26. A fuel cell cathode comprising a catalyst as claimed in any of claims 1 to 19.

27. A fuel cell cathode as claimed in claim 26 wherein the catalyst is provided in a gas diffusion layer.

28. A fuel cell cathode as claimed in claim 27 wherein silver is provided in the gas diffusion layer which is modified with a surfactant salt solution.

29. A method for manufacturing a fuel cell cathode comprising:-

providing silver in a gas diffusion layer; and

modifying the silver with a surfactant - salt solution.

30. A method as claimed in claim 29 comprising:-

providing a porous substrate; and

applying the silver to the porous substrate.

31. A method as claimed in claim 30 wherein the silver is applied to the porous substrate by printing.

32. A method as claimed in claim 30 or 31 wherein the silver is in the form of an ink for application to the substrate.

33. Use of a catalyst as claimed in any of claims 1 to 19 in

- fuel cells;
- batteries;
- chemical synthesis; and/or
- decomposition processes.

34. A method of detecting a peroxide comprising the steps of:

- providing a silver electrode;
- modifying the electrode with a surfactant-salt solution; and
- rinsing the electrode with distilled water.

35. A method as claimed in claim 34 comprising rinsing the electrode with water before exposing the electrode to the sample.

36. A method as claimed in claim 34 or 35 wherein the peroxide is hydrogen peroxide.

37. A catalyst substantially as hereinbefore described.

38. A sensor substantially as hereinbefore described.

39. A fuel cell substantially as hereinbefore described.

40. A fuel cell cathode substantially as hereinbefore.

41. A method for manufacturing a fuel cell cathode substantially as hereinbefore described.

42. A detection method substantially as hereinbefore described.

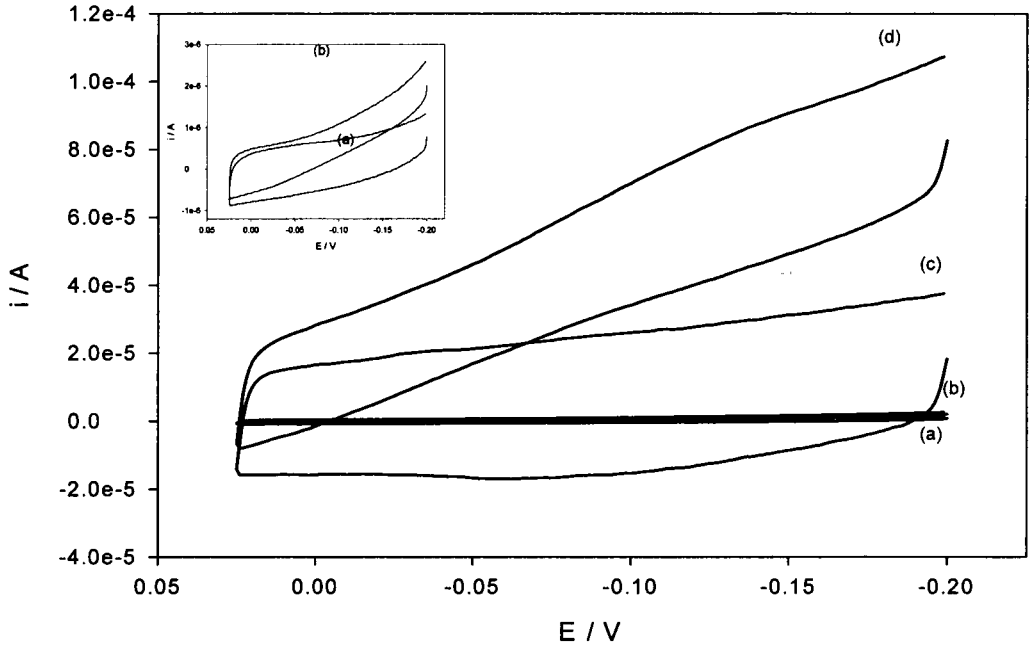
1.2e-4
1.0e-4
8.0e-5
6.0e-5
4.0e-5
2.0e-5
0.0
-2.0e-5
-4.0e-5
i / A
0.05
0.00
-0.05
-0.10
-0.15
-0.20
E / V
(a)
(b)
(c)
(d)
(e)

Fig. 1

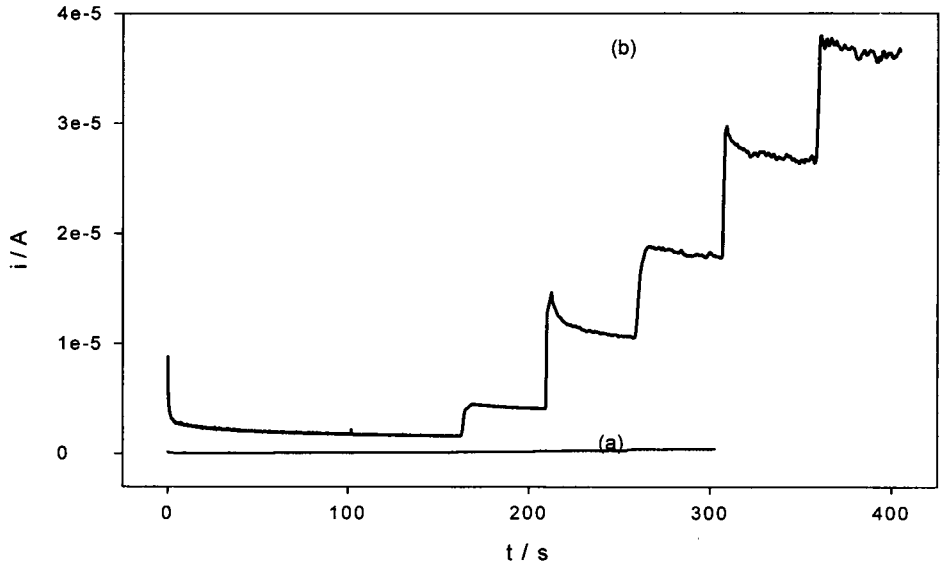
4e-5
3e-5
2e-5
1e-5
0
i / A
0
100
200
300
400
t / s
(a)
(b)

Fig. 2

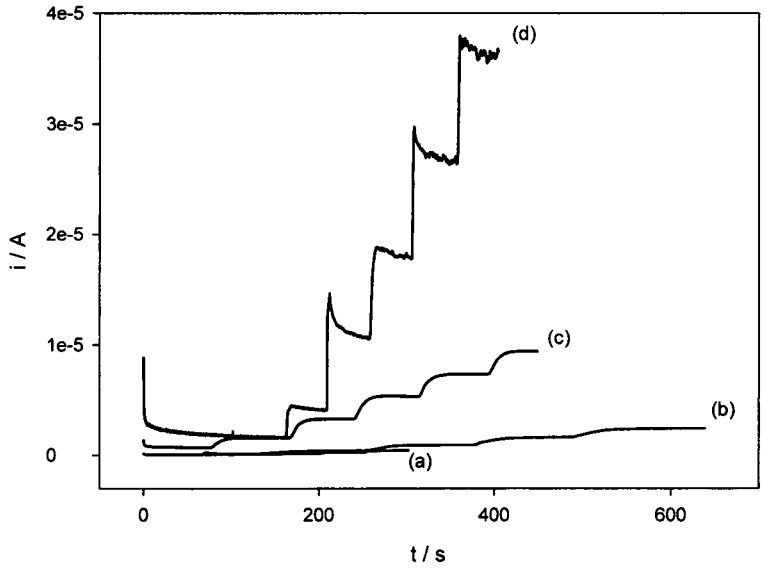
4e-5
3e-5
2e-5
1e-5
0
i / A
0
200
400
600
t / s
(a)
(b)
(c)
(d)

Fig. 3

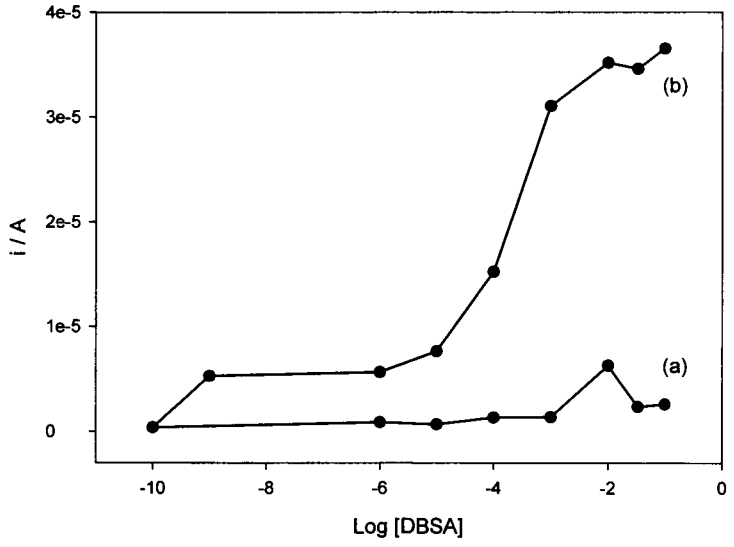
4e-5
3e-5
2e-5
1e-5
0
i / A
-10
-8
-6
-4
-2
0
Log [DBSA]
(a)
(b)

Fig. 4

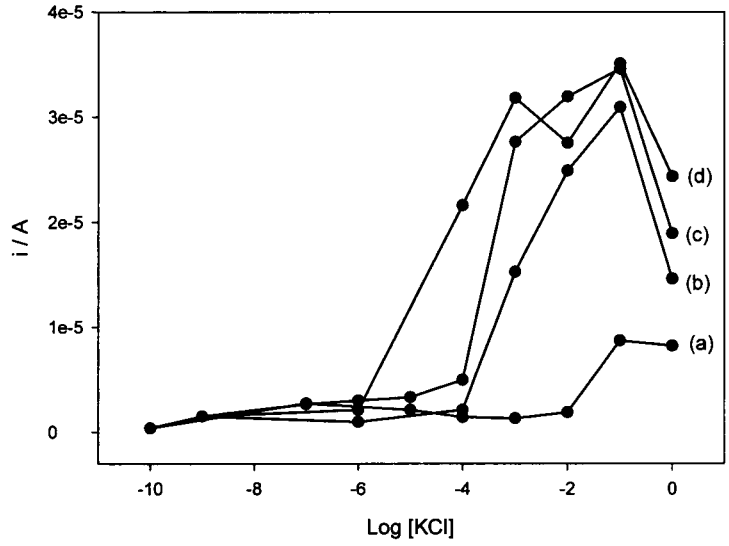
4e-5
3e-5
2e-5
1e-5
0
i / A
-10
-8
-6
-4
-2
0
Log [KCl]
(d)
(c)
(b)
(a)

Fig. 5

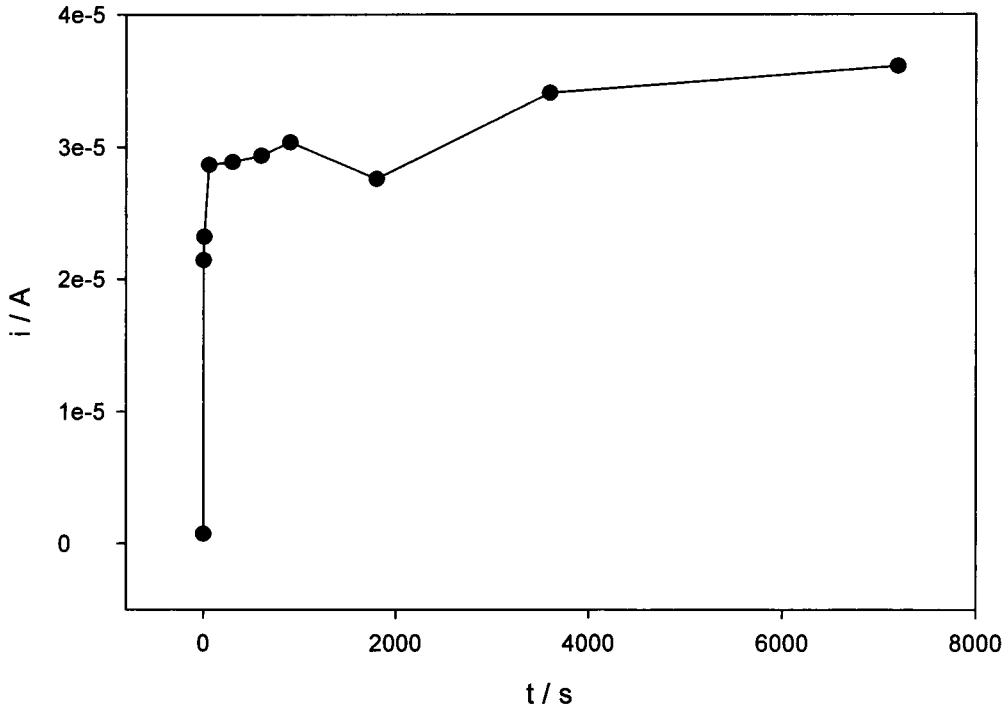
4e-5
3e-5
2e-5
1e-5
0
i / A
0
2000
4000
6000
8000
t / s

Fig. 6

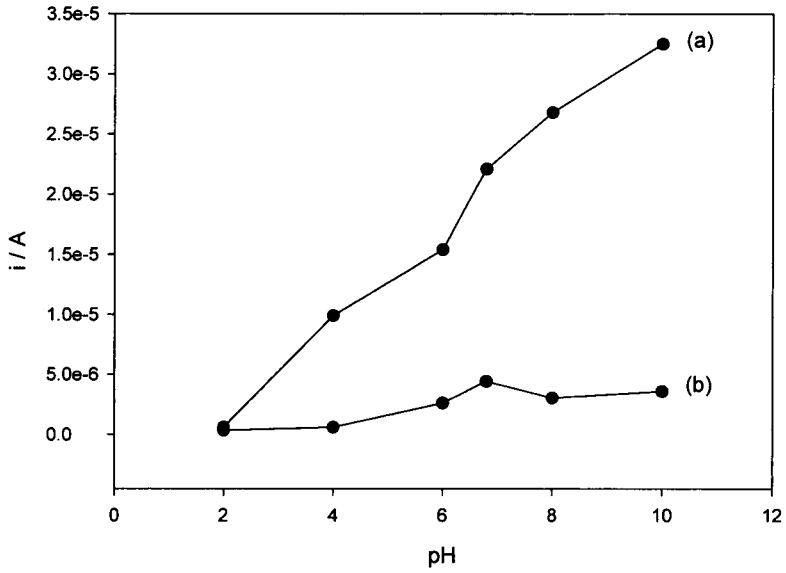
3.5e-5
3.0e-5
2.5e-5
2.0e-5
1.5e-5
1.0e-5
5.0e-6
0.0
i / A
0
2
4
6
8
10
12
pH
(a)
(b)

Fig. 7

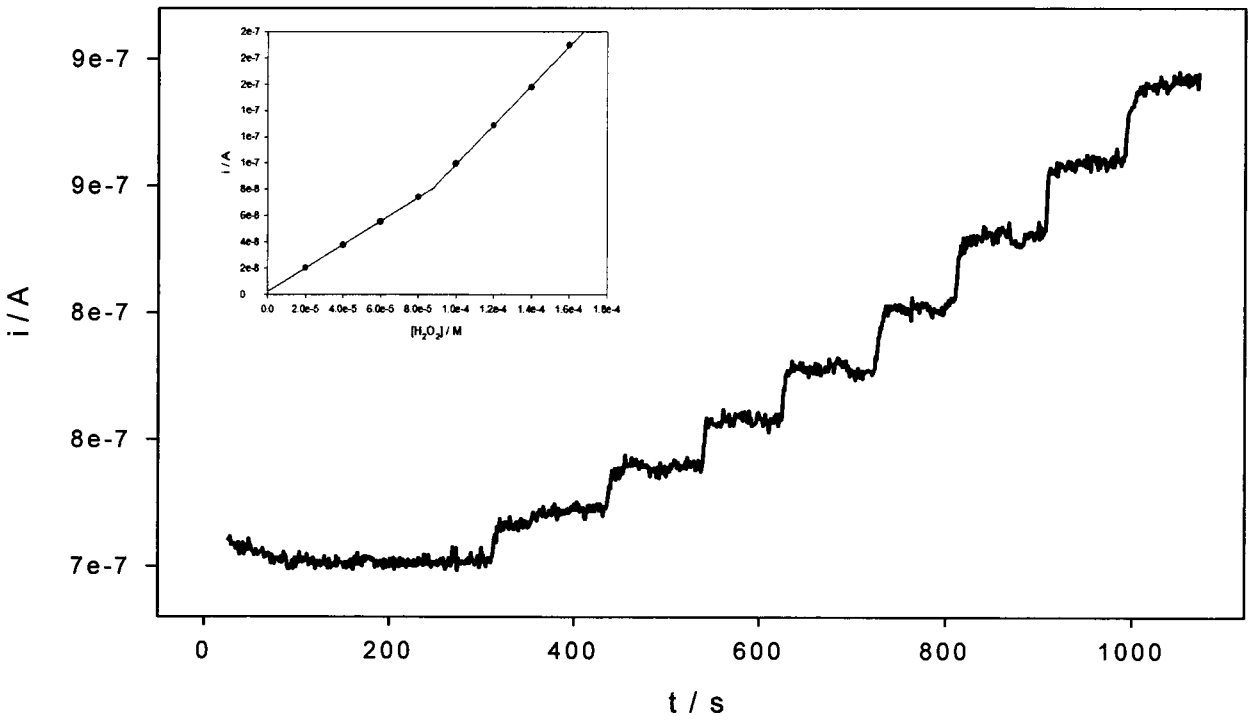
9e-7
9e-7
8e-7
8e-7
7e-7
i / A
0
200
400
600
800
1000
t / s
i / A
[H2O2] / M

Fig. 8

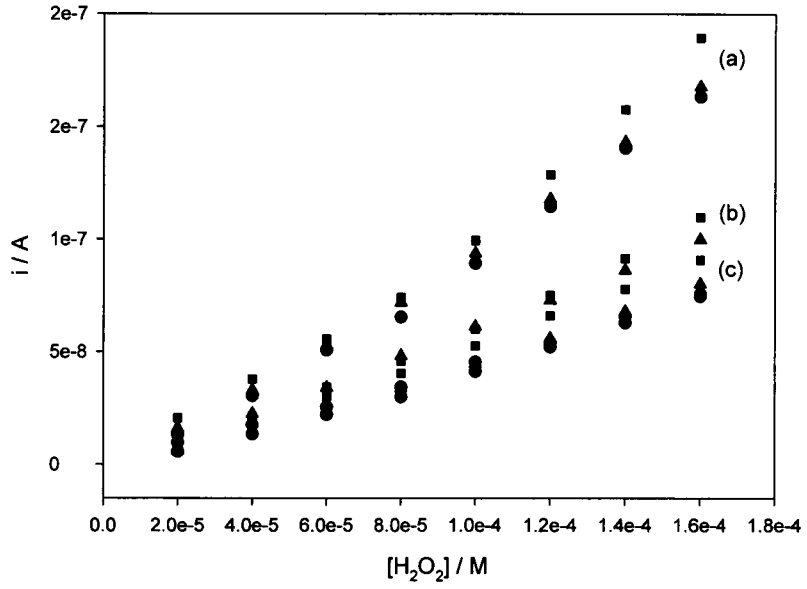
2e-7
2e-7
1e-7
5e-8
0
i / A
(a)
(b)
(c)
0.0
2.0e-5
4.0e-5
6.0e-5
8.0e-5
1.0e-4
1.2e-4
1.4e-4
1.6e-4
1.8e-4
[H2O2] / M

Fig. 9

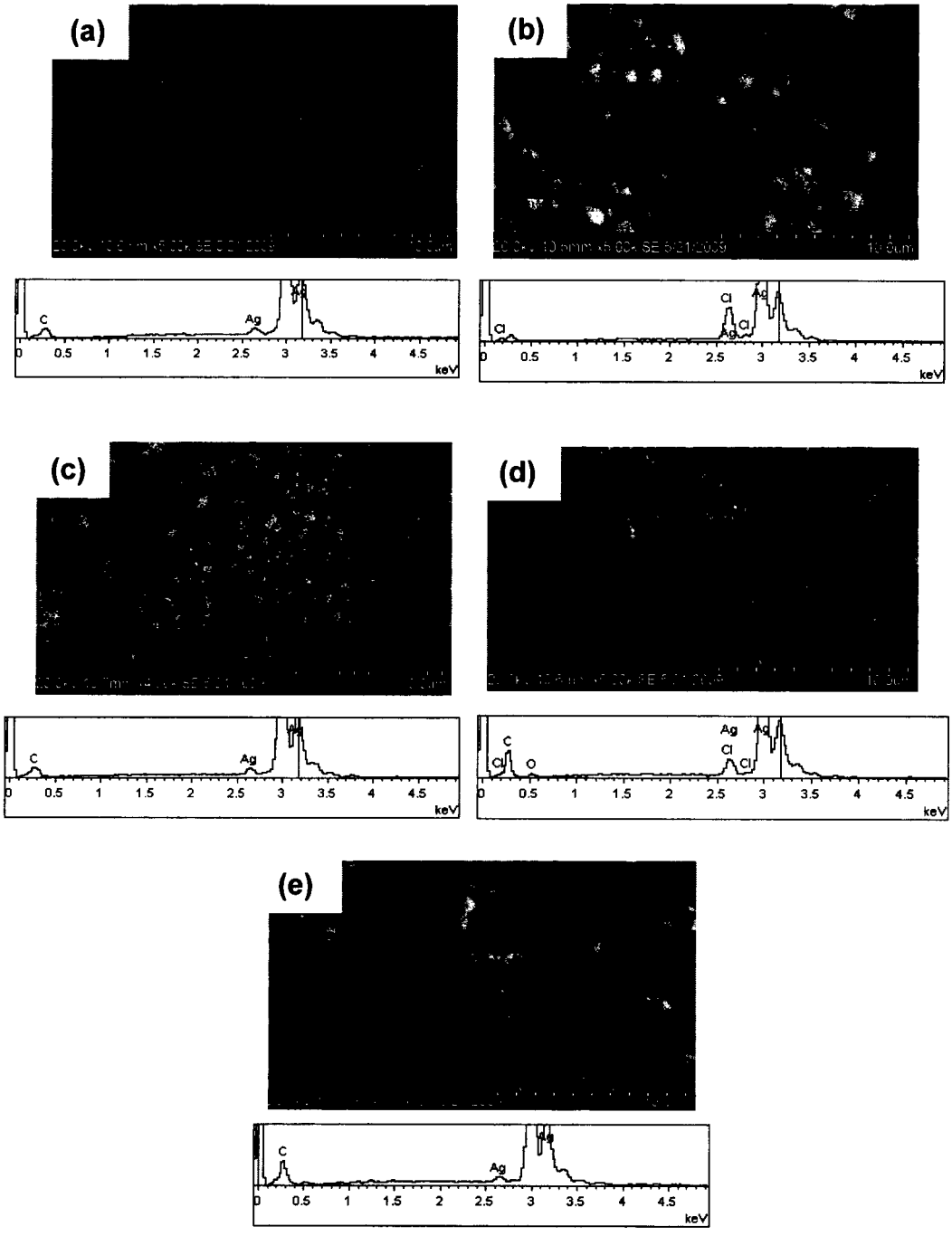

Fig. 10

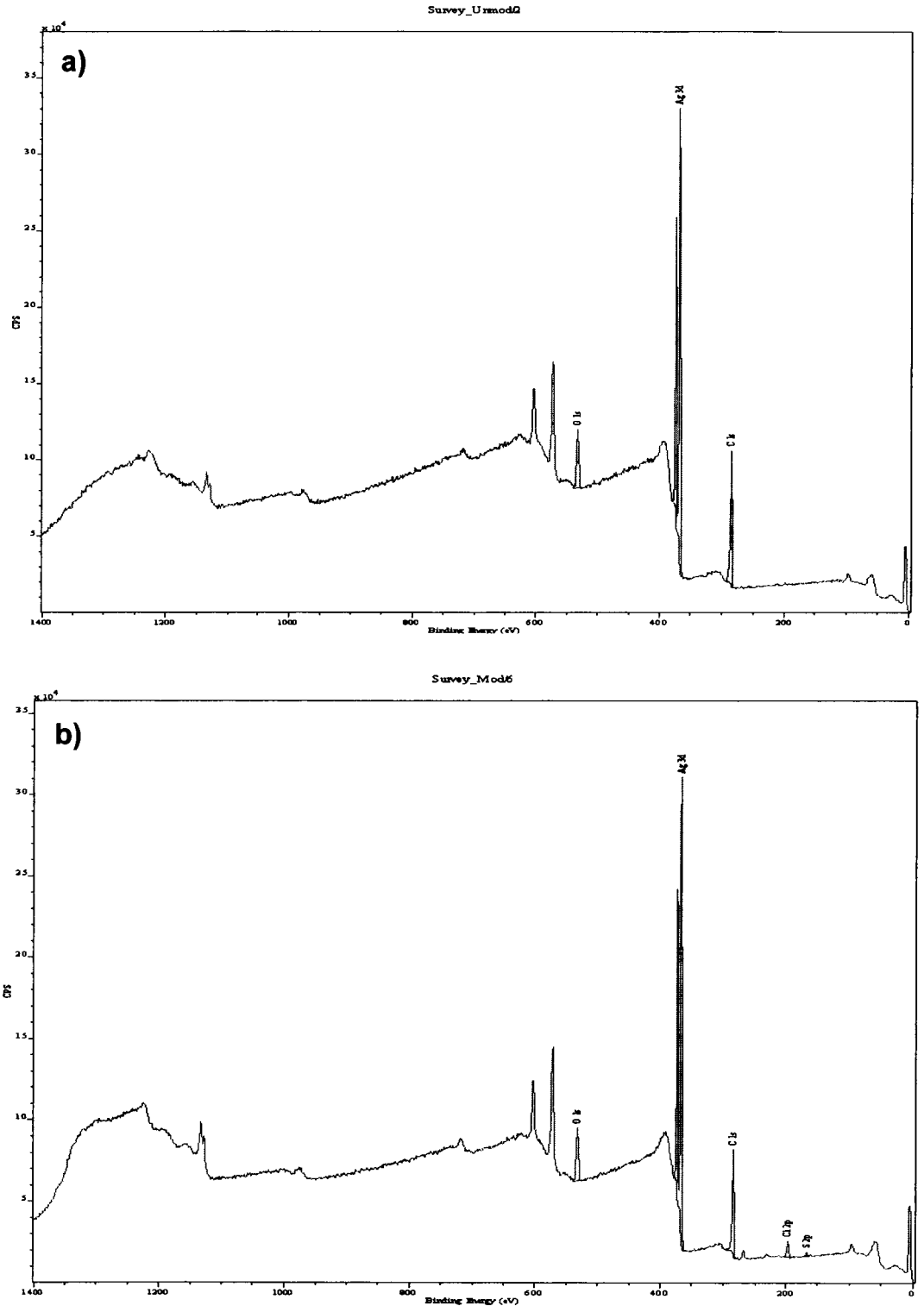
Survey_Unmod2
a)
Ag3d
O1s
C1s
CPS
Binding Energy (eV)
Survey_Mod6
b)
Ag3d
O1s
C1s
Cl2p
Ag3s

Fig. 11

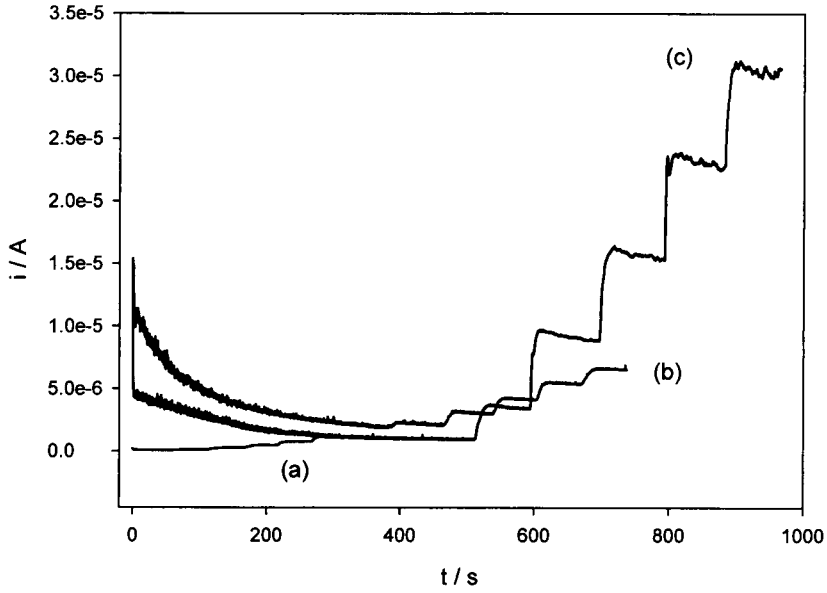
3.5e-5
3.0e-5
2.5e-5
2.0e-5
1.5e-5
1.0e-5
5.0e-6
0.0
i / A
0
200
400
600
800
1000
t / s
(a)
(b)
(c)

Fig. 12

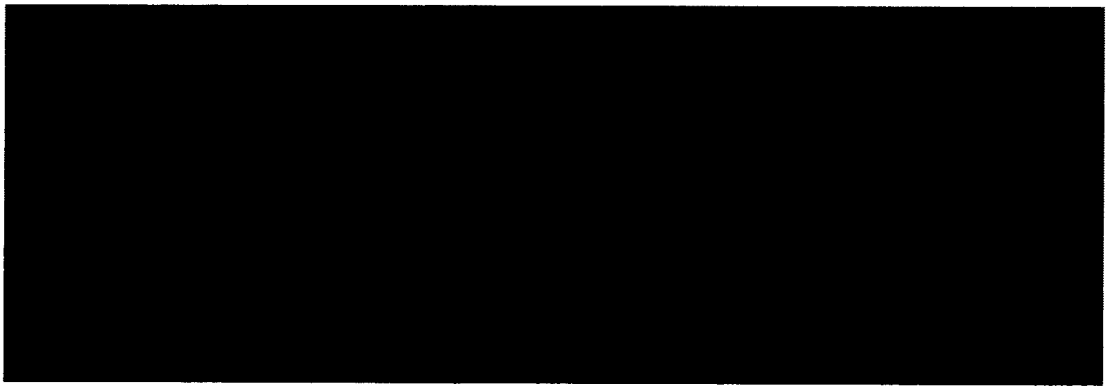

Fig. 13

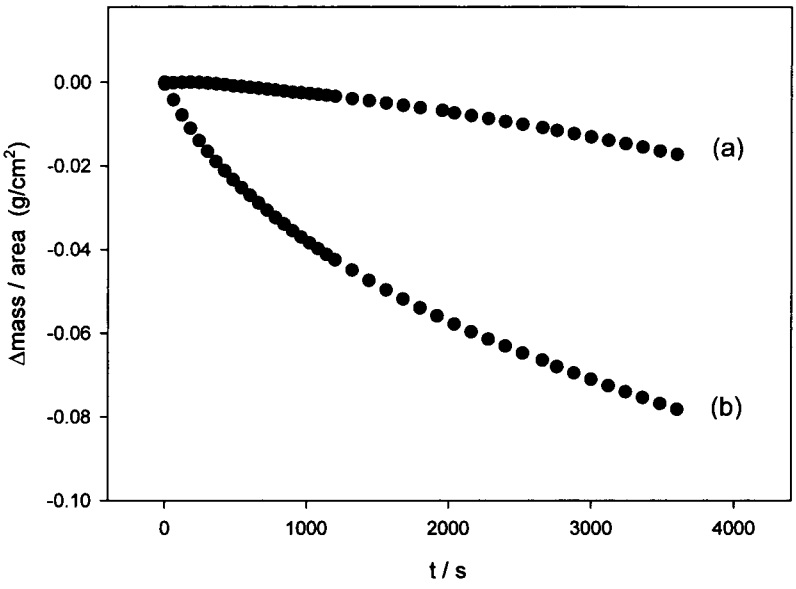
0.00
-0.02
-0.04
-0.06
-0.08
-0.10
Δmass / area (g/cm²)
0
1000
2000
3000
4000
t / s
(a)
(b)

Fig. 14

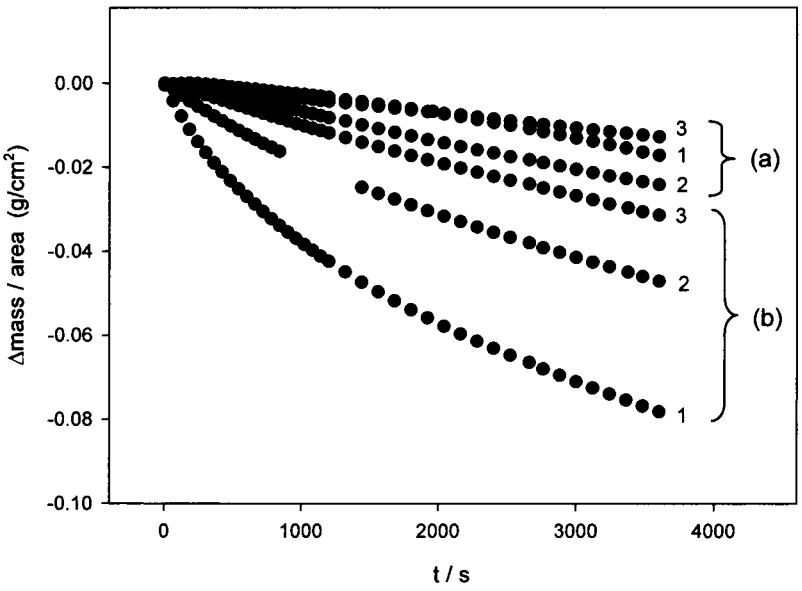
0.00
-0.02
-0.04
-0.06
-0.08
-0.10
Δmass / area (g/cm²)
0
1000
2000
3000
4000
t / s
3
1
2
(a)
3
2
1
(b)

Fig. 15

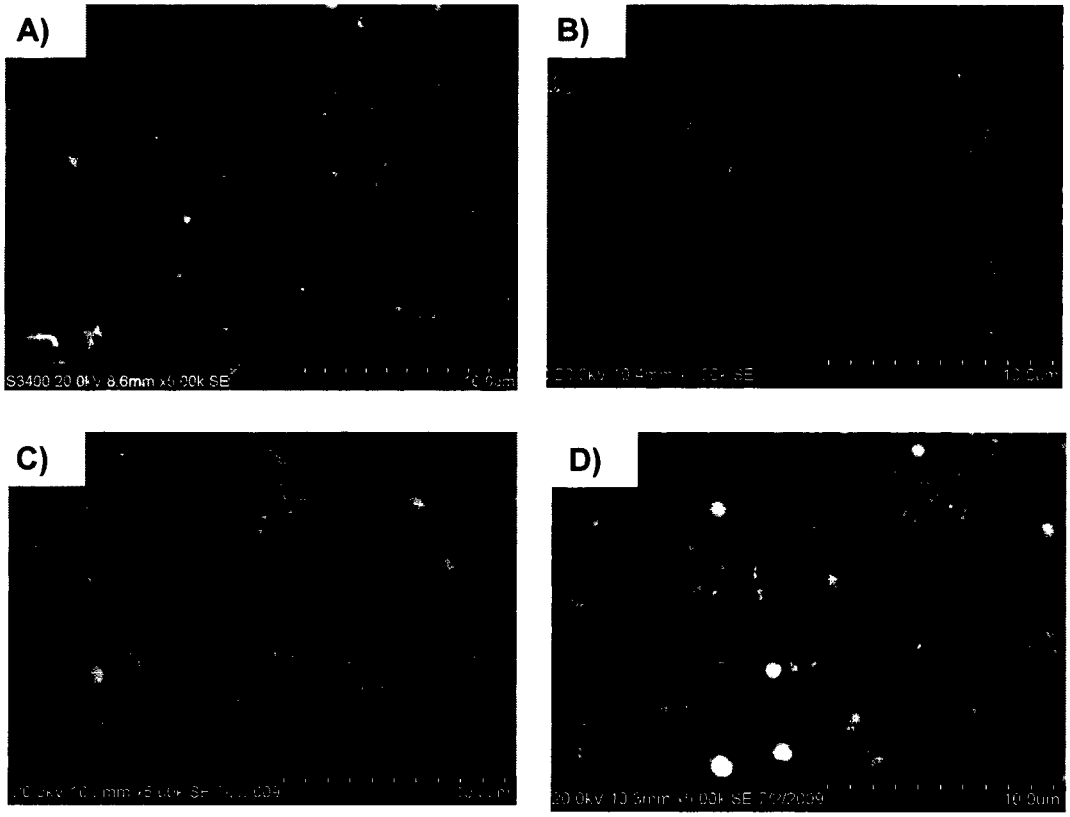

Fig. 16

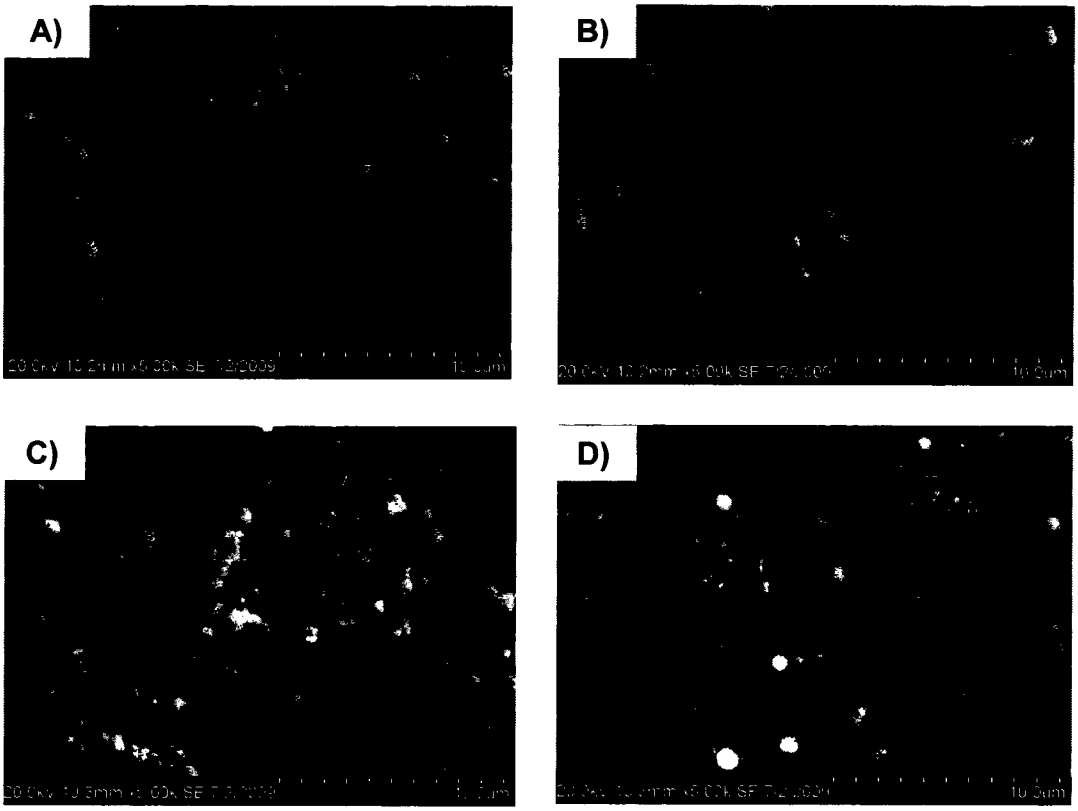

Fig. 17

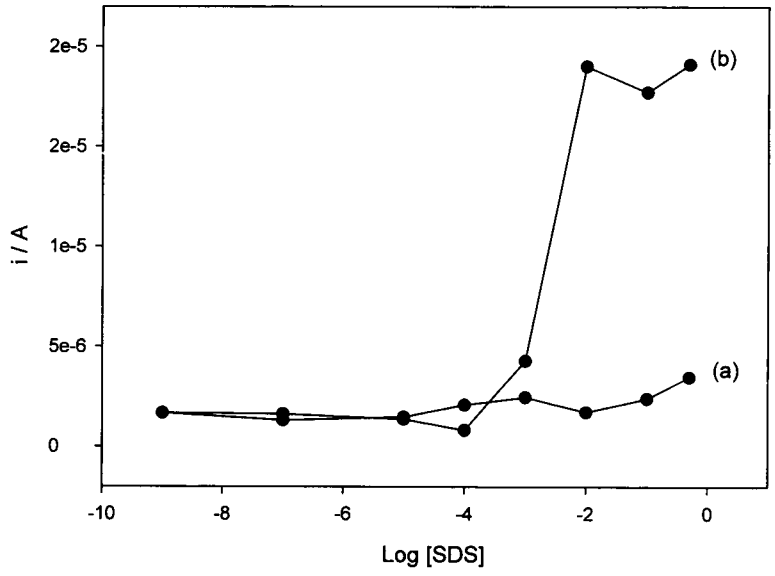

Fig. 18

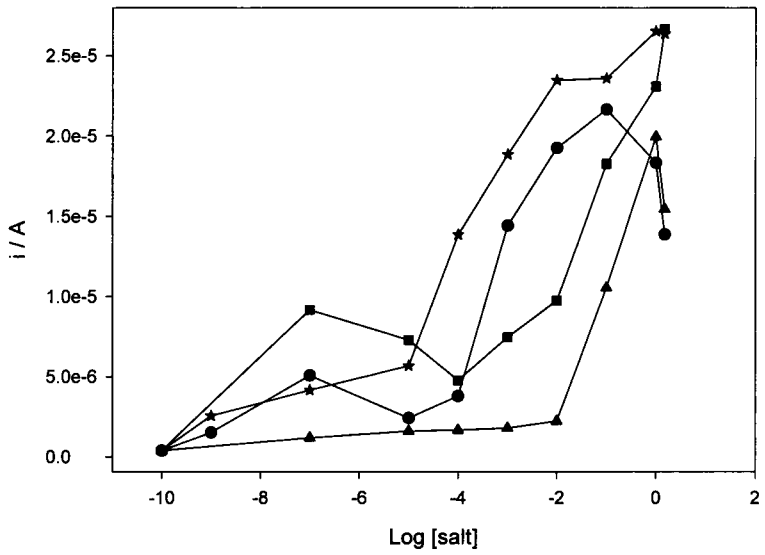
2.5e-5
2.0e-5
1.5e-5
1.0e-5
5.0e-6
0.0
i / A
-10
-8
-6
-4
-2
0
2
Log [salt]

Fig. 19

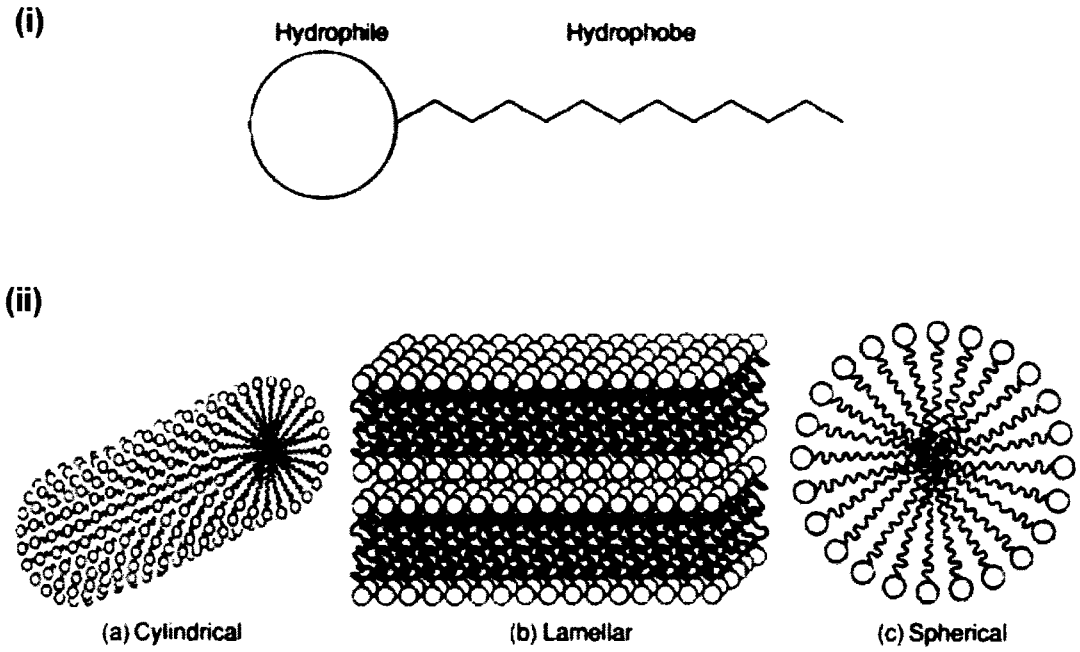
(i)
Hydrophile
Hydrophobe
(ii)
(a) Cylindrical
(b) Lamellar
(c) Spherical

Fig. 20

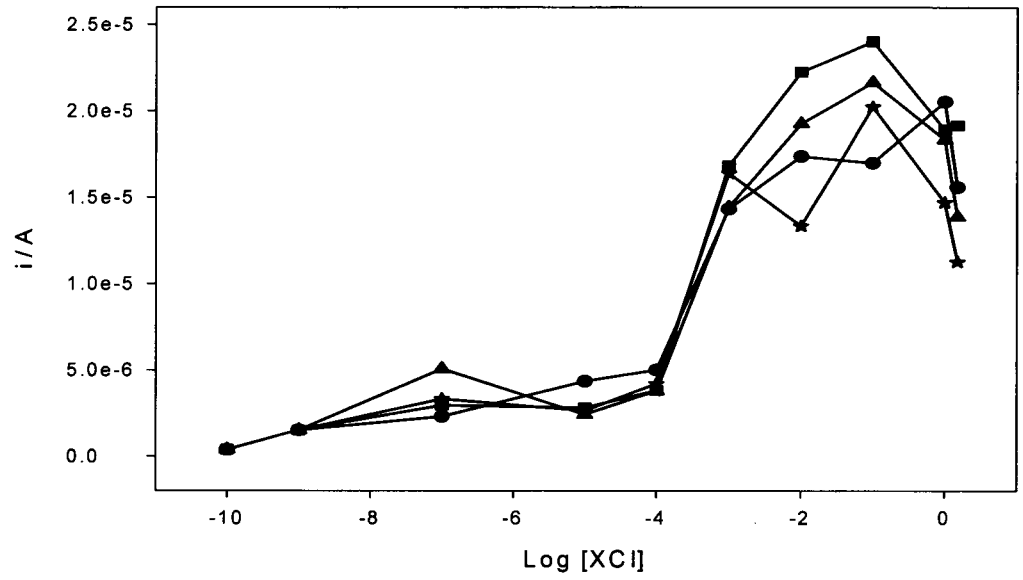
2.5e-5
2.0e-5
1.5e-5
1.0e-5
5.0e-6
0.0
i / A
-10
-8
-6
-4
-2
0
Log [XCl]

Fig. 21

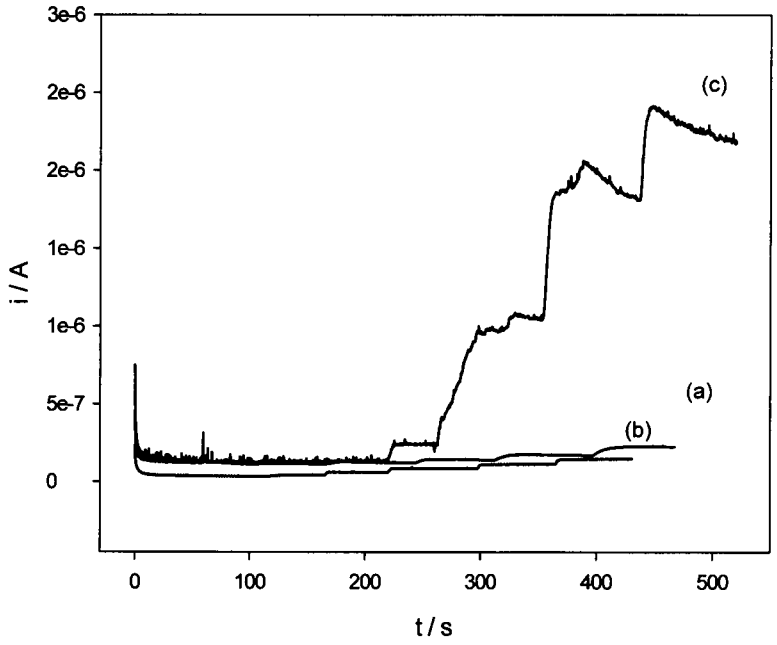
3e-6
2e-6
2e-6
1e-6
1e-6
5e-7
0
i / A
(c)
(a)
(b)
0
100
200
300
400
500
t / s

Fig. 22

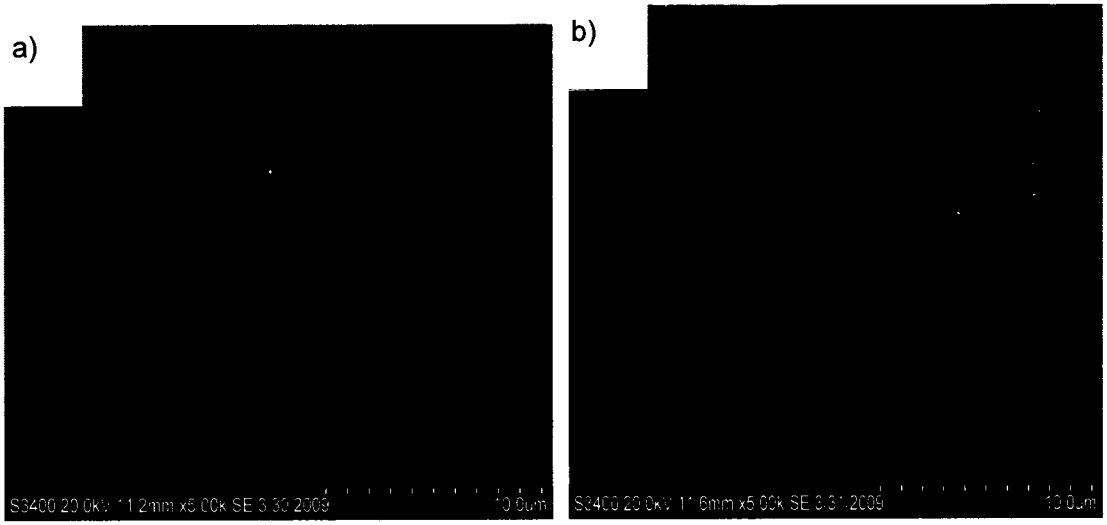

Fig. 23

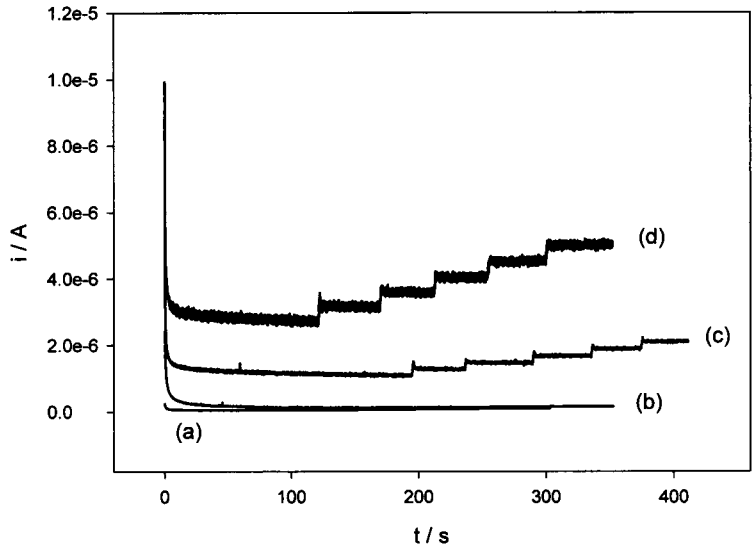

Fig. 24

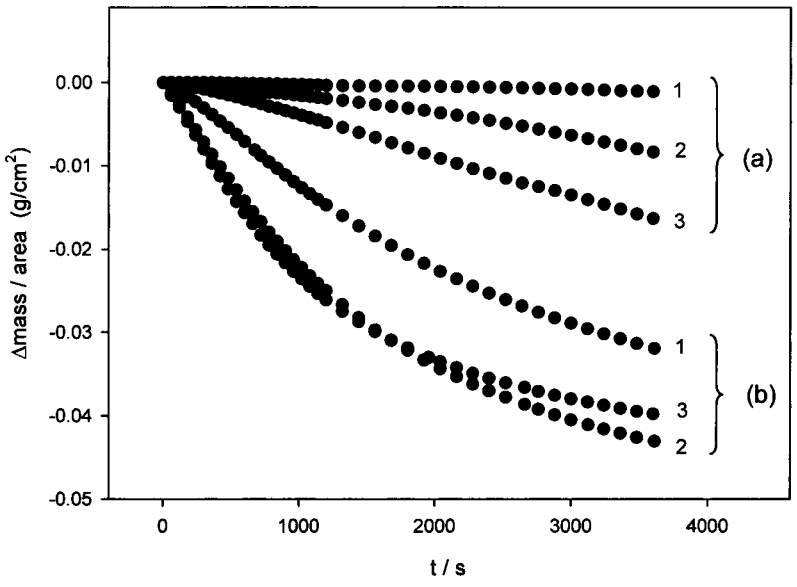
0.00
-0.01
-0.02
-0.03
-0.04
-0.05
Δmass / area (g/cm²)
0
1000
2000
3000
4000
t / s
1
2
3
(a)
1
3
2
(b)

Fig. 25

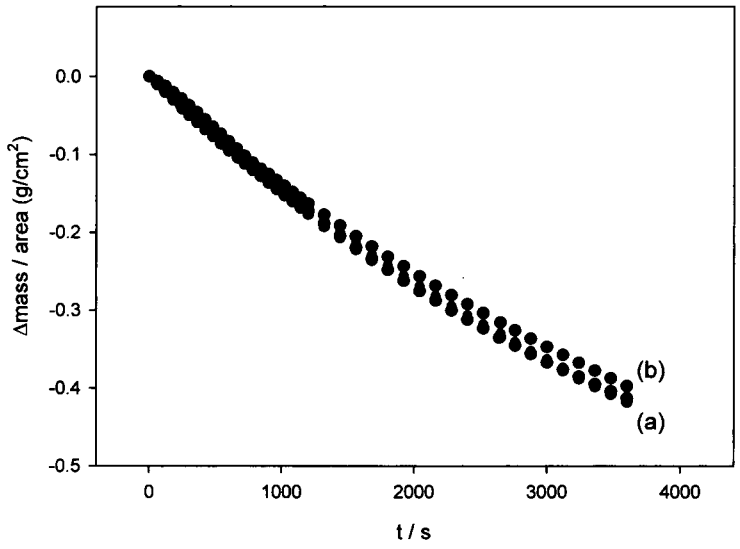
0.0
-0.1
-0.2
-0.3
-0.4
-0.5
Δmass / area (g/cm²)
0
1000
2000
3000
4000
t / s
(b)
(a)

Fig. 26

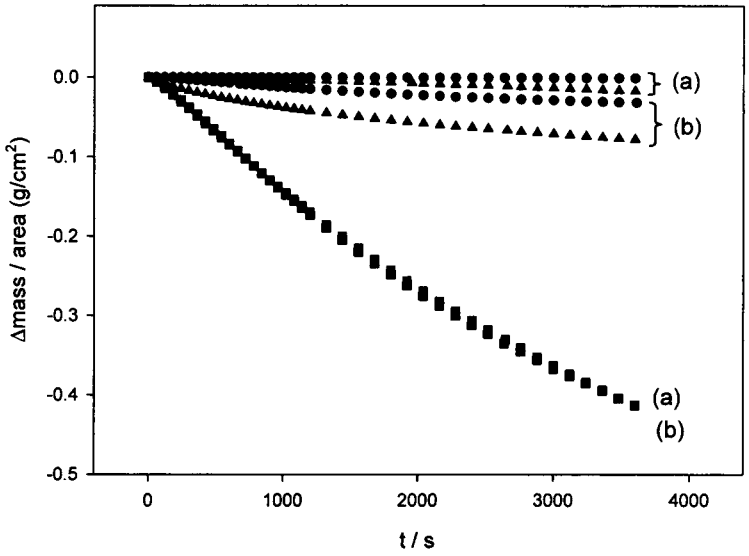
0.0
-0.1
-0.2
-0.3
-0.4
-0.5
Δmass / area (g/cm²)
0
1000
2000
3000
4000
t / s
(a)
(b)
(a)
(b)

Fig. 27

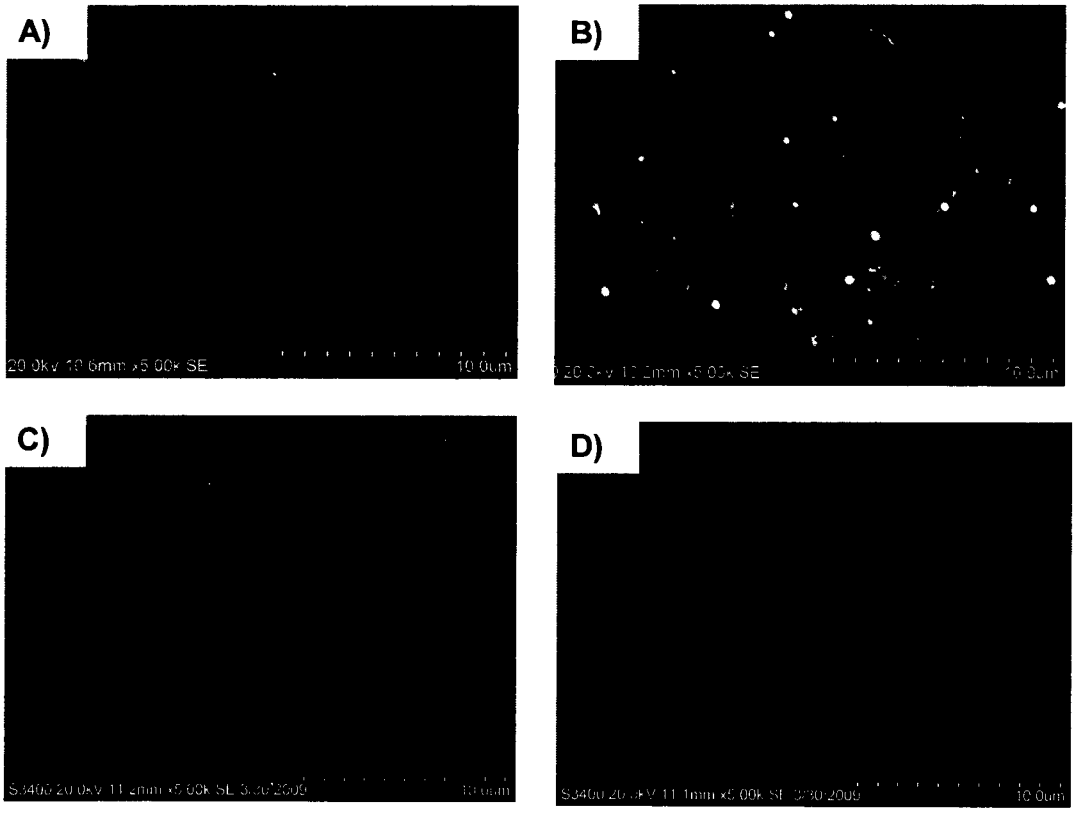
A)
B)
C)
D)

Fig. 28

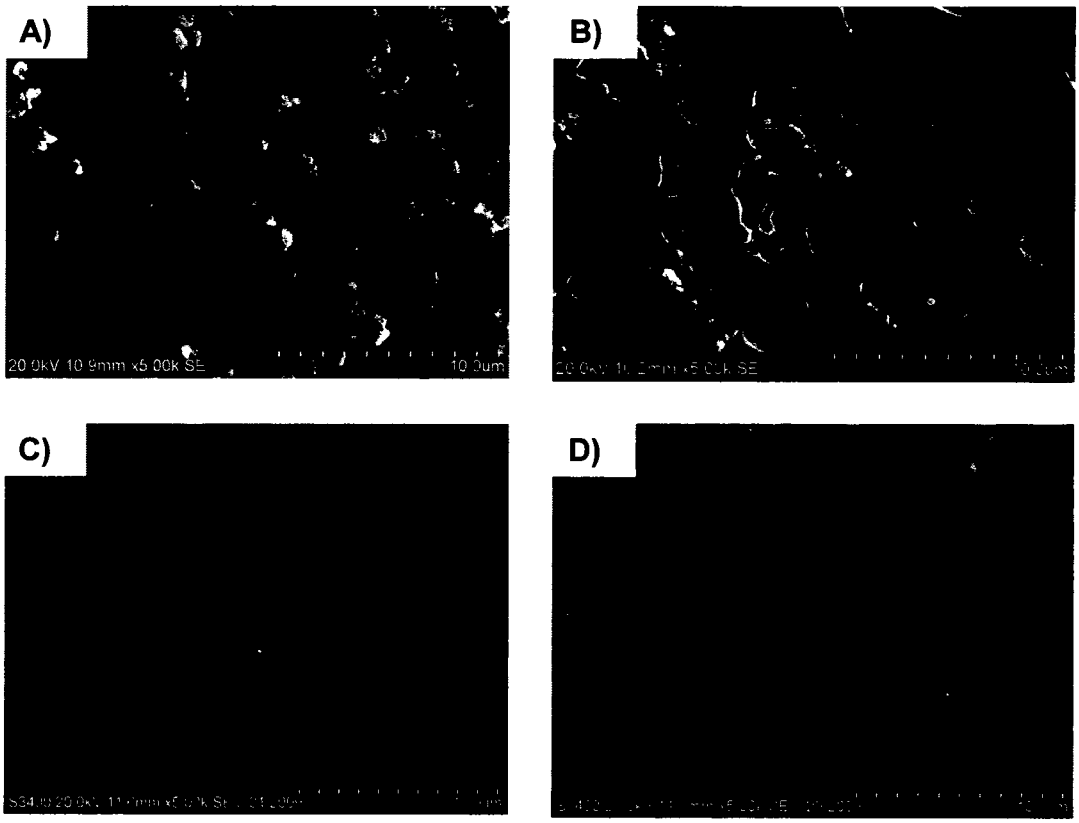

Fig. 29

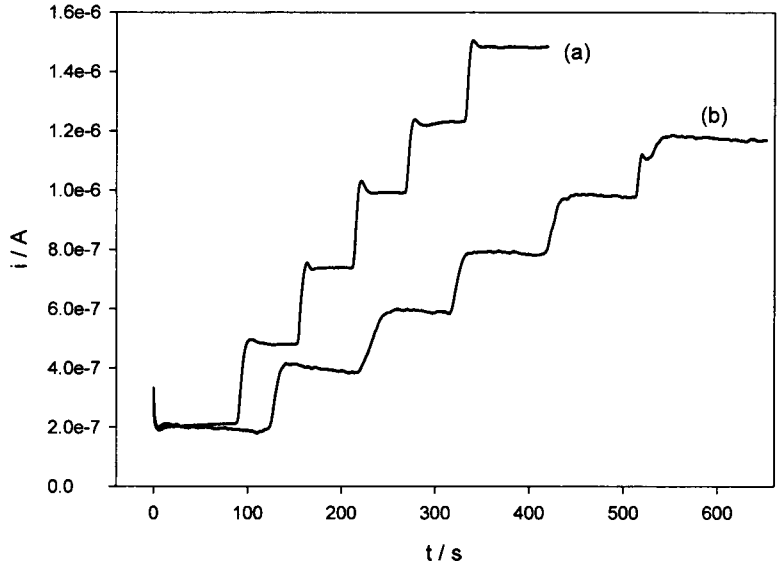
1.6e-6
1.4e-6
1.2e-6
1.0e-6
8.0e-7
6.0e-7
4.0e-7
2.0e-7
0.0
i / A
0
100
200
300
400
500
600
t / s
(a)
(b)

Fig. 30

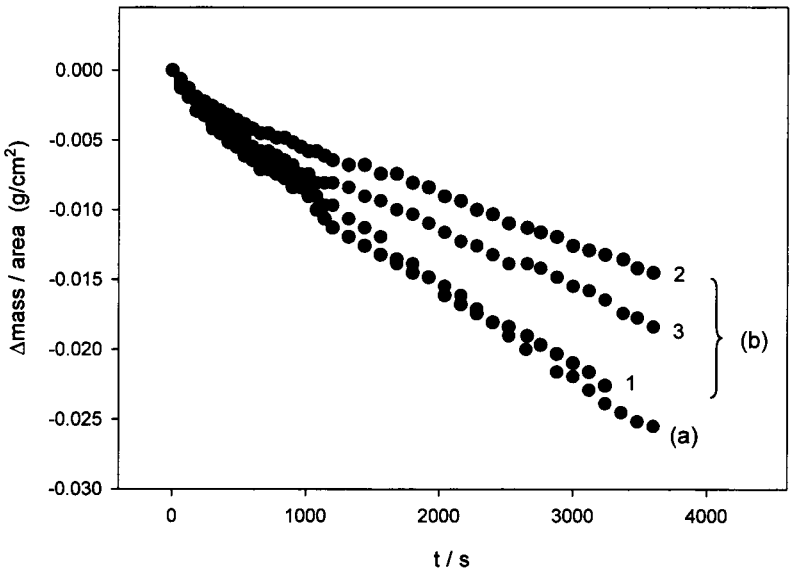
0.000
-0.005
-0.010
-0.015
-0.020
-0.025
-0.030
Δmass / area (g/cm²)
0
1000
2000
3000
4000
t / s
2
3
1
(b)
(a)

Fig. 31

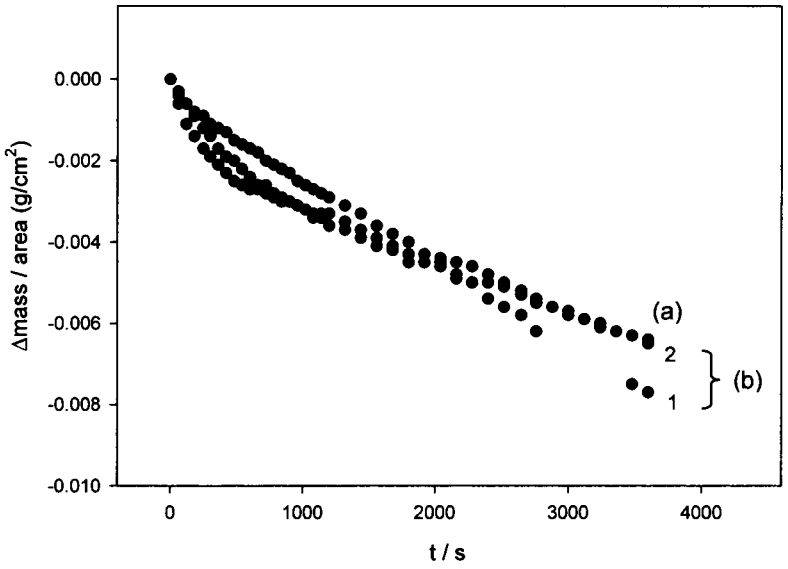
0.000
-0.002
-0.004
-0.006
-0.008
-0.010
Δmass / area (g/cm²)
0
1000
2000
3000
4000
t / s
(a)
2
1
(b)

Fig. 32

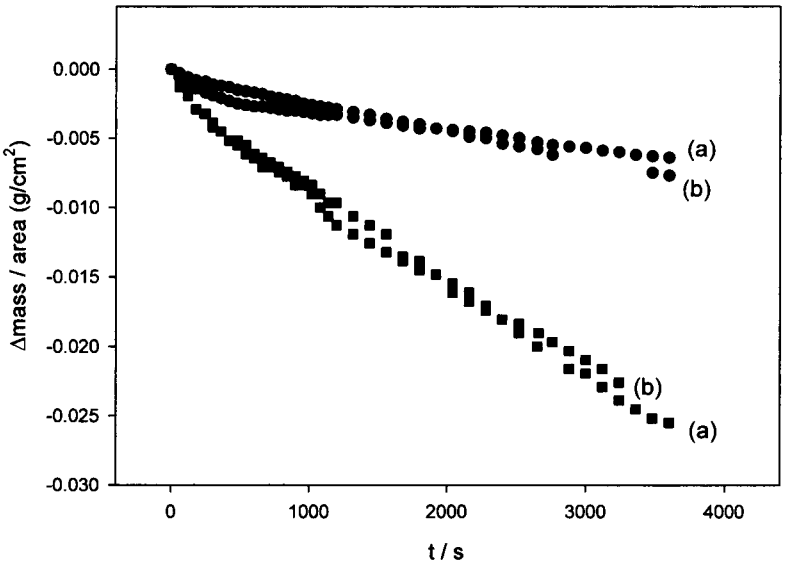
0.000
-0.005
-0.010
-0.015
-0.020
-0.025
-0.030
Δmass / area (g/cm²)
0
1000
2000
3000
4000
t / s
(a)
(b)
(b)
(a)

Fig. 33

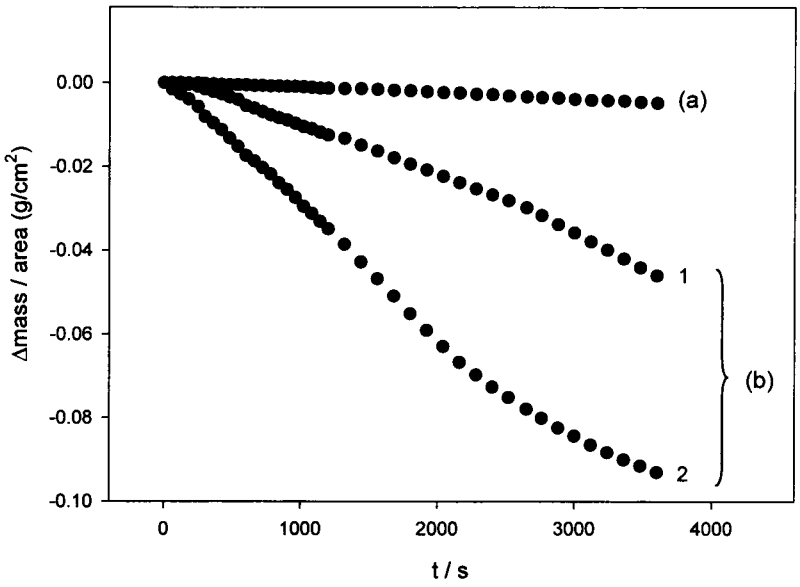
0.00
-0.02
-0.04
-0.06
-0.08
-0.10
Δmass / area (g/cm²)
0
1000
2000
3000
4000
t / s
(a)
1
(b)
2

Fig. 34

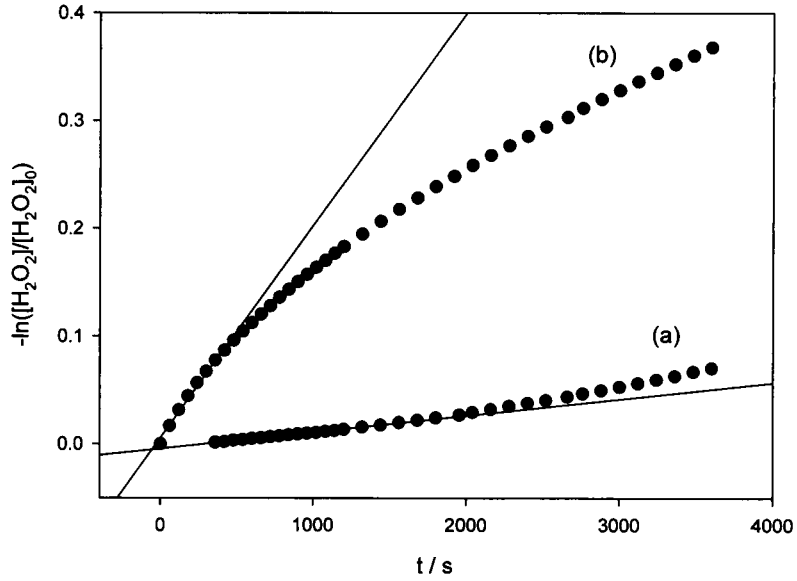
0.4
0.3
0.2
0.1
0.0
-ln([H₂O₂]/[H₂O₂]₀)
0
1000
2000
3000
4000
t / s
(b)
(a)

Fig. 35

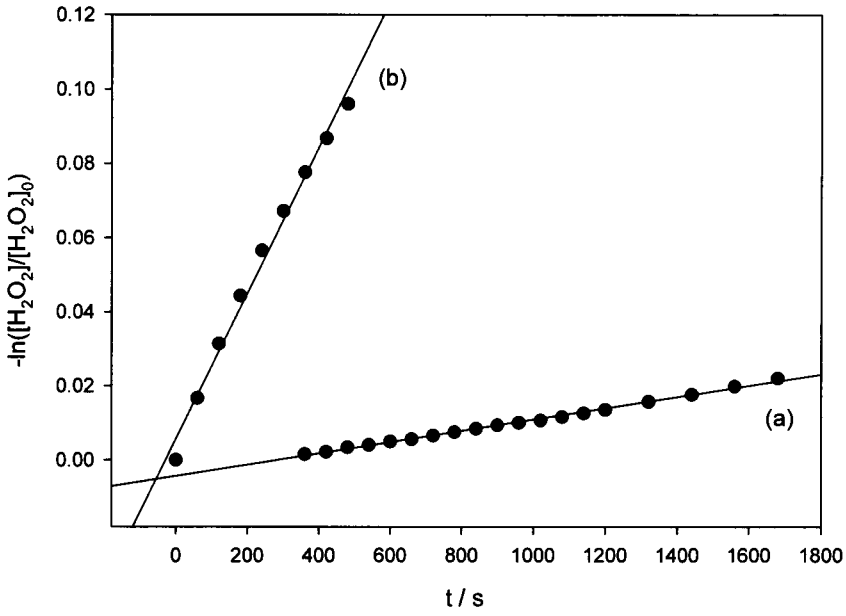
0.12
0.10
0.08
0.06
0.04
0.02
0.00
-ln([H2O2]/[H2O2]0)
(b)
(a)
0
200
400
600
800
1000
1200
1400
1600
1800
t / s

Fig. 36

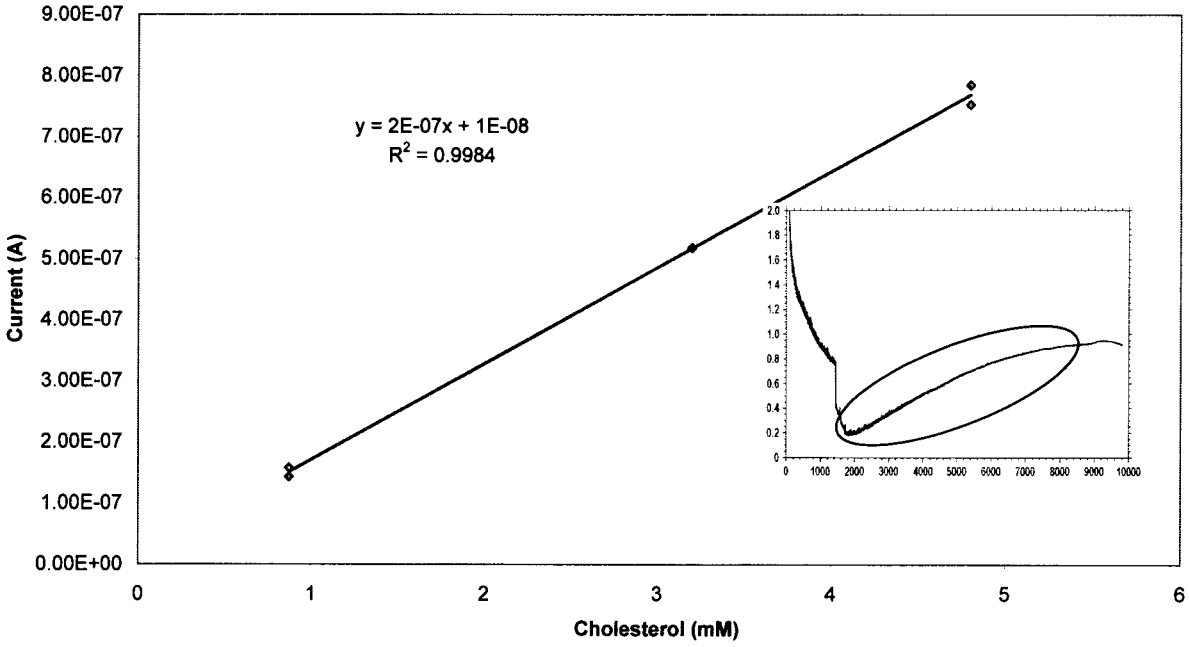
9.00E-07
8.00E-07
7.00E-07
6.00E-07
5.00E-07
4.00E-07
3.00E-07
2.00E-07
1.00E-07
0.00E+00
Current (A)
y = 2E-07x + 1E-08
R2 = 0.9984
0
1
2
3
4
5
6
Cholesterol (mM)

Fig. 37

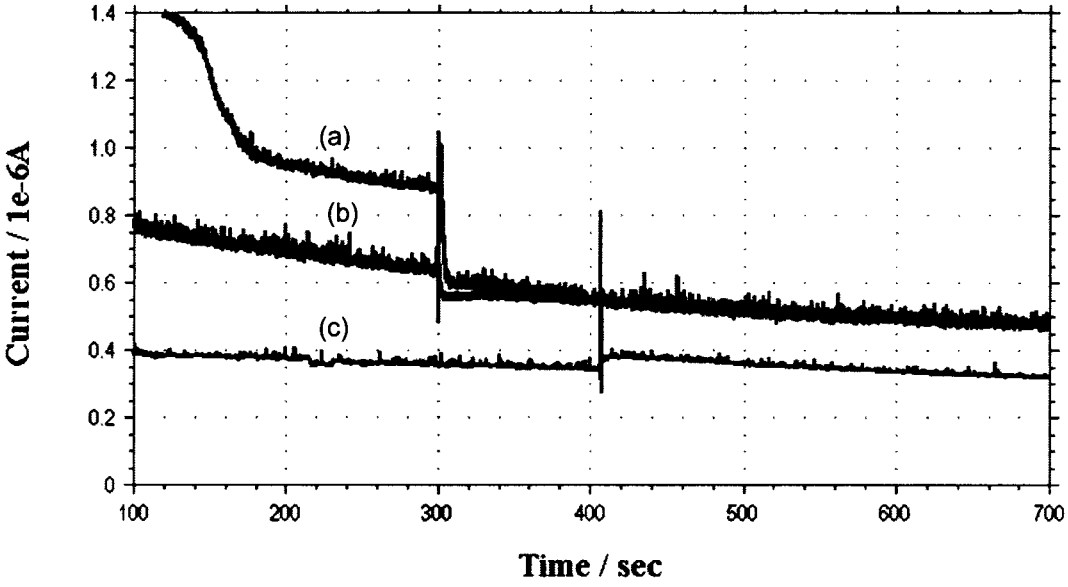
Current / 1e-6A
Time / sec
(a)
(b)
(c)
1.4
1.2
1.0
0.8
0.6
0.4
0.2
0
100
200
300
400
500
600
700

Fig. 38

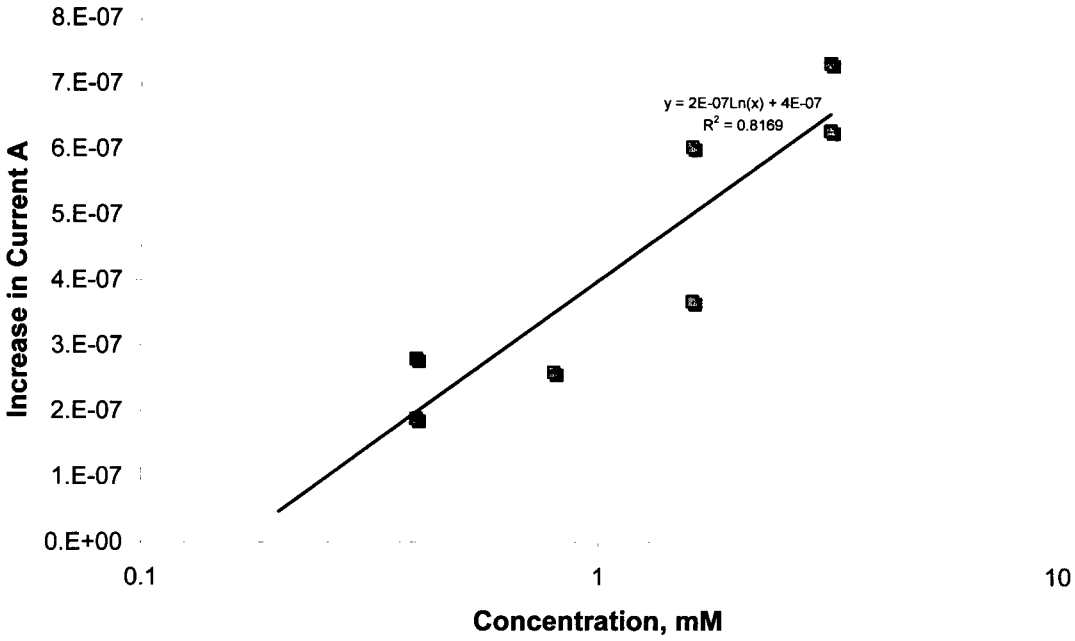
Increase in Current A
Concentration, mM
y = 2E-07Ln(x) + 4E-07
R² = 0.8169
8.E-07
7.E-07
6.E-07
5.E-07
4.E-07
3.E-07
2.E-07
1.E-07
0.E+00
0.1
1
10

Fig. 39

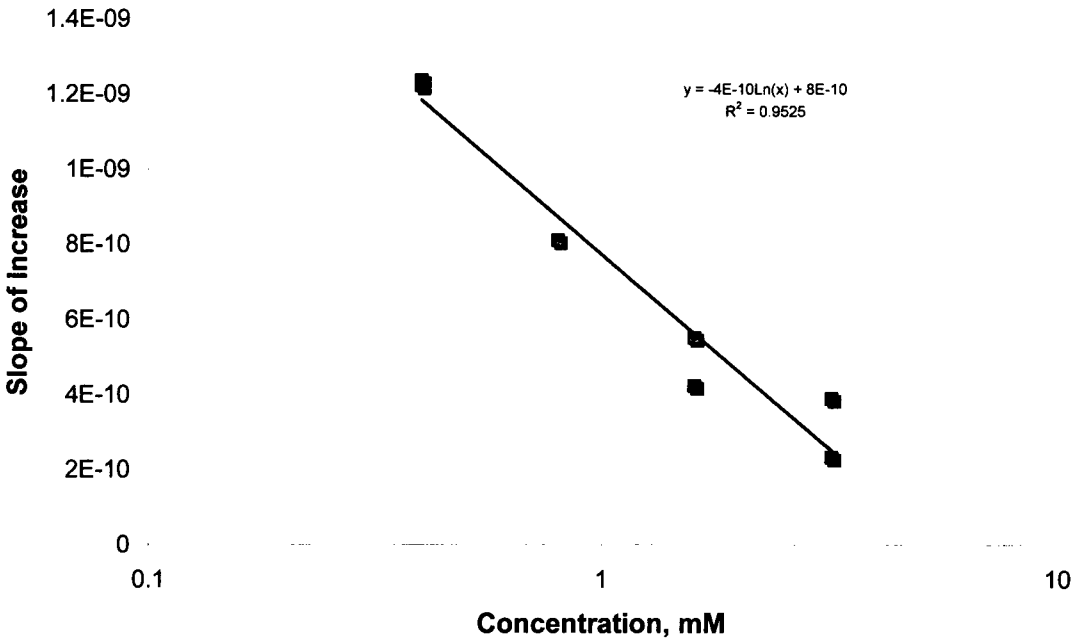
1.4E-09
1.2E-09
1E-09
8E-10
6E-10
4E-10
2E-10
0
Slope of Increase
y = -4E-10Ln(x) + 8E-10
R2 = 0.9525
0.1
1
10
Concentration, mM

Fig. 40

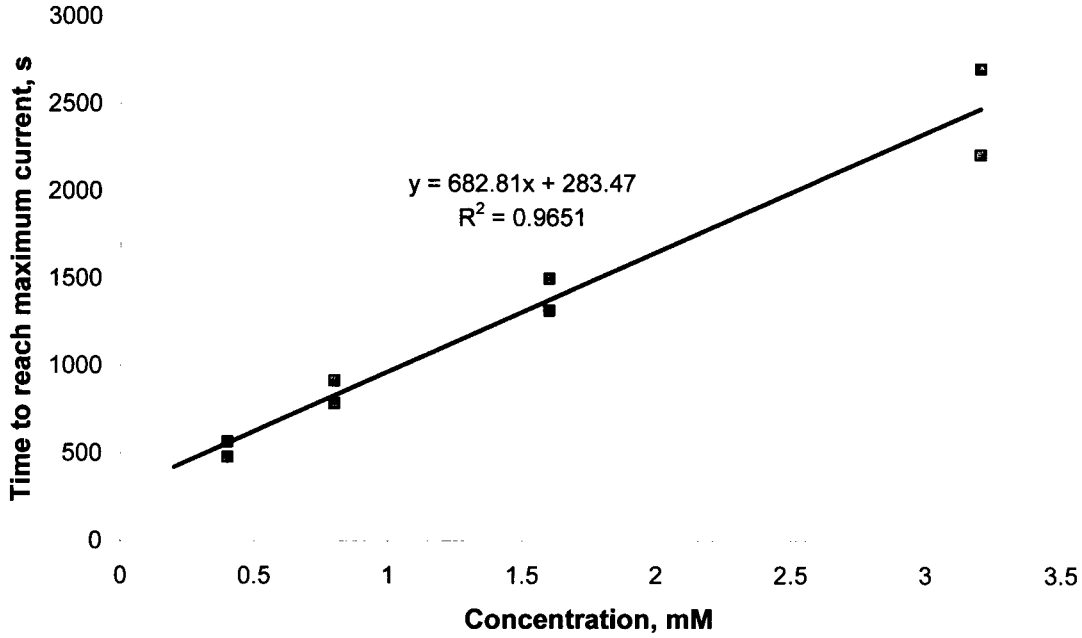
3000
2500
2000
1500
1000
500
0
Time to reach maximum current, s
y = 682.81x + 283.47
R2 = 0.9651
0
0.5
1
1.5
2
2.5
3
3.5
Concentration, mM

Fig. 41

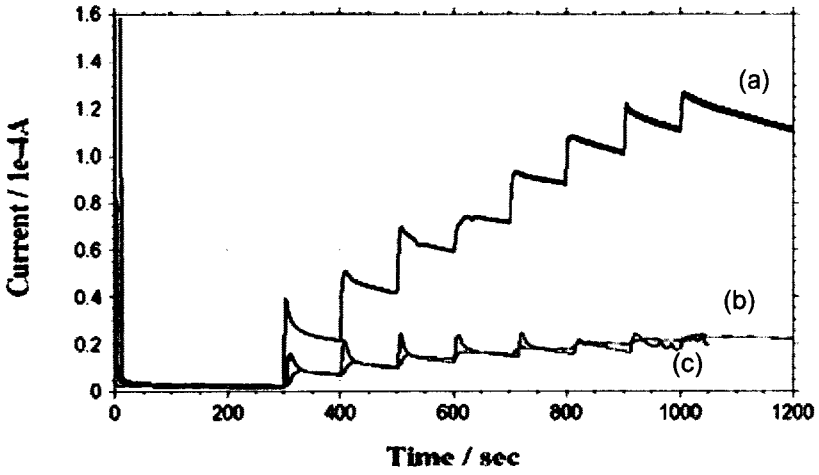
Current / 1e-4A
Time / sec
(a)
(b)
(c)

Fig. 42

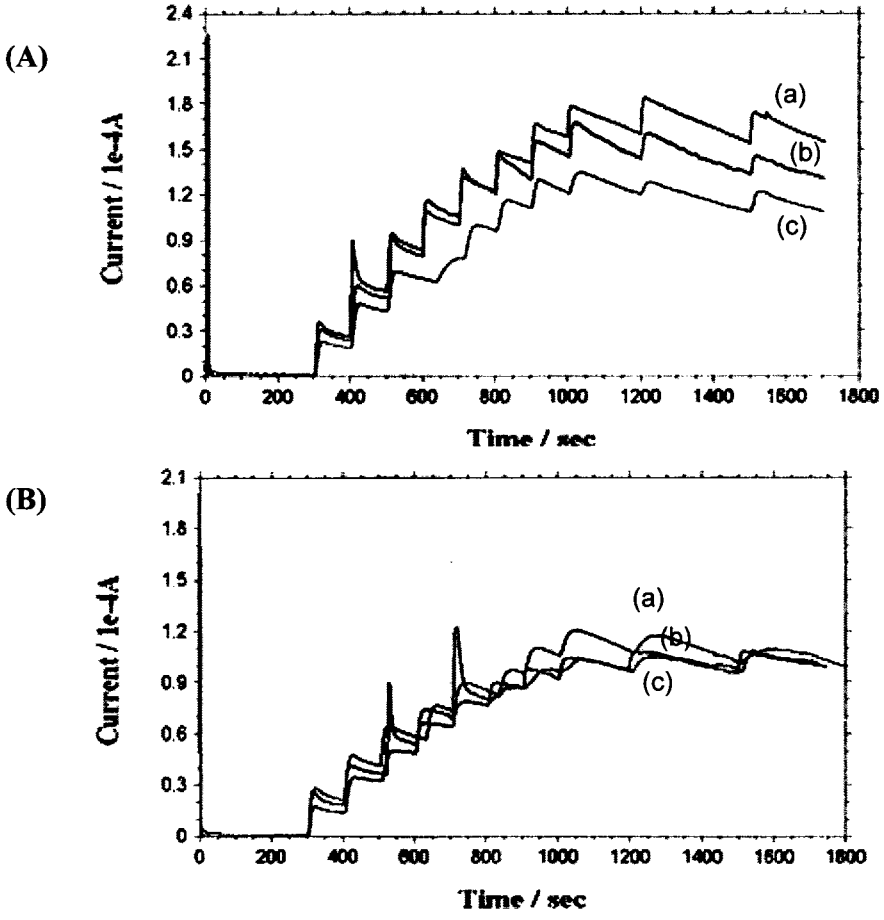
(A)
Current / 1e-4A
Time / sec
(a)
(b)
(c)
(B)
Current / 1e-4A
Time / sec
(a)
(b)
(c)

Fig. 43

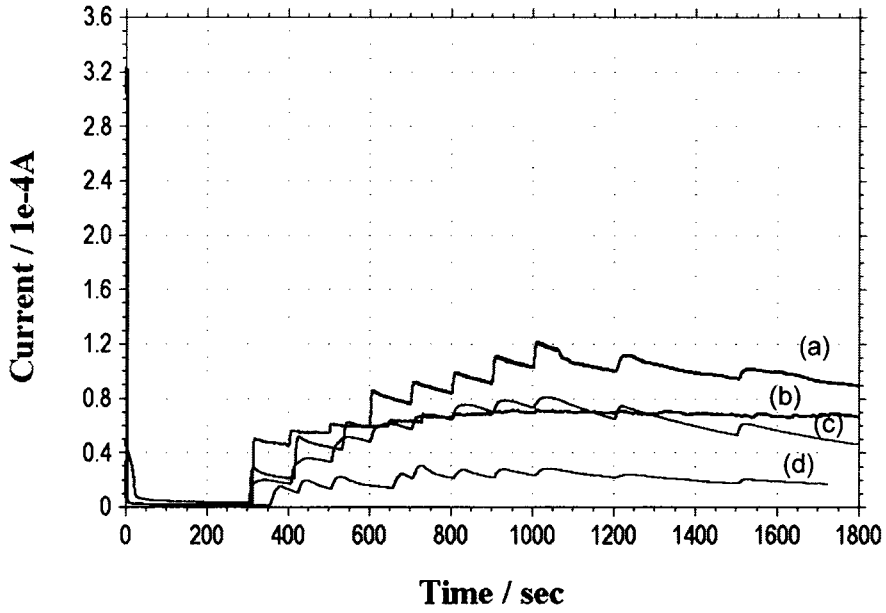
Current / 1e-4A
Time / sec
(a)
(b)
(c)
(d)
0
0.4
0.8
1.2
1.6
2.0
2.4
2.8
3.2
3.6
0
200
400
600
800
1000
1200
1400
1600
1800

Fig. 44

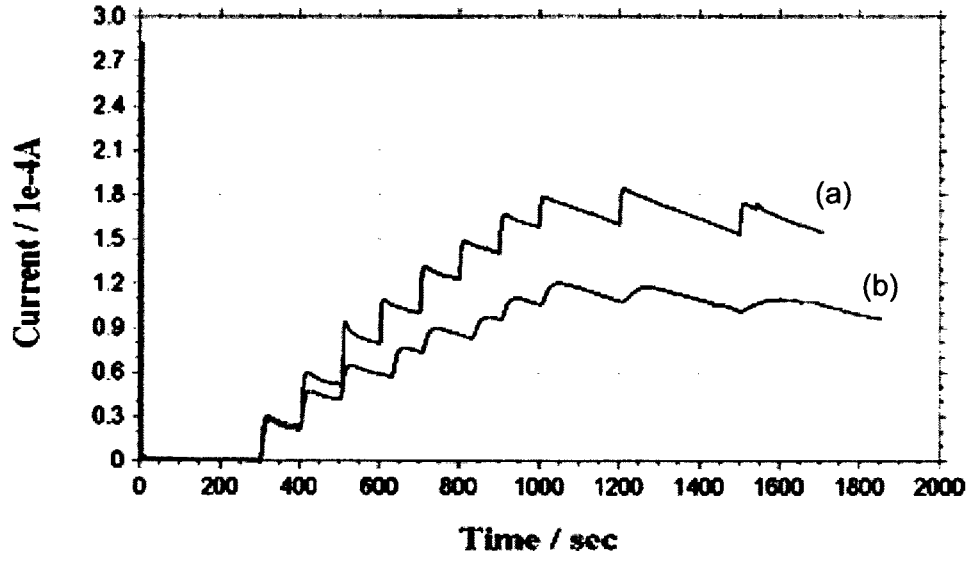
Current / 1e-4A
Time / sec
(a)
(b)
0
0.3
0.6
0.9
1.2
1.5
1.8
2.1
2.4
2.7
3.0
0
200
400
600
800
1000
1200
1400
1600
1800
2000

Fig. 45

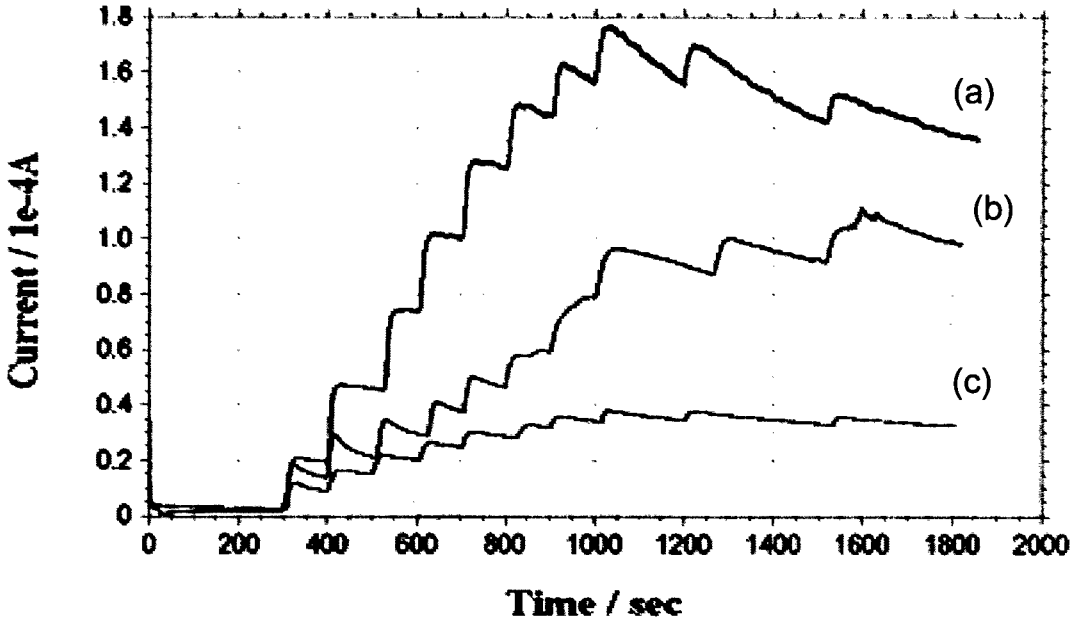
Current / 1e-4A
Time / sec
(a)
(b)
(c)
0
0.2
0.4
0.6
0.8
1.0
1.2
1.4
1.6
1.8
0
200
400
600
800
1000
1200
1400
1600
1800
2000

Fig. 46

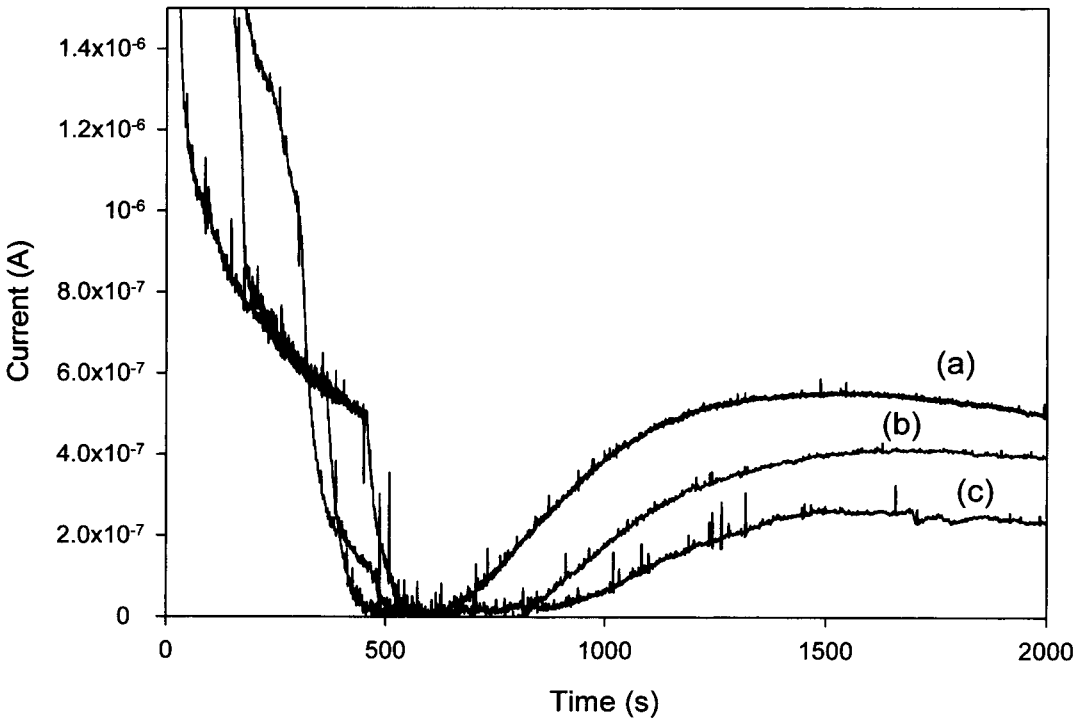
Current (A)
Time (s)
(a)
(b)
(c)
1.4x10-6
1.2x10-6
10-6
8.0x10-7
6.0x10-7
4.0x10-7
2.0x10-7
0
0
500
1000
1500
2000

Fig. 47

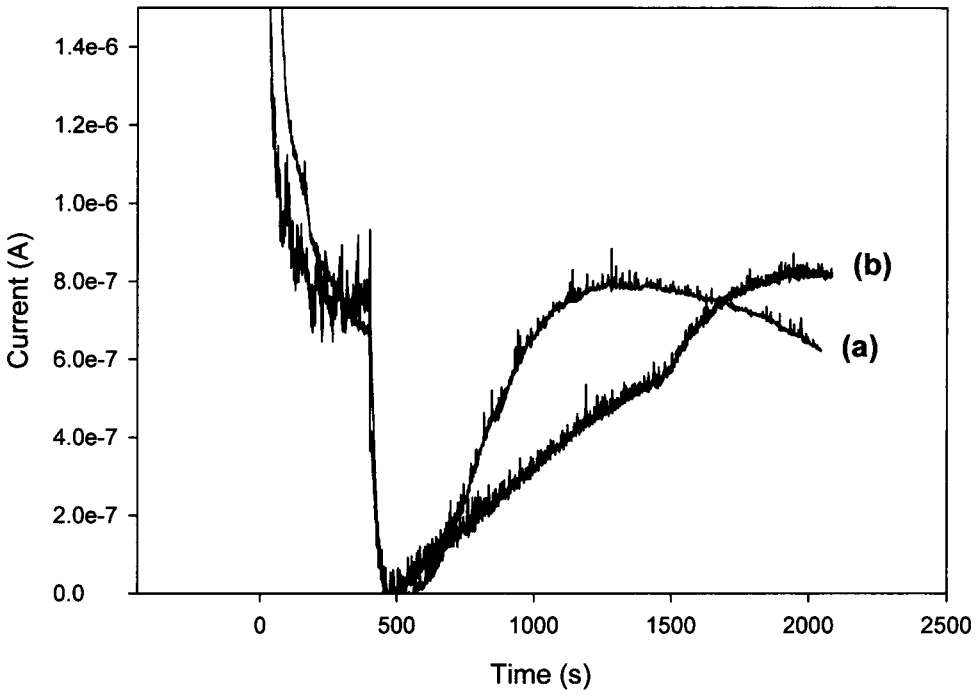
1.4e-6
1.2e-6
1.0e-6
8.0e-7
6.0e-7
4.0e-7
2.0e-7
0.0
Current (A)
0
500
1000
1500
2000
2500
Time (s)
(b)
(a)

Fig. 48

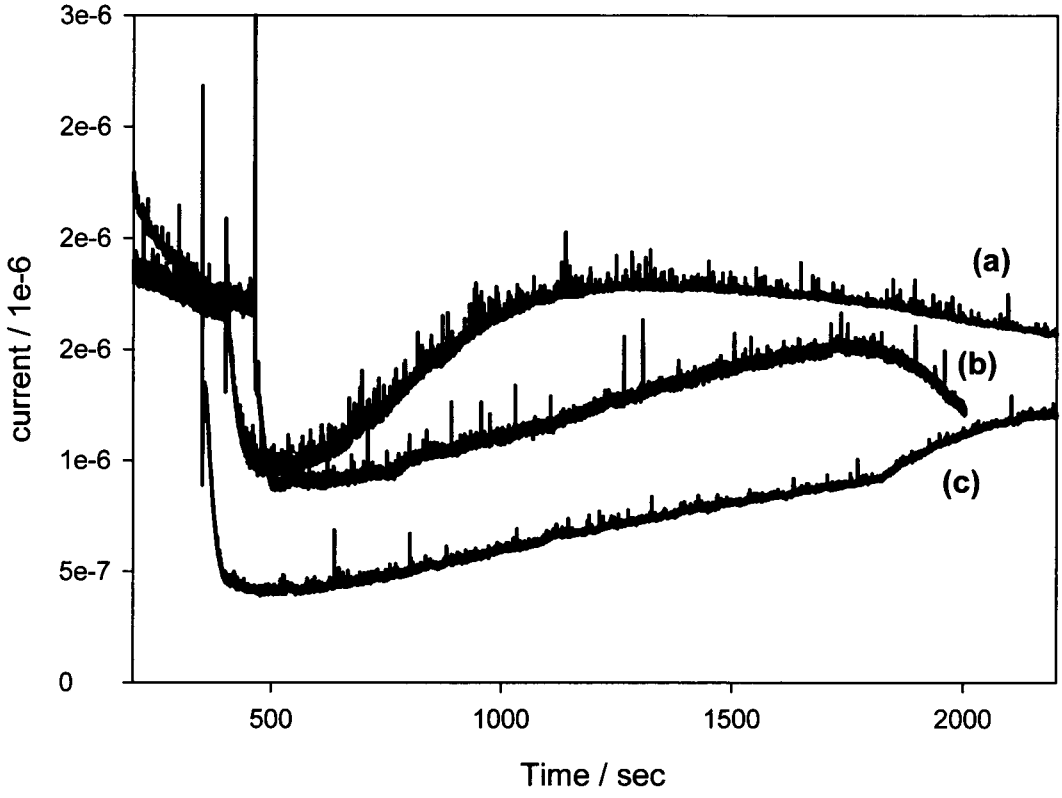
3e-6
2e-6
2e-6
2e-6
1e-6
5e-7
0
current / 1e-6
500
1000
1500
2000
Time / sec
(a)
(b)
(c)

Fig. 49

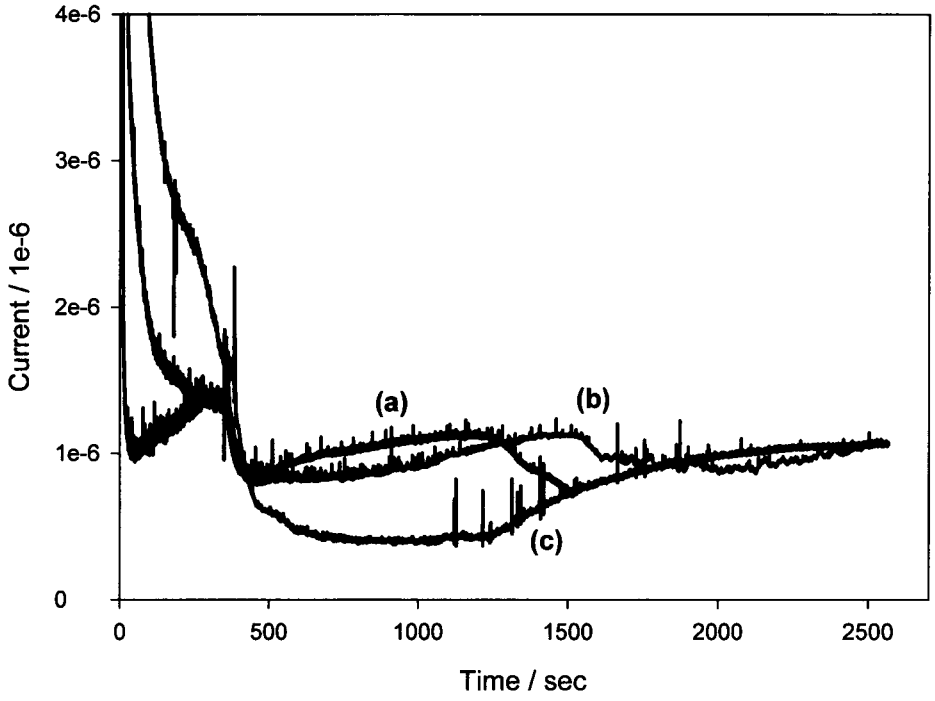
4e-6
3e-6
2e-6
1e-6
0
Current / 1e-6
0
500
1000
1500
2000
2500
Time / sec
(a)
(b)
(c)

Fig. 50

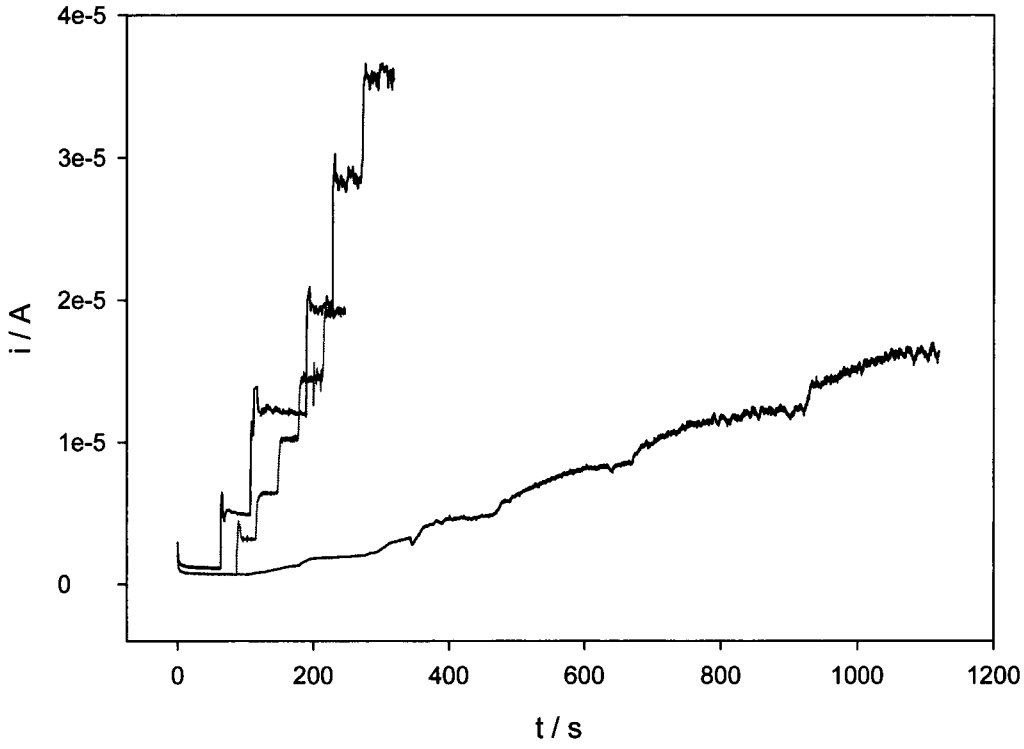
4e-5
3e-5
2e-5
1e-5
0
i / A
0
200
400
600
800
1000
1200
t / s

Fig. 51

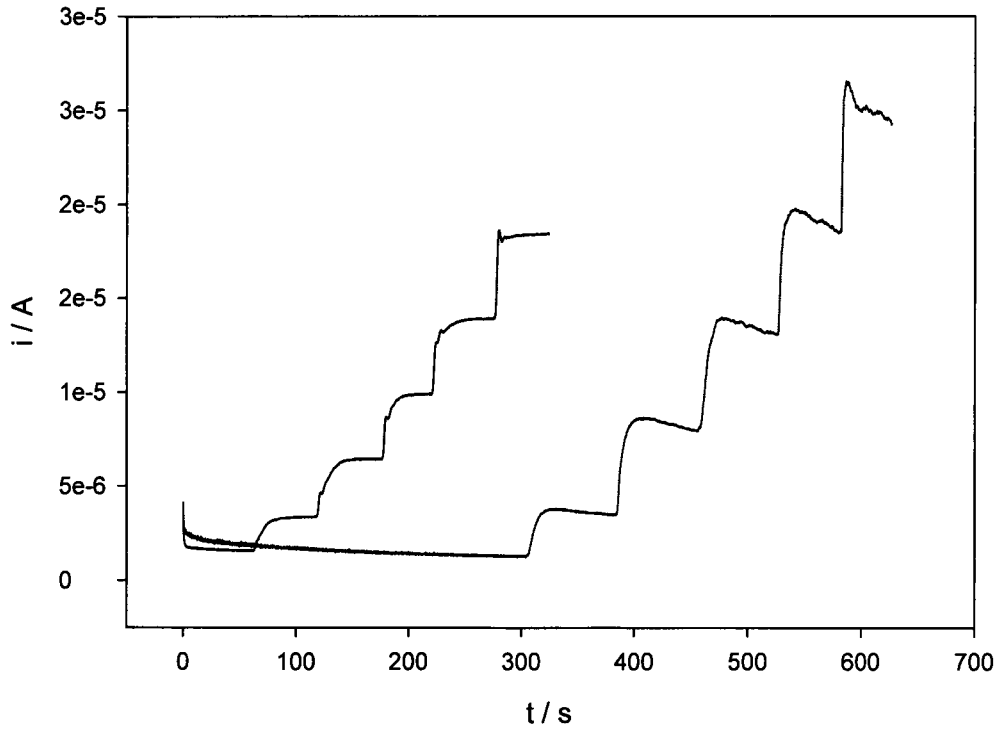
3e-5
3e-5
2e-5
2e-5
1e-5
5e-6
0
i / A
0
100
200
300
400
500
600
700
t / s

Fig. 52

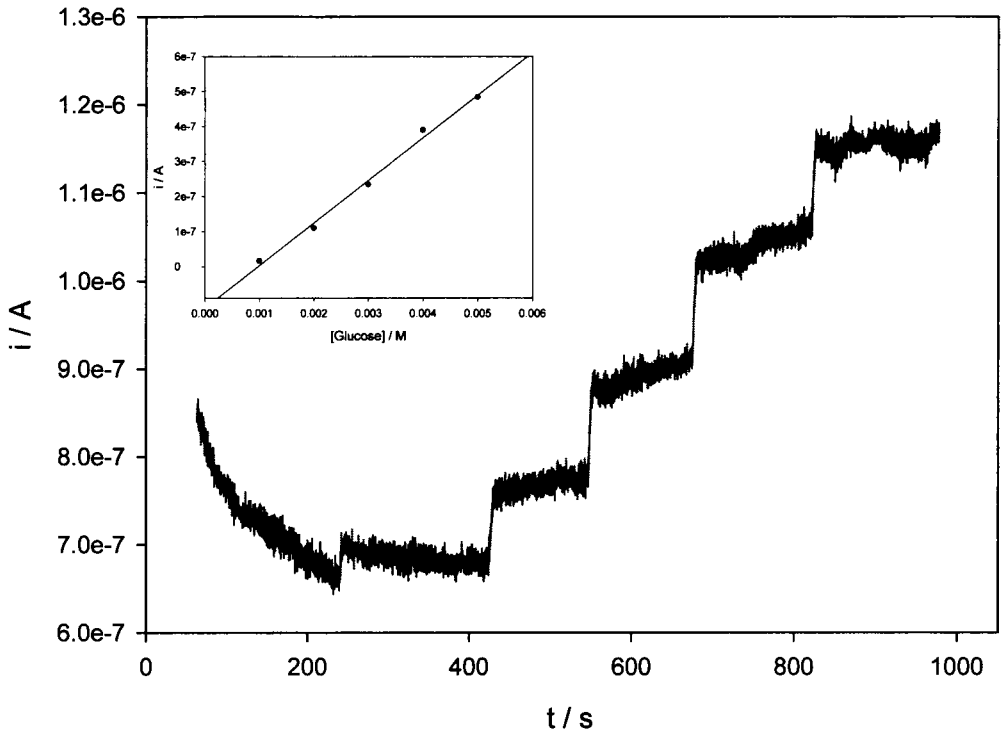
1.3e-6
1.2e-6
1.1e-6
1.0e-6
9.0e-7
8.0e-7
7.0e-7
6.0e-7
i / A
0
200
400
600
800
1000
t / s
6e-7
5e-7
4e-7
3e-7
2e-7
1e-7
0
i / A
0.000
0.001
0.002
0.003
0.004
0.005
0.006
[Glucose] / M

Fig. 53

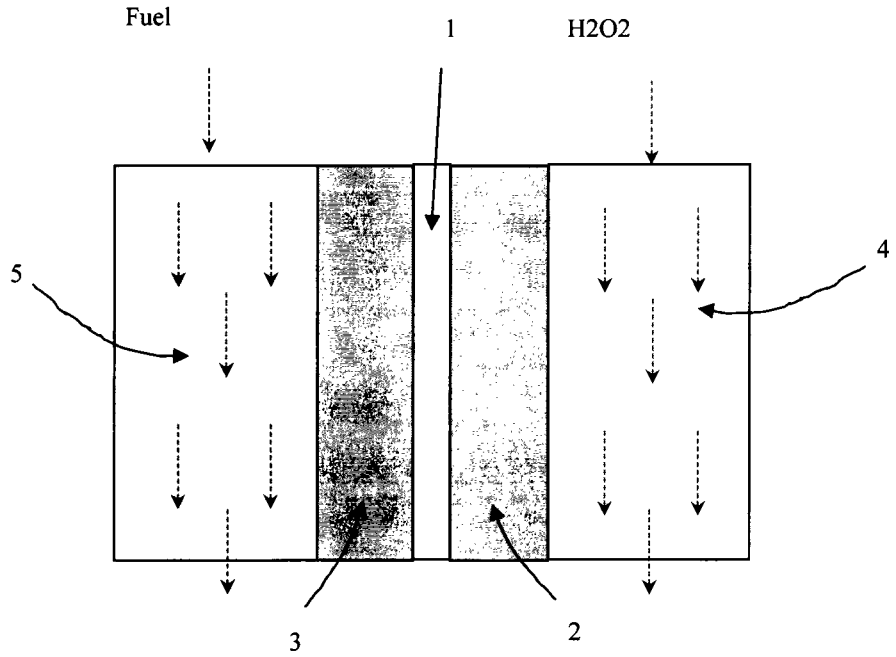
Fuel
1
H2O2
5
4
3
2

Fig. 54

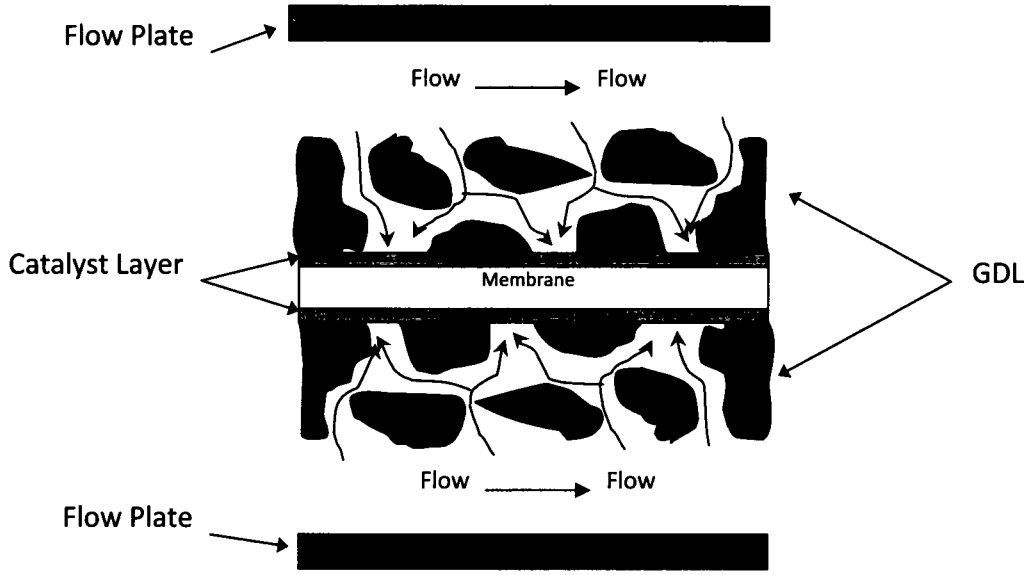
Flow Plate
Flow
Flow
Catalyst Layer
Membrane
GDL
Flow
Flow
Flow Plate

Fig. 55

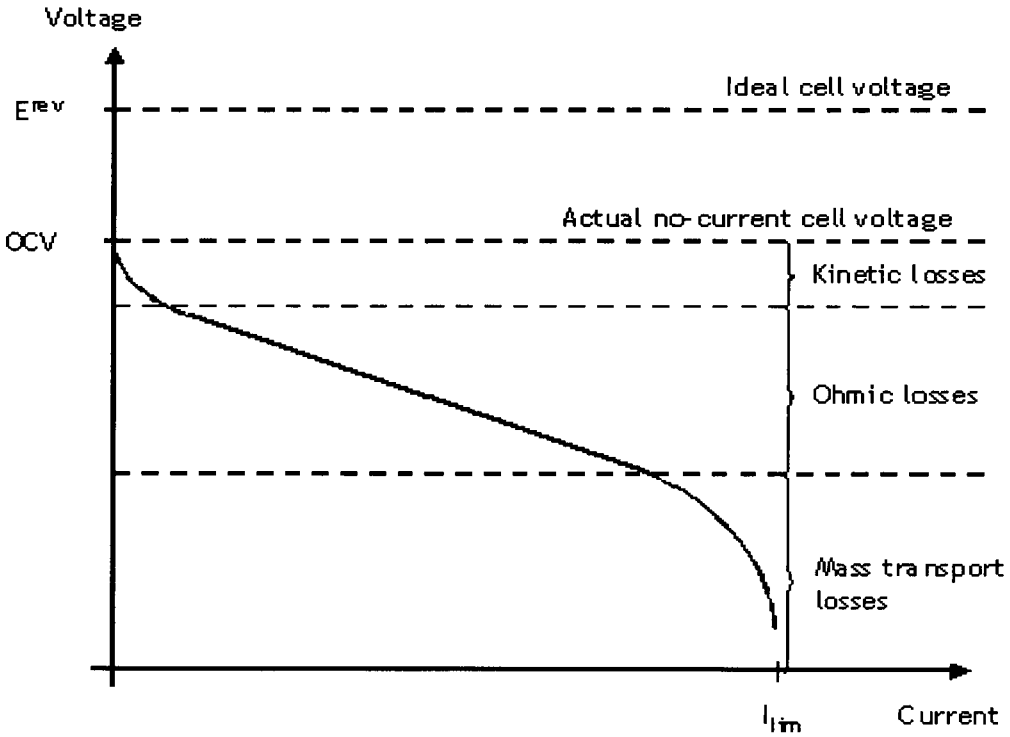
Voltage
Ideal cell voltage
E rev
Actual no-current cell voltage
OCV
Kinetic losses
Ohmic losses
Mass transport losses
I lim
Current

Fig. 56

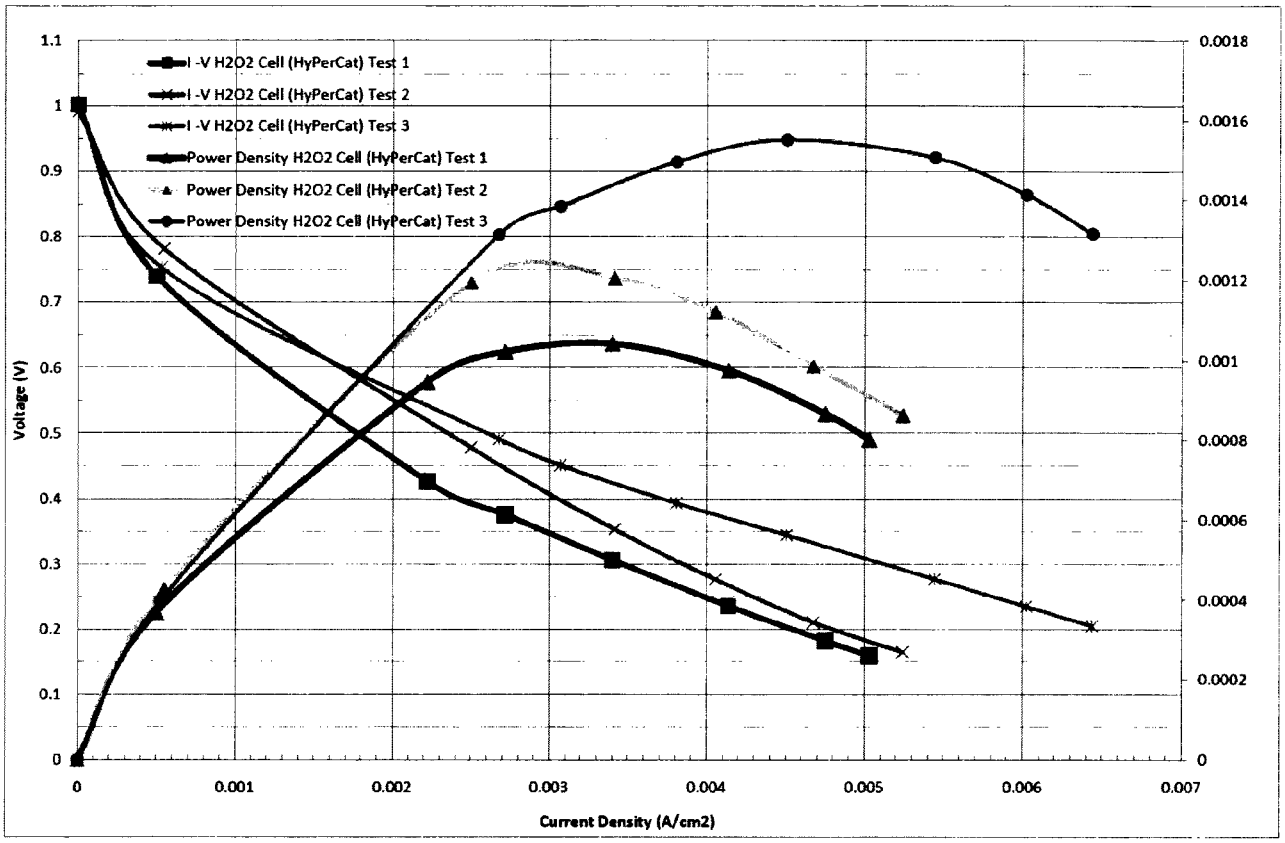
I -V H2O2 Cell (HyPerCat) Test 1
I -V H2O2 Cell (HyPerCat) Test 2
I -V H2O2 Cell (HyPerCat) Test 3
Power Density H2O2 Cell (HyPerCat) Test 1
Power Density H2O2 Cell (HyPerCat) Test 2
Power Density H2O2 Cell (HyPerCat) Test 3
Voltage (V)
Current Density (A/cm2)
1.1
1
0.9
0.8
0.7
0.6
0.5
0.4
0.3
0.2
0.1
0
0.0018
0.0016
0.0014
0.0012
0.001
0.0008
0.0006
0.0004
0.0002
0
0.001
0.002
0.003
0.004
0.005
0.006
0.007

Fig. 57

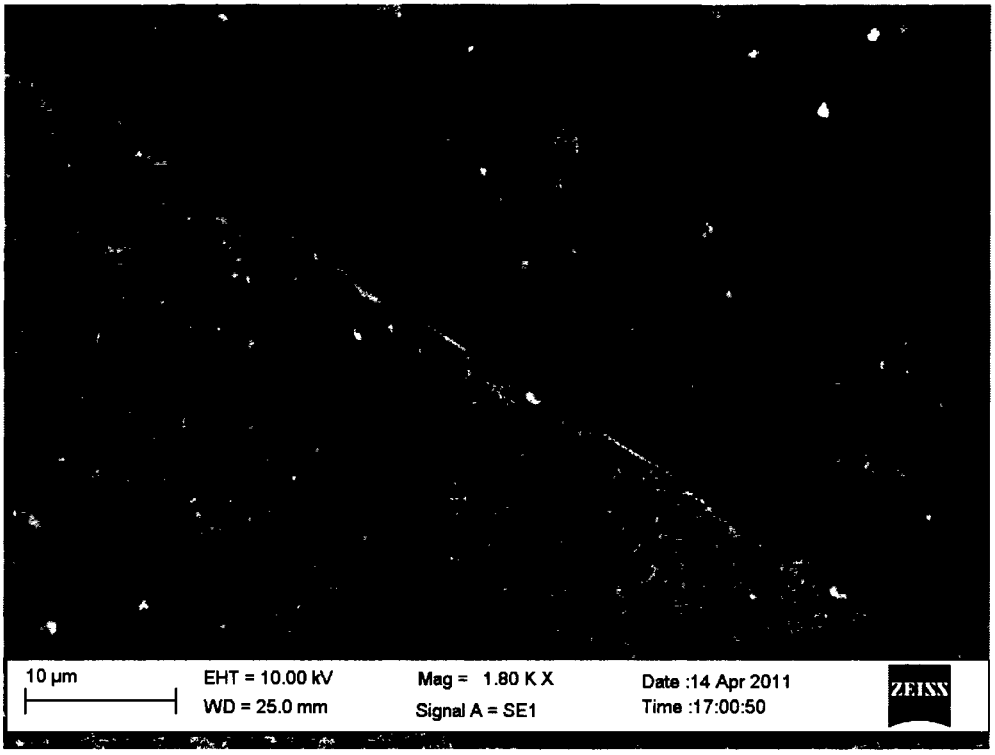
10 µm
EHT = 10.00 kV
WD = 25.0 mm
Mag = 1.80 K X
Signal A = SE1
Date :14 Apr 2011
Time :17:00:50
ZEISS

Fig. 58

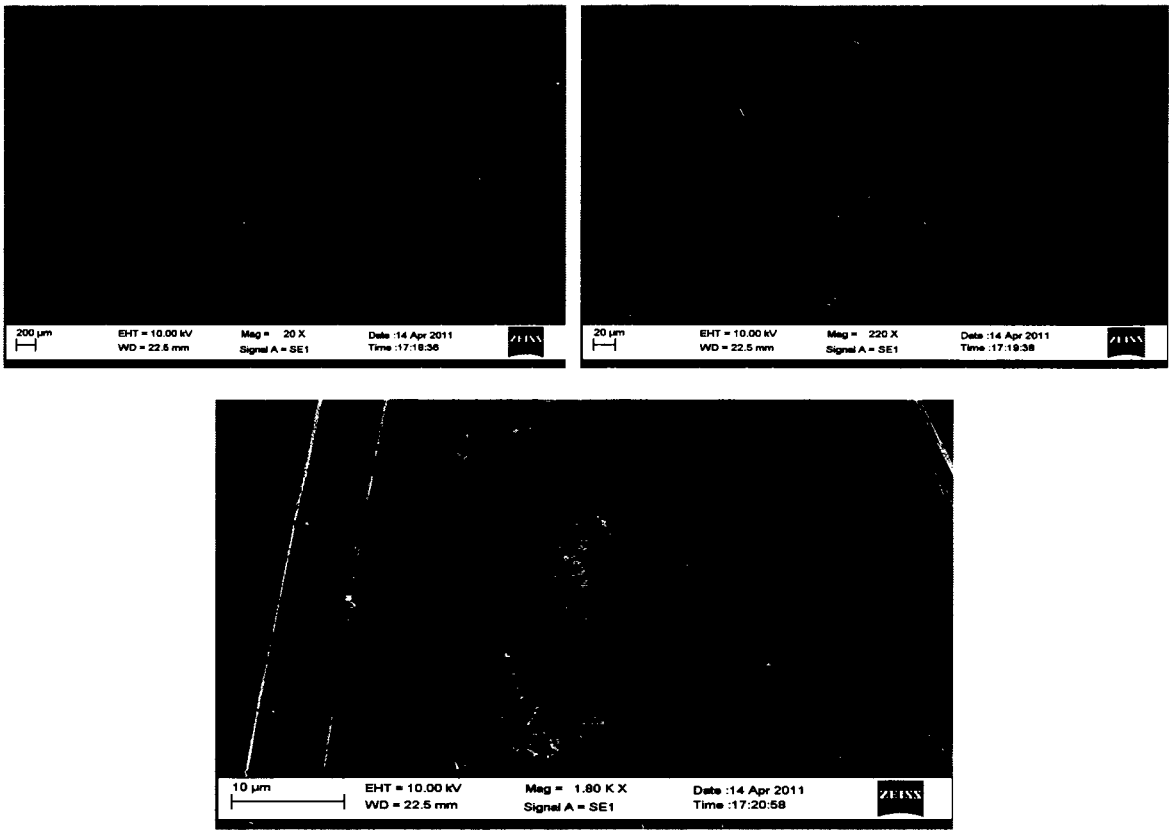
200 µm
EHT = 10.00 kV
WD = 22.5 mm
Mag = 20 X
Signal A = SE1
Date :14 Apr 2011
Time :17:18:36
20 µm
EHT = 10.00 kV
WD = 22.5 mm
Mag = 220 X
Signal A = SE1
Date :14 Apr 2011
Time :17:19:38
10 µm
EHT = 10.00 kV
WD = 22.5 mm
Mag = 1.80 K X
Signal A = SE1
Date :14 Apr 2011
Time :17:20:58

Fig. 59

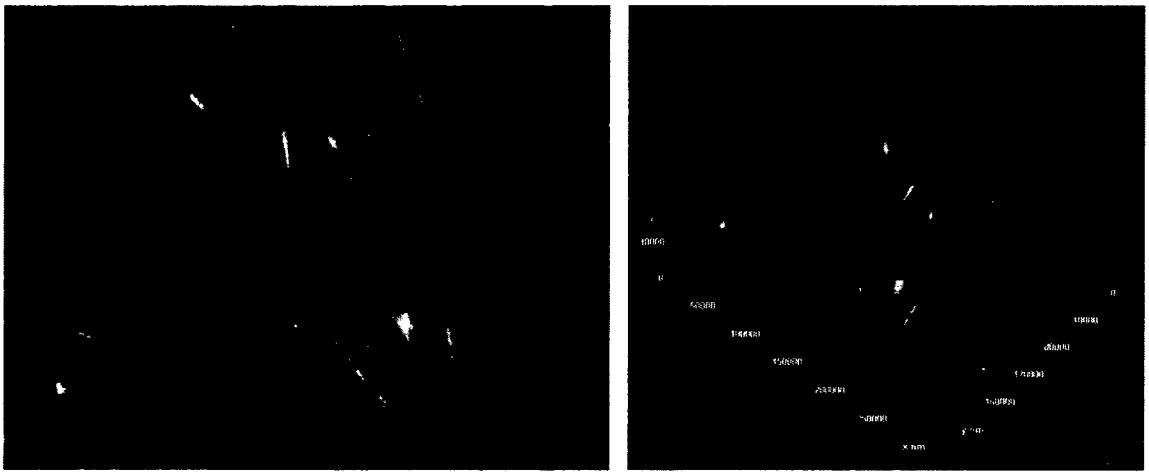

Fig. 60